VILNIUS TECH
Vilniaus Gedimino technikos universitetas

Andžej BOREL

INVESTIGATION OF BEHAVIORAL MODELS USED FOR LINEARIZATION OF RADIO FREQUENCY POWER AMPLIFIERS OVER A WIDE CARRIER FREQUENCY RANGE

DOCTORAL DISSERTATION

TECHNOLOGICAL SCIENCES
ELECTRICAL AND ELECTRONIC ENGINEERING (T 001)

Vilnius, 2026

2026-026-M

VILNIUS GEDIMINAS TECHNICAL UNIVERSITY

Andžej BOREL

INVESTIGATION OF BEHAVIORAL MODELS USED FOR LINEARIZATION OF RADIO FREQUENCY POWER AMPLIFIERS OVER A WIDE CARRIER FREQUENCY RANGE

DOCTORAL DISSERTATION

TECHNOLOGICAL SCIENCES
ELECTRICAL AND ELECTRONIC ENGINEERING (T 001)

Vilnius, 2026

The doctoral dissertation was prepared at Vilnius Gediminas Technical University in 2019–2026.

Supervisor

Prof. Dr Vaidotas BARZDĖNAS (Vilnius Gediminas Technical University, Electrical and Electronic Engineering – T 001).

The Dissertation Defense Council of the Scientific Field of Electrical and Electronic Engineering of Vilnius Gediminas Technical University:

Chairman

Prof. Dr Darius PLONIS (Vilnius Gediminas Technical University, Electrical and Electronic Engineering – T 001).

Members:

Prof. Dr Vitalij NOVICKIJ (Vilnius Gediminas Technical University, Electrical and Electronic Engineering – T 001),

Prof. Dr Šarūnas PAULIKAS (Vilnius Gediminas Technical University, Electrical and Electronic Engineering – T 001),

Dr Habil. Mariusz STĘPIEŃ (Silesian University of Technology, Poland, Electrical and Electronic Engineering – T 001),

Prof. Dr Algimantas VALINEVIČIUS (Kaunas University of Technology, Electrical and Electronic Engineering – T 001).

The dissertation will be defended at the public meeting of the Dissertation Defense Council of the Scientific Field of Electrical and Electronic Engineering in the *Aula Doctoralis* Meeting Hall of Vilnius Gediminas Technical University at **10 a.m. on 9 June 2026.**

Address: Saulėtekio al. 11, LT-10223 Vilnius, Lithuania.
Tel.: +370 5 274 4956; fax +370 5 270 0112; e-mail: doktor@vilniustech.lt

A notification on the intended defense of the dissertation was sent on 8 May 2026. A copy of the doctoral dissertation is available for review at the Vilnius Gediminas Technical University repository https://etalpykla.vilniustech.lt, the Library of Vilnius Gediminas Technical University (Saulėtekio al. 14, LT-10223 Vilnius, Lithuania), and the Wroblewski Library of the Lithuanian Academy of Sciences (Žygimantų g. 1, LT-01102 Vilnius, Lithuania).

Vilnius Gediminas Technical University book No. 2026-026-M

https://doi.org/10.20334/2026-026-M

Vilnius Gediminas Technical University, 2026

andzej.borel@vilniustech.lt

VILNIAUS GEDIMINO TECHNIKOS UNIVERSITETAS

Andžej BOREL

RADIJO DAŽNIŲ GALIOS STIPRINTUVAMS LINEARIZUOTI TAIKOMŲ ELGSENOS MODELIŲ TYRIMAS PLAČIAME NEŠLIO DAŽNIŲ DIAPAZONE

DAKTARO DISERTACIJA

TECHNOLOGIJOS MOKSLAI,
ELEKTROS IR ELEKTRONIKOS INŽINERIJA (T 001)

Vilnius, 2026

Disertacija rengta 2019–2026 metais Vilniaus Gedimino technikos universitete.

Vadovas

prof. dr. Vaidotas BARZDĖNAS (Vilniaus Gedimino technikos universitetas, Elektros ir elektronikos inžinerija – T 001).

Vilniaus Gedimino technikos universiteto Elektros ir elektronikos inžinerijos mokslo krypties disertacijos gynimo taryba:

Pirmininkas

prof. dr. Darius PLONIS (Vilniaus Gedimino technikos universitetas, Elektros ir elektronikos inžinerija – T 001).

Nariai:

prof. dr. Vitalij NOVICKIJ (Vilniaus Gedimino technikos universitetas, Elektros ir elektronikos inžinerija – T 001),

prof. dr. Šarūnas PAULIKAS (Vilniaus Gedimino technikos universitetas, Elektros ir elektronikos inžinerija – T 001),

habil. dr. Mariusz STĘPIEŃ (Silezijos technologijos universitetas, Lenkija, Elektros ir elektronikos inžinerija – T 001),

prof. dr. Algimantas VALINEVIČIUS (Kauno technologijos universitetas, Elektros ir elektronikos inžinerija – T 001).

Disertacija bus ginama viešame Elektros ir elektronikos inžinerijos mokslo krypties disertacijos gynimo tarybos posėdyje **2026 m. birželio 9 d. 10 val.** Vilniaus Gedimino technikos universiteto *Aula Doctoralis* posėdžių salėje.

Adresas: Saulėtekio al. 11, LT-10223 Vilnius, Lietuva.
Tel.: (0 5) 274 4956; faksas (0 5) 270 0112; el. paštas *doktor@vilniustech.lt*

Pranešimai apie numatomą ginti disertaciją išsiųsti 2026 m. gegužės 8 d.
Disertaciją galima peržiūrėti Vilniaus Gedimino technikos universiteto talpykloje *https://etalpykla.vilniustech.lt/*, Vilniaus Gedimino technikos universiteto bibliotekoje (Saulėtekio al. 14, LT-10223 Vilnius, Lietuva) bei Lietuvos mokslų akademijos Vrublevskių bibliotekoje (Žygimantų g. 1, LT-01102 Vilnius, Lietuva).

Abstract

The dissertation examines the impact of carrier frequency variation on the accuracy of behavioral models used for power amplifier linearization in radio frequency (RF) systems. In reconfigurable, wideband communication networks, such as those employing cognitive radio and 5G/6G technologies, power amplifiers (PAs) are often required to operate over a range of carrier frequencies. Conventional behavioral models, typically developed for a single frequency, may exhibit decreased accuracy when applied outside their original training conditions.

The work is structured around three chapters. The First Chapter is a review of common PA linearization techniques, including feedforward, feedback, and digital predistortion, with an emphasis on their operational principles, implementation considerations, and known limitations.

The Second Chapter describes the development of a semi-automated measurement setup designed to characterize PA behavior under varying operating conditions. It discusses different types of PA behaviors, instruments, and techniques needed to excite and capture them. It proposes methods for setup calibration. The regression polynomial model extraction technique is discussed. The parametrization of the memory polynomial model is proposed, as well as measurement metrics to evaluate the modeling error.

The Third Chapter experimentally investigates how modeling error varies as the carrier frequency changes. Experimental results indicate that model accuracy decreases with increasing deviation from the training frequency, and that this trend is influenced by the modulation bandwidth of the excitation signal. The proposed parametrization technique is experimentally investigated. The results show a significant modeling error reduction compared to the standard memory polynomial model.

The dissertation outlines a methodology for characterizing frequency-dependent modeling error. The proposed modeling technique allows for reducing the error associated with applying the amplifier model to different carrier frequencies. The methods and findings may be applicable in contexts where behavioral models are used in adaptive RF transmitter systems that operate over broad or dynamically changing frequency ranges.

Reziumė

Disertacija nagrinėja nešlio dažnio kitimo įtaka elgsenos modelių, taikomų galios stiprintuvams linearizuoti radijo dažnių sistemose, tikslumui. Perkonfigūruojamuose ir plačiajuosčiuose ryšio tinkluose, tokiuose kaip sistemos, kuriose naudojamos kognityvinio radijo ir 5G ir 6G technologijos, galios stiprintuvai dažnai turi veikti skirtingais nešlio dažniais. Įprastai vienam dažniui sukurti elgsenos modeliai gali prarasti tikslumą, kai taikomi už savo pradinių mokymo sąlygų ribų.

Darbas suskirstytas į tris skyrius. Pirmame skyriuje apžvelgiami dažniausiai naudojami galios stiprintuvų linearizavimo metodai, įskaitant grįžtamojo ryšio, tiesioginio koregavimo ir skaitmeninės išankstinės iškraipymų kompensacijos metodus, jų veikimo principai, įgyvendinimo aspektai ir žinomi apribojimai.

Antrame skyriuje aprašomas pusiau automatinės matavimo sistemos, skirtos galios stiprintuvų elgsenai įvairiomis veikimo sąlygomis charakterizuoti, kūrimas. Nagrinėjami skirtingi stiprintuvų elgsenos tipai, reikalingi prietaisai ir metodai tokioms elgsenoms sužadinti ir užfiksuoti. Pateikiami sistemos kalibravimo metodai. Aprašoma regresinių daugianarių pagrindu paremta modelio išskyrimo technika. Pasiūloma atminties daugianarių parametrizacijos metodika, taip pat – metrikos modeliavimo paklaidai įvertinti.

Trečiajame skyriuje eksperimentiniu būdu tiriama, kaip modelio paklaida kinta keičiantis nešlio dažniui. Eksperimentų rezultatai rodo, kad modelio tikslumas mažėja, kai nešlio dažnis vis labiau nutolsta nuo mokymo dažnio, ir kad ši tendencija priklauso nuo sužadinimo signalo moduliacijos juostos pločio. Eksperimentiškai ištirta pasiūlyta atminties daugianario parametrizacijos metodika. Rezultatai parodo reikšmingą modeliavimo klaidos sumažėjimą, palyginti su standartiniu atminties daugianario modeliu.

Disertacijoje pateikiama metodika, skirta galios stiprintuvams modeliuoti esant skirtingiems nešlių dažniams. Pasiūlyta modeliavimo metodika leidžia sumažinti modeliavimo klaidą, atsirandančią taikant stiprintuvo modelį esant skirtingiems nešlių dažniams. Siūlomi metodai ir gauti rezultatai gali būti taikomi sistemose, kuriose elgsenos modeliai naudojami adaptuojamuose radijo dažnių siųstuvuose, veikiančiuose plačiame arba dinamiškai kintančiame dažnių ruože.

Notations

Symbols

A – analog amplifier gain (liet. *analoginio stiprintuvo stiprinimas*);

B – analog couplers coupling ratio (liet. *analoginių šakotuvų susiejimo koeficientas*);

C_1, C_2 – active feedback couplers (liet. *aktyvaus grįžtamojo ryšio šakotuvai*);

G – digital system gain (liet. *skaitmeninės sistemos stiprinimas*);

S point, Q point – power amplifier saturation and quiescent points (liet. *galios stiprintuvo soties ir darbo taškai*);

$IMSR_a$, $IMSR_0$ – ratio of intermodulation power to signal power before and after the error cancellation circuit (liet. *intermoduliacijos ir signalo galių santykis prieš ir po klaidų kompensavimo grandinės*);

β – feedback constant (liet. *grįžtamojo ryšio konstanta*);

a_i, $a_{MRAS,i}$, $a_{STR,i}$ – DPD, MRAS-DPD, and STR-DPD coefficients (liet. *adaptyviųjų skaitmeninių sistemų koeficientai*);

T_{dn} – delay time of time-delay element (liet. *laiko vėlinimo elemento vėlinimo trukmė*);

τ – maximal delay time error in feedforward circuit (liet. *didžiausia vėlinimo trukmės paklaida tiesioginio ryšio grandinėje*);

P_{in}, P_{out} – input and output power (liet. *įėjimo ir išėjimo galia*);

V, V_{out} – input and output voltages of the feedback amplifier (liet. *grįžtamojo ryšio stiprintuvo įėjimo ir išėjimo įtampos*);

k_n – *n*-th harmonic coefficient of a nonlinear system (liet. *netiesinės sistemos n-osios harmonikos koeficientas*);

$x(t)$, $y(t)$, $y_{RF}(t)$ – input and output analog signals (liet. *įėjimo ir išėjimo analoginiai signalai*);

$x_I(t)$, $x_Q(t)$ – in-phase and quadrature signal components (liet. *fazinė ir kvadratūrinė signalo dedamosios*);

$x(n)$, $x_{DPD}(n)$, $x_{STR}(n)$, $y(n)$ – input, DPD output, STR output, and output digital signals (liet. *skaitmeninių sistemų įejimo ir išėjimo skaitmeniniai signalai*);

$z(n)$, $e(n)$ – output and error signal of post-inverse adaptive filter (liet. *postinversinio adaptyviojo filtro išėjimo ir klaidos signalai*).

Abbreviations

5G – 5th Generation of cellular networks (liet. *penktoji mobiliojo ryšio tinklų karta*);

ACLR – Adjacent Channel Leakage Ratio (liet. *gretimo kanalo nutekėjimo santykis*);

ADC – Analog to Digital Converter (liet. *analoginis-skaitmeninis keitiklis*);

DAC – Digital to Analog Converter (liet. *skaitmeninis-analoginis keitiklis*);

DPD – Digital Predistortion (liet. *skaitmeninis išankstinis iškraipymas*);

DUT – Device Under Test (liet. *tiriamas įrenginys*);

IF – Intermediate Frequency (liet. *tarpinis dažnis*);

IMD – Intermodulation Distortion (liet. *intermoduliaciniai iškraipymai*);

LTE – Long-Term Evolution (liet. *ilgalaikė evoliucija*);

LTE-A – LTE Advanced (liet. *pažangioji LTE*);

LUT – Look-Up Table (liet. *paieškos lentelė*);

MIMO, mMIMO – (Massive) Multiple Input Multiple Output (liet. *didelės apimties įėjimų ir išėjimų sistema*);

MP – Memory Polynomial (liet. *atminties daugianaris*);

MRAS – Model Reference Adaptive System (liet. *modeliu pagrįsta adaptyvioji sistema*);

NMSE – Normalized Mean Squared Error (liet. *normalizuota vidutinė kvadratinė paklaida*);

PA – Power Amplifier (liet. *galios stiprintuvas*);

PAE – Power Added Efficiency (liet. *pridėtinės galios efektyvumo koeficientas*);

PAPR – Peak-to-Average Power Ratio (liet. *didžiausios ir vidutinės galių santykis*);

PC – Personal Computer (liet. *asmeninis kompiuteris*);

PLL – Phase-Locked Loop (liet. *fazės sinchronizavimo kilpa*);

PMP – Parametrical Memory Polynomial (liet. *parametrinis atminties daugianaris*);

QAM – Quadrature Amplitude Modulation (liet. *kvadratūrinė amplitudinė moduliacija*);

QPSK – Quadrature Phase Shift Keying (liet. *kvadratūrinė fazinė moduliacija*);

RB – Receiver Bandwidth (liet. *imtuvo praleidžiamų dažnių juostos plotis*);

RF – Radio Frequency (liet. *radijo dažnis*);

SFDR – Spurious-Free Dynamic Range (liet. *dinaminis diapazonas be iškraipymų*);

STR – Self-Tuning Regulator (liet. *save derinantis reguliatorius*);

VSA – Vector Signal Analyzer (liet. *vektorinis signalų analizatorius*);

VSG – Vector Signal Generator (liet. *vektorinis signalų generatorius*).

Contents

Introduction

Problem Formulation

Power amplifiers (PAs) are essential in modern communication systems, enabling reliable signal transmission but introducing nonlinear distortions that degrade signal quality, especially near peak efficiency; these effects are commonly mitigated using techniques such as digital predistortion (DPD), which relies on behavioral models such as memory polynomials (MP). However, such models are typically valid only under their original extraction conditions and do not account for performance outside that range, a limitation in frequency-agile applications like cognitive radio. This dissertation addresses the issue by proposing a behavioral modeling approach that parameterizes MP model coefficients as functions of carrier frequency, allowing a single model to capture frequency-dependent variations in gain, phase, and memory effects across a continuous range. Focusing on moderate-power (1–2 W) amplifiers in the 5G FR-1 band (410–7125 MHz) and using standard communication signals with bandwidths from 10 kHz to 2 MHz, the work aims to improve model robustness, reduce the need for repeated characterization, and support efficient linearization in adaptive transmitter systems.

Relevance of the Dissertation

This dissertation investigates whether a power amplifier (PA) model extracted at one carrier frequency can be reliably applied to others, addressing a key challenge in modern wideband and multi-band wireless systems such as cognitive radio. It evaluates the modeling errors introduced by frequency changes and proposes methods to mitigate them by characterizing frequency-dependent PA behavior and enabling a single model to operate across multiple operating points. The work introduces metrics for quantifying these inaccuracies and explores compensation techniques that improve model robustness. Overall, it demonstrates that with proper treatment of frequency dependence, PA linearization can be made more flexible and efficient, reducing the need for repeated multi-frequency characterization while lowering development effort.

In Lithuania, PAs were researched earlier by Dr Aleksandr Vasjanov and Prof. Dr Vaidotas Barzdėnas. Their contributions include studies into different PA architectures (Vasjanov & Barzdenas, 2016, 2018) and general CMOS amplifier chip design (Barzdenas & Navickas, 2009; Vasjanov & Barzdenas, 2020).

Research Object

The object of the research is a behavioral model of a radio-frequency power amplifier.

Aim of the Dissertation

The dissertation aims to develop and validate a frequency-robust behavioral modeling framework for radio-frequency power amplifiers that ensures accurate performance prediction across a wide range of carrier frequencies.

Tasks of the Dissertation

To achieve the aim of the dissertation, the following tasks need to be completed:

1. Develop a characterization system that allows for modeling a power amplifier by measuring its excitation and response signals.
2. Investigate and propose metrics for PA modeling error caused by carrier frequency variation.
3. Experimentally examine the impact of excitation signal characteristics on PA modeling error caused by carrier frequency variation.

4. Propose methods for reducing PA modeling error caused by carrier frequency variation.

Research Methodology

The following methods are used in the present dissertation:

1. A literature review identified key trends in PA linearization and defined the research problem.
2. The PA was experimentally characterized using continuous-wave and modulated signals.
3. Measured data were used to extract behavioral models via polynomial regression.
4. MATLAB was used for measurement control, data processing, modeling, and visualization.

Scientific Novelty of the Dissertation

The research presented in this dissertation has yielded the following novel results in the field of Electrical and Electronic Engineering:

1. A semi-automatic system is developed for PA characterization across a wide range of operating conditions.
2. A method is introduced to quantify carrier-frequency-dependent modeling error and to analyze its variation across various frequencies.
3. A multi-frequency dataset of PA input-output signals is created to support reproducible error analysis.
4. A parameterized memory polynomial model with frequency-dependent coefficients is proposed, achieving near-per-frequency accuracy with fewer measurements and lower extraction effort.

Practical Value of the Research Findings

The proposed parameterized memory polynomial modeling methodology for power amplifiers requires fewer computations and measurements compared to the conventional memory polynomial modeling approach, as it enables the behavioral model to operate at carrier frequencies different from those used for model extraction. The developed methodology can reduce measurement and calibration time in telecommunication systems operating with varying carrier frequencies while

preserving deterministic computational complexity suitable for real-time digital predistortion-based power amplifier linearization. Unlike approaches that require large volumes of measurement data, the proposed parameterization method achieves comparable modeling accuracy using significantly fewer measurement datasets.

Defended Statements

1. A method was developed for evaluating the generalization capability of power amplifier behavioral models with respect to carrier frequency. It determines the rate of change of frequency-dependent modeling error, analyzes the dependence of memory polynomial model error on carrier frequency, and assesses the influence of excitation signal parameters, including average power, modulation bandwidth, and peak-to-average power ratio.
2. It was experimentally determined that the variation of modeling error with changes in carrier frequency is strongly correlated with the modulation bandwidth of the excitation signal (correlation coefficient up to 0.99). Meanwhile, the average signal power and PAPR do not exhibit significant correlation, or correlation is observed only at one of the tested frequencies. As the frequency deviates further from the model extraction point, the error increases. In the case of the 3.3–3.8 GHz power amplifier, increasing the modulation bandwidth of the excitation signal from 0.01 MHz to 2 MHz caused the rate of change of the modeling error with respect to frequency to increase from 0.08 dB/MHz to 0.11 dB/MHz, based on the normalized mean square error metric.
3. A proposed parameterized memory polynomial model with frequency-dependent coefficients enables accurate approximation of power amplifier behavior over the 3.3–3.8 GHz range, achieving an average NMSE of approximately −39 dB when using 10 or more interpolation points. This corresponds to the result obtained when modeling the amplifier at 51 different carrier frequencies, thereby significantly reducing the measurement requirements.

Approval of the Research Findings

Two publications referenced in the *Clarivate Analytics Web of Science* database were published on the topic of the dissertation (Borel et al., 2021; Borel et al., 2025).

One publication was published in the conference proceedings (Borel & Barzdėnas, 2020).

The results of the research were presented in four scientific conferences:

- Open International Conference of Electrical, Electronic, and Information Sciences (eStream), 2020, Vilnius, Lithuania.
- Open International Conference of Electrical, Electronic, and Information Sciences (eStream), 2021, Vilnius, Lithuania.
- Workshop on Microwave Theory and Techniques in Wireless Communications (MTTW), 2021, Riga, Latvia.
- Conference of Doctoral Students and Young Scientists (FizTeCh), 2025, Vilnius, Lithuania.

Structure of the Dissertation

The dissertation consists of the introduction, 3 chapters and general conclusions.

The dissertation is 99 pages, without a summary in Lithuanian. It has 54 numbered formulas in text, 38 figures, and 10 tables. The dissertation used 100 literature sources.

Acknowledgments

A scientific work is never the achievement of its author alone. This work, too, would not have been possible without the help and support of others.

I would like to thank my scientific supervisor, Prof. Dr Vaidotas Barzdėnas, for his constant and comprehensive support during the preparation of this dissertation, for the long hours spent in discussions, and for helping me not to give up halfway through the journey.

I express my sincere gratitude to my colleague, Assoc. Prof. Dr Aleksandr Vasjanov, for his creativity and experience, the impact of which on this work is difficult to overestimate.

I thank my parents, Daiva and Valerij, and my sister Jolanta for their patience and support. I thank my beloved Rusnė and her parents, Sigitas and Rasa, for their support. Finally, I thank the society of Lithuania, whose work creates the conditions for the development of science and studies.

1

Literature Survey on Power Amplifier Linearization Methods

This chapter reviews the trade-off between linearity and efficiency and methods to address it. Three main groups of linearization methods are discussed. It discusses the problem of behavioral modeling over a range of carrier frequencies. The results of the review are published (Borel et al., 2021), (Borel & Barzdėnas, 2020).

1.1. Linearity Versus Efficiency Trade-Off

A power amplifier is a device used to increase the power of a signal and deliver it to a load, typically an antenna in wireless communications. To achieve this amplification, a PA draws power from the supply. The ratio of output power, delivered to the load (P_{out}) to the power drawn from the supply (P_{DC}), is called the *drain efficiency* of the amplifier. A more rigorous efficiency metric, which also accounts for the input signal power (P_{in}), is known as *power added efficiency* (PAE).

$$PAE = \frac{P_{\text{out}} - P_{\text{in}}}{P_{\text{DC}}}. \tag{1.1}$$

Higher PAE is desirable as it helps reduce the overall power consumption of communication networks, since the PA is the most power-hungry component in the infrastructure. This is particularly important in mobile applications, where improved power efficiency directly contributes to longer battery life.

Over its full operating range, a PA is an inherently nonlinear device. Figure 1.1 shows a typical PA transfer characteristic. Ideally, the characteristic would remain linear up to the clipping point; however, due to the nature of semiconductor physics, this is not achievable in transistor-based amplifiers. The transfer characteristic can be divided into three regions: linear, nonlinear, and saturation. An amplifier typically achieves its highest PAE in the saturation region.

When amplifying a constant-amplitude signal, the quiescent point (Q point) can be set near the saturation point (S point), enabling high PAE. However, to achieve spectral efficiency, variable-amplitude signals are usually required. To transmit such signals linearly, the Q point must be placed within the linear region of the transfer characteristic; otherwise, unwanted nonlinear distortion is introduced into the transmitted signal. This, in turn, degrades the amplifier's PAE.

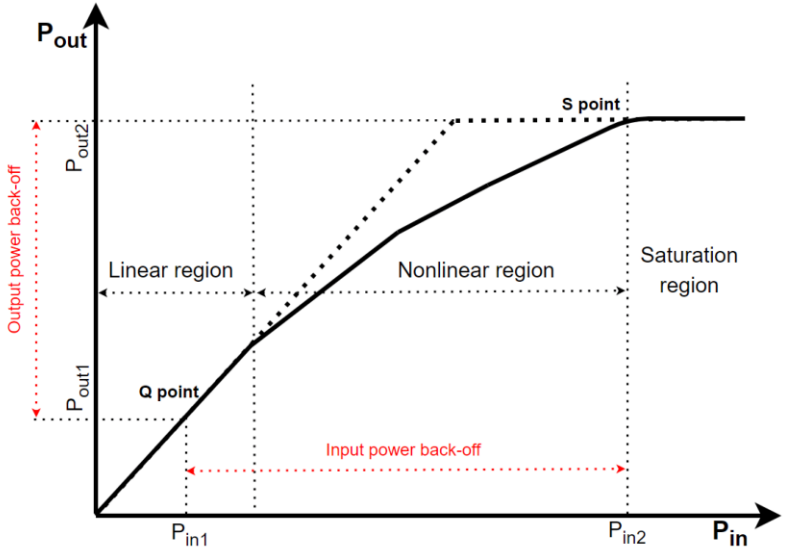

Fig. 1.1. General amplifier transfer characteristic (created by the author)

Linearization is the process of making an inherently nonlinear circuit behave more linearly. Setting the Q point within the PA's linear region is therefore already a basic linearization technique. When the Q point is positioned to allow

amplification of the entire signal amplitude with minimal nonlinear distortion, the amplifier operates in Class A. This approach relies on *power back-off*, which is the difference between the S point and the Q point in terms of either input or output power. Although Class A amplification is highly spectrally efficient, it is also extremely power-inefficient. The maximum theoretical drain efficiency is 50%, but practical implementations often fall below 25%.

1.2. Common Linearization Techniques

Biasing the PA into class A operation may be a linearization technique, but it does not address the trade-off between linearity and efficiency, merely prioritizing the former over the latter. Three main groups of techniques are used to improve linearity without entirely sacrificing power efficiency: feedforward, feedback, and predistortion.

1.2.1. Feedforward

The feedforward linearization technique was the first linearization method invented. However, it was widely adopted later than other linearization methods (Black, 1977), which can be explained by examining the principle of feedforward operation and the development of communication technologies. The operational diagram of the method is given in Figure 1.2. The feedforward circuitry attempts to isolate an error generated by a main amplifier so that this error can be further minimized, or ideally, eliminated from the output signal. The feedforward circuitry consists of signal and error cancellation sub-circuits. The signal cancellation circuit isolates the main amplifier's error, and the error cancellation circuit subtracts the received error from the main signal.

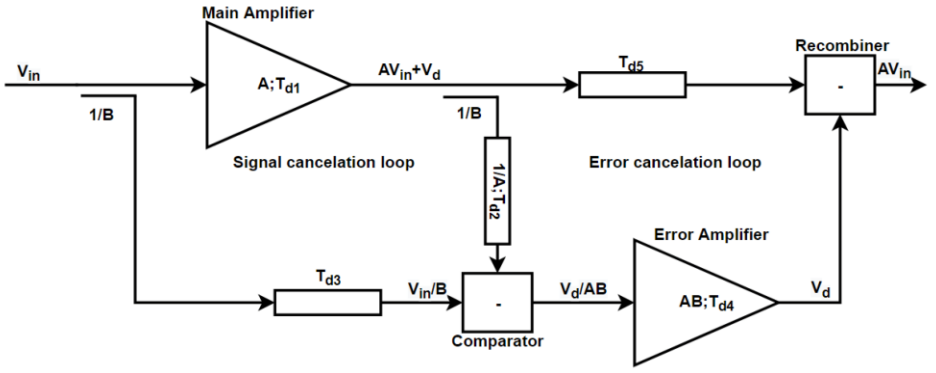

Fig. 1.2 Simplified feedforward operational diagram (created by the author)

The input signal is divided into two parts: one is fed to the input of the power amplifier, and the other is delayed by T_{d3} and fed to the comparator of the signal cancellation circuit. For simplicity, it was assumed that coupling ratio $B >> 1$, so that the coupler has no noticeable effect on the input and output signal powers of the amplifier. The output signal of the main amplifier consists of the sum of the amplified input signal and the distortion generated by the amplifier ($AV_{in} + V_d$). Part of the output signal is coupled to the signal cancellation loop comparator via an attenuator. Setting the delay time T_{d3} so that it compensates for the delays caused by the main amplifier and the attenuator, i.e., $T_{d3} = T_{d1} + T_{d2}$, at the output of the signal cancellation comparator, will ideally obtain the attenuated value of the distortions generated by the main amplifier. The value obtained in the signal cancellation circuit is then amplified by an error amplifier and fed to an output comparator. The delay time $T_{d5} = T_{d2} + T_{d4}$ ensures the same phases of both compared signals. Ideally, the error signal is subtracted from the main amplifier signal, receiving a distortion-free signal at the output.

The concept of the feedforward method is intuitive and simple, but it was clear to Howard Black, the developer of the methodology, that the implementation of this concept has many practical difficulties with respect to the stability of component parameters (Black, 1977; Pothecary, 1999). The accuracy of the circuit parameters has a decisive influence on the value of nonlinear distortion suppression, since almost identical values are compared. During his time, Howard Black faced the problem that vacuum tube amplifiers lacked sufficient stability in temperature, age, and frequency parameters. For example, he developed the feedforward amplifier system, which had to be manually adjusted every six hours because the fluctuation in supply voltage caused a gain change, which drastically lowered distortion suppression. Eventually, Black solved his problem by developing another linearization technique – feedback linearization, which will be discussed later. The feedforward method was forgotten until the early 1970s.

By the 1970s, vacuum tube amplifiers were being replaced by solid-state devices. Communication networks were expanding, and solutions were needed to ensure the use of wider bandwidth channels. Around this time, researchers returned their attention to feedforward amplifiers. In 1973, Bennett and Clements published an article (Bennett & Clements, 1974) reviewing the disadvantages of the feedback linearization technique, used commonly at that time, and the potential advantages of the feedforward method. The authors noted that, as the frequencies of the signals used increased, the gain and phase margins of the feedback structure decreased, and, therefore, it became more difficult or even impossible to ensure circuit stability. Several years earlier, similar statements were made by Seidel et al. (1968). Seidel contended that the feedback method faced the problem of causality. The problem was at the heart of the feedback method: one attempts to correct an event that has already happened by changing its cause. This works

up to a certain limit when the “past” and the “present” are not clearly separated in terms of the signal, i.e., the delay of the amplifier is much shorter than the wave period of the received signal. As the signal period approaches the amplifier delay time, this limitation arises, and the contradiction of the method becomes apparent: unwanted oscillation occurs at the amplifier’s output. Unlike feedback, the feedforward circuit structure is unconditionally stable at all frequencies, because the signal is compared to a time-delayed reference signal. This advantage of feedforward was a cornerstone that often did not even leave a real choice between the two methods. Together with this main advantage, feedforward also has a less drastic reduction in gain compared to feedback, does not depend on the delay nature of the amplifier used, and does not require the use of a portion of the gain-bandwidth product to ensure amplifier stability.

After identifying all the potential advantages of feedforward, it was necessary to come up with ways to minimize or circumvent the shortcomings of this structure. The disadvantages of feedforward can be roughly divided into two groups: distortions due to extremely high requirements for component tolerance and power losses due to additional amplifier and passive components. The stability of the values of the components used is critical when the circuit compares two nearly identical signals. Unlike feedback, feedforward does not have a self-regulating mechanism to compensate for component value shifts due to temperature, age, supply voltage fluctuations, etc. This means that, as the environmental conditions change, the classical feedforward scheme collapses quickly. Therefore, to achieve an acceptable distortion suppression value, it is necessary to provide a way to compensate for natural fluctuations in the values of the circuit elements. There are also questions about the power efficiency of such a structure. The error amplifier used must not introduce its own distortions to the signal, which usually means that it must be used in class A mode with a significant power back-off. In addition, the use of additional couplers and comparators inevitably reduces the power efficiency of the system. Researchers have been working on these problems since the 1970s.

Additional power loss is one of the serious factors limiting the use of feedforward. When developing this methodology, Black was primarily thinking about reducing intermodulation distortions, and energy efficiency was a secondary consideration for him. Today, to reduce the energy consumption of communication networks, the energy efficiency of the amplifier system requires much more attention. From an energy efficiency viewpoint, an additional power amplifier in the error cancellation circuit becomes a key issue in the feedforward system. The power consumed by the error amplifier is not directly used to amplify the input signal, so its amount is inversely proportional to the total value of the system power efficiency factor. One of the factors that determines the power consumed by the error amplifier is the amplifier’s output power coupler ratio. A lower power

error amplifier can be used by transferring more power to the error cancellation circuit; however, this reduces the output power level, because there is no way to compensate for the losses caused by the power coupler. This problem is solvable by choosing optimal coefficients of the utilized power couplers to get the desired linearity and efficiency. Reactive devices (such as transformers) can also be used instead of hybrid directional couplers, sacrificing insulation between the main and error correction circuits for lower power losses.

With certain assumptions, Bennett and Clements (1974), Kenington (1992), and Parsons and Kenington (1994) provided a quantitative theoretical analysis of feedforward circuit power efficiency parameters. The authors single out the main factors determining power efficiency: variation of the gain of the main amplifier in the signal bandwidth, the value of the output coupler, and the total insertion losses of time delay elements. The power consumption of the error amplifier increases as the variation of the gain of the main amplifier increases. For example, if the gain of the main amplifier drops by 2 dB in the bandwidth and the phase fluctuates by ± 9°, the error amplifier must provide −12 dB of power compared to the main amplifier. Similarly, the relative power of the error amplifier can be calculated for other values of gain and phase variation (Bennett & Clements, 1974). The theoretical dependence of power efficiency on the value of the output coupler used is given in (Kenington, 1992). This study shows that the peak value of the efficiency curve is sharply defined using more efficient amplifiers (e.g., with a class C power amplifier, the feedforward system achieves a theoretical efficiency of 43.25% at an 8.2 dB output coupler value). In the case of less efficient amplifiers in the system, the peak of the efficiency curve is wider (e.g., with a class A amplifier, the feedforward system achieves a theoretical power efficiency of 24.1% at 17.6 dB output coupler value; however, when increasing the coupler value by 10 dB, efficiency drops only by 1.6% to 22.5%). Although both these results are only approximate due to the assumptions made, the dependence revealed is illustrative. Further mathematical analysis showed that the efficiency of the feedforward circuit drops drastically when estimating the insertion losses of the time delay elements (Parsons & Kenington, 1994). For example, a 1 dB input loss reduces the efficiency of the theoretical Class C amplifier feedforward system from 43% to ~34%, and a 2 dB input loss reduces the theoretical efficiency to ~28%.

To solve the problem of low component tolerance and natural parameter drift, the adaptive feedforward linearization technique is used. Based on the available knowledge, Cavers (Cavers, 1995; Smith & Cavers, 1998) was among the first researchers to theoretically investigate this method. He investigated the adaptation parameters of a so-called gradient feedforward amplifier. The essence of the method is to adjust the parameters of the feedforward circuit (delay time, complex gain, etc.) using a mathematically calculated gradient signal.

Analyzing the feedforward circuit, Cavers found that the accuracy α of the signal cancellation circuit elements must be in the order of 10^{-4} over the entire signal frequency range to achieve 40 dB intermodulation distortion (IMD) attenuation.

$$IMSR_0 = |\beta - 1|^2 \, IMSR_a, \tag{1.2}$$

where β is the unity gain of the error amplifier, $IMSR_a$ and $IMSR_0$ are the ratios of intermodulation power to signal power before and after the error cancellation circuit, respectively. For example, to suppress intermodulation interference by 40 dB, one needs an accuracy of 1% in error amplifier parameters in the whole operational bandwidth. It was also determined that the error in the delay times of the branches of the circuit must not exceed 0.3% of the signal period. For example, to achieve 40 dB intermodulation distortion suppression when a 10 MHz bandwidth signal is used, the maximum delay time error τ is calculated in Equation (1.3). Considering that modern communication networks aim to use bandwidths considerably higher than 10 MHz, the accuracy requirements for delay elements can easily become impractical.

$$\tau = 0.3\ \% \times \frac{1}{10\ \text{MHz}} = 0.3\ \text{ns}, \tag{1.3}$$

One of the shortcomings of the analysis is that it ignores the memory effects of the amplifier. The least mean squares adaptation estimating the amplifier memory effects using the Wiener–Hammerstein memory model has been thoroughly investigated in (Gokceoglu et al., 2012). Both analyses propose methods to alleviate the component tolerance requirements for the feedforward circuit. A method of pilot signal adaptation was also described in the literature (Braithwaite, 2008). Unlike the gradient method, this method adds a pilot signal outside of the channel bandwidth to the input signal. The power of the added signal is then measured at the output, thus evaluating the level of distortion suppression and adjusting the parameters of the error cancellation circuit.

Table 1.1. Feedforward method results (Created by the author)

Source	Output Power, dBm	Efficiency, %	ACLR (lowest), dBc	Carrier Frequency, MHz	Bandwidth, MHz
(Cho et al., 2005)	44.7	10.9 (PAE)	−60	2140	4

End of Table 2.1

Source	Output Power, dBm	Effi-ciency, %	ACLR (lowest), dBc	Carrier Frequen-cy, MHz	Band-width, MHz
(Xiang & Wang, 2009)	49	27.2	−53.5	945	N/A
(Choi et al., 2010)	43	19.4 (PAE)	−53.2	2140	20
(Braithwaite & Khanifar, 2013)	52.7	25	−62.0	880	10
(Braithwaite, 2015)	51.4	21.4	−63.0	880	10

Table 1.1 shows the results obtained with the feedforward method to the best of the authors' knowledge. The selected studies considered the following: the date of publication – only the results of the last 15 years were included; whether the work provided a measurement of a physical prototype; and whether both spectral and energy efficiency parameters were specified.

Five works were investigated according to the specified criteria. The highest achieved energy efficiency was 27.2% (drain efficiency) and 19.4% PAE. The highest achieved Adjacent channel leakage ratio was −63 dBc. The best ratio of spectral to energy efficiency was demonstrated in Braithwaite's study (2013). Typically, the error amplifier is set to Class A or AB, which significantly reduces the efficiency of the feedforward circuit. In the mentioned study, the error amplifier was a nonlinear Doherty structure amplifier. By appropriately controlling the nonlinear distortions generated by the main amplifier, the author determined a mode of operation in which the distortions generated by the main amplifier were inverse to the distortions created by the error amplifier; thus, these distortions compensate for each other. This is achieved by including an offset calculated in the value function.

1.2.2. Feedback

As mentioned earlier, the feedback linearization technique was developed by the same author as the feedforward technique. While today, feedback is one of the most often used design techniques for amplifiers, it is interesting to note that, in an initial attempt to patent it, the patent was denied because this method was thought to be some variation of the perpetual motion machine. However, later, due to its simplicity and efficiency, this methodology became widely used. A simplified operational diagram of the feedback circuit is presented in Figure 1.3.

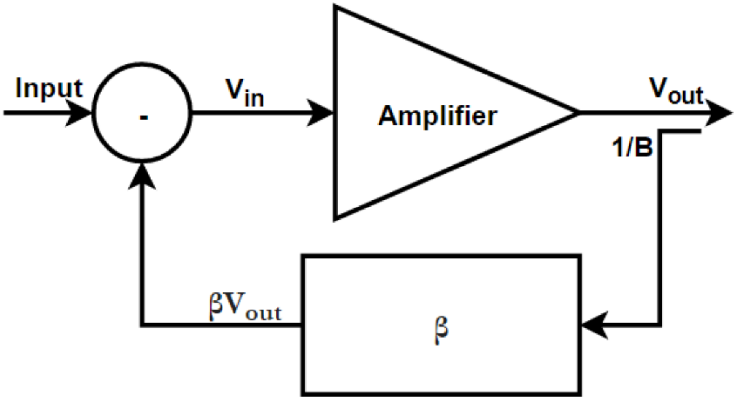

Fig. 1.3. Simplified feedback operational diagram (created by the author)

Mathematical interpretation of the operation of a feedback circuit is given below. It is known that, algebraically, the output signal V_{out} of an amplifier can be described as follows:

$$V_{\text{out}} = k_1 V + \sum_{n=2}^{\infty} k_n V^n, \tag{1.4}$$

where V is the input signal, k_n is the weight of the corresponding harmonic. Ideally, all k_n with coefficients $n > 1$ are equal to 0. Of course, virtually any amplifier distorts the shape of the input signal and creates new spectral components. If part of the signal β is returned to the amplifier's input via the negative feedback circuit, the expression of the output signal can be overwritten (Denny, 1970):

$$V_{\text{out}} = k_1 V_{\text{in}} + \frac{1}{1 + k_1 \beta} \sum_{n=2}^{\infty} k_n V_{\text{in}}^n, \tag{1.5}$$

where

$$V_{\text{in}} = V - \beta V_{\text{out}}. \tag{1.6}$$

The simplest feedback circuit reduces the amplitudes of the side harmonics by a factor of $\frac{1}{1 + k_1 \beta}$. It is not difficult to notice that, together with the side harmonics, distortions caused by other reasons are suppressed: temperature fluctuations, aging, supply voltage fluctuations, etc., so in general, the feedback circuit does not require additional system adjustment. It is also said that feedback is a self-regulating circuit. It can also be shown that, in the case of negative feedback,

the frequency-dependent gain is replaced by a much smaller but more stable feedback gain. The physical essence of this process is that, by turning the phase of the output signal by 180° and returning it to the input, the power of the generated side harmonics is subtracted from the input signal, so it can be later compensated by the amplifier. This methodology is applied at relatively low frequencies, but the transition to RF and microwave reveals a contradiction in causality that had been described earlier. This contradiction is partially resolved by using part of the gain-bandwidth to ensure stability, i.e., creating sufficient gain and phase margin. It is also obvious that returning part of the output signal to the input results in an irreversible loss of the output signal power. It is not difficult to notice that, in the case of simple feedback, the attenuation of side harmonics in decibels is equal to the value of the gain in decibels lost (Kenington, 2000). The problems of ensuring stability and compensating for gain reduction are relatively easily solved in low-frequency systems, but are much more difficult to solve at higher frequencies. This is because, as the frequencies increase, each decibel of the gain becomes technologically more expensive, and the delay of the feedback circuit approaches the propagation rate of the signal.

To use feedback linearization at RF frequencies, several different methods have been proposed (Kenington, 2000; Raab et al., 2002; Wood, 2014): active feedback, envelope feedback, polar feedback, and Cartesian feedback. These are the most widely used feedback linearization methods. At the same time, references to so-called distortion and difference-frequency methods can be found in the literature, but they are rarely used and will not be discussed in more detail.

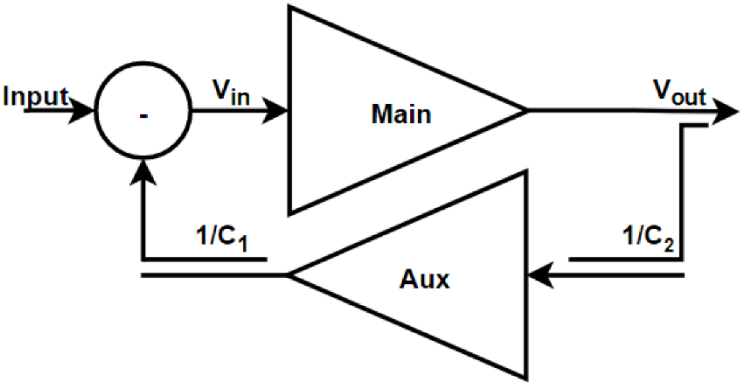

Fig. 1.4. Simplified active feedback operational diagram (created by the author)

The active feedback methodology was proposed (Ballesteros et al., 1988; Perez et al., 1985) in the mid-1980s. A simplified operational diagram of active feedback is shown in Figure 1.4. Passive component feedback is replaced by active

component feedback. Couplers C1 and C2 are also used in the system, whose values are adjusted to achieve optimal system performance. It is clear from Eq. (1.5) that the greater the portion of the output signal returned to the input, the greater the attenuation of the side harmonics. By using active components in the feedback circuit, it is possible to ensure the suppression of intermodulation distortions of the same magnitude by using a smaller part of the output signal power. It is also possible to suppress the intermodulation distortions of the main amplifier by controlling the operational point of the secondary amplifier. To do so, the form of the distortion in the secondary amplifier must be complementary to the distortion form generated by the main amplifier. The authors were able to demonstrate a 3.2 dB increase in output power at the same level of distortion compared to a conventional feedback scheme (Ballesteros et al., 1988). However, at the same time, it was noted that such a system was sensitive to changes in temperature due to the variation in gain of the secondary amplifier. Therefore, one of the main advantages of feedback, circuit self-regulation, is lost in this methodology. To our knowledge, this method is not widely used, although recently, several papers utilizing active feedback (and variations) techniques have been presented and reported quite promising results (Kang et al., 2017, 2018; J. Liu et al., 2019; Xu, 2021).

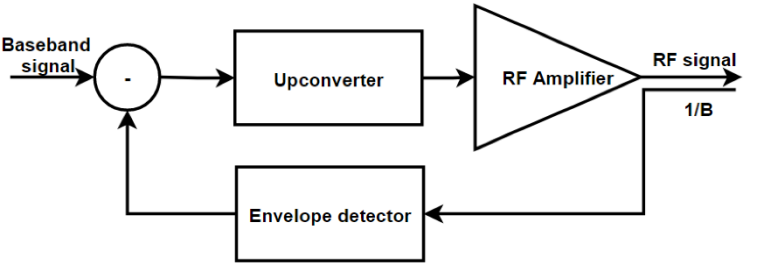

Fig. 1.5. Envelope feedback transmitter operational diagram (created by the author)

Another feedback problem, the lack of stability at higher frequencies, is solved by the so-called modulation or envelope feedback. An operational diagram of such a transmitter is shown in Figure 1.5. In this case, an output signal envelope is detected in the feedback path. It makes it possible to compare low-frequency signal envelopes, which in turn allows it to more easily ensure the stability of the circuit. Frequency bandwidth of the detector generally depends on the type of signal modulation used and, in some cases, (for example, in a two-tone test) can reach relatively high values (Kenington, 2000). It should be noted that such a circuit no longer consists of a single power amplifier, but it contains the entire transmitter system, as the input signal is an unmodulated low-frequency signal, and the output

signal is a modulated RF signal. In case it is not possible to work with the base-band signal (for example, in repeaters), the detection of the input signal, using an additional coupler at the amplifier's input, can be applied, as shown in (Macchiarella et al., 2004). One of the main disadvantages of such a system is a simple envelope detector, which cannot compensate for the phase distortions generated by the nonlinearities in the AM/PM characteristic of the amplifier (Kenington, 2000). As a result, the following modifications of the methodology are most used: polar and Cartesian feedback.

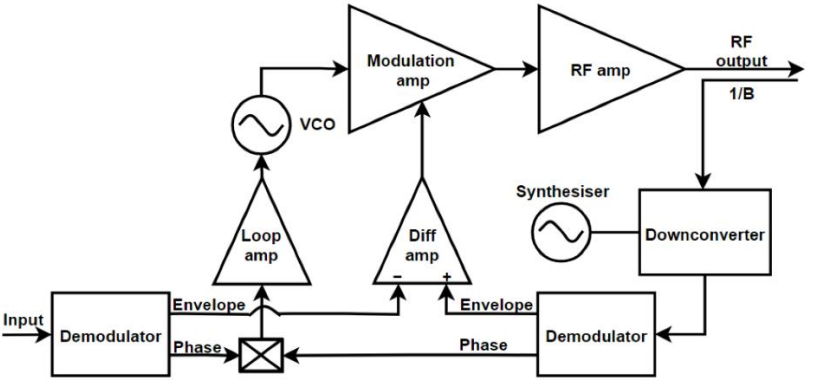

Fig. 1.6. Polar feedback transmitter operational diagram (created by the author)

The simplified schematic of the polar feedback transmitter proposed by Petrovic and Gosling (1979) is presented in Figure 1.6. In this case, one is again considering the entire transmitter system, not just the power amplifier. Similar to the previously described envelope feedback circuit, the output signal of the power amplifier is initially shifted to lower frequencies. Unlike the modulation feedback circuit described above, in this case, the output signal is fed to a splitter circuit, which, in the simplest case, can be a combination of a demodulator and an amplitude limiter (Kenington, 2000). After, the signal is split into envelope and phase components, i.e., converted to its polar form. The input and output signal envelopes are then compared. The received error signal is fed to a modulation amplifier. The oscillator, commonly a phase-locked loop, is controlled by the phase difference between input and output signals. In a modulation amplifier, the signal is raised to the required RF frequency and further fed to the RF amplifier. In this way, a circuit with two separate feedback loops is obtained, one of which corrects for amplitude and the other for phase distortions. The circuit presented in Figure 1.6 can achieve up to 50 dBc distortion attenuation in a two-harmonic test (Kenington, 2000). The distortion suppression value of the circuit directly depends on the accuracy of the phase-locked loop used, as well as its operating limitations. It is often difficult to ensure the stable operation of the phase-locked loop over a

wide frequency range. Additionally, due to the peculiarities of polar modulation, the widths of the phase and amplitude spectra of the components differ significantly, which creates additional problems while designing the system. Polar transmitters are currently being tested using partially or fully digital structures (P. Li et al., 2016; Zheng & Luong, 2013). There is research about ways to reduce the influence of group delay on transmitter operation by using phase and amplitude feedback separately (Kousai et al., 2012), although in this case, a non-polar signal image is used.

Before talking about Cartesian feedback transmitters, the differences between quadrature and polar modulation should be discussed. In the case of polar modulation, the signal is divided into amplitude and phase components. A constant amplitude signal is applied to the power amplifier and is modulated in phase. Amplitude modulation is obtained by modulating not the input signal but usually the power supply voltage of the power amplifier. In the case of quadrature modulation, the signal is divided into in-phase and quadrature components, which are shifted by 90° with respect to each other (Fig. 1.7). By modifying the amplitudes of the component signals, different modulations are obtained. As a result of the modulation, one can achieve an input signal with a variable amplitude. By amplifying a constant amplitude signal, in the case of polar modulation, one can use a power amplifier in the saturation region.

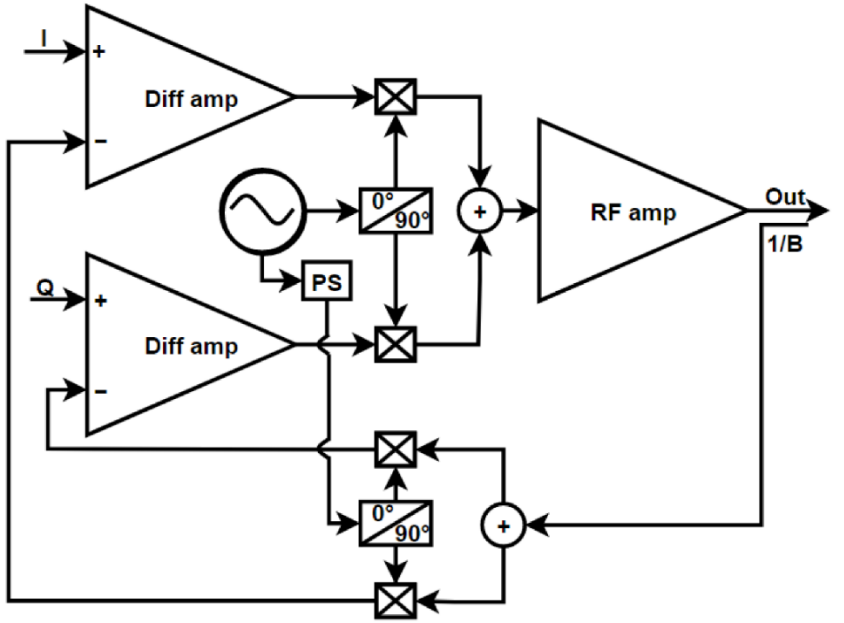

Fig. 1.7. Cartesian feedback transmitter operational diagram (created by the author)

Conversely, while using quadrature modulation, one must ensure the linearity of the amplifier within the variation range of the signal amplitude. Nevertheless, it is the quadrature modulation and, accordingly, the Cartesian feedback transmitters that are more common in practice. This is mainly because quadrature modulation allows for more efficient use of the frequency spectrum.

The simplified schematic diagram of the Cartesian feedback transmitter is shown in Figure 1.7. In this case, the signal is not divided into amplitude and phase components, but into in-phase and quadrature components (commonly referred to as I and Q, respectively). This means that one can dispense with difficult-to-implement phase-locked loops in the transmitter, achieving the necessary modulation using a combination of I and Q signals. Unlike polar form components, IQ is characterized by the fact that both the in-phase and quadrature components of the signal have a similar bandwidth (Dawson & Lee, 2004; Katz et al., 2016).

Figure 1.7 shows a transmitter whose input is a combination of I and Q signals. The phase and quadrature signal components are fed to the inputs of the differential amplifiers, where they are compared to the output signals. The resulting error signal is modulated using a quadrature RF modulator. The signal is amplified by a power amplifier. A portion of the signal is coupled to the feedback circuit, where it is decomposed into I and Q components using a feedback demodulator. The signals are amplified if necessary and fed back to the input. A phase change circuit is placed between the input and feedback quadrature RF oscillators to provide a phase shift for synchronous signal modulation and demodulation. This circuit is required to ensure transmitter stability. The Cartesian feedback scheme is relatively easy to implement and offers both amplitude and phase control without the use of complicated broadband phase-locked loops. This is one of the reasons why it is the quadrature modulation amplifiers that have become classical and the most widely applied and researched.

The accuracy of system operation is limited by the parameters of the feedback circuit: the total circuit delay and the integrity of the demodulator. Researchers proposed a method for compensating errors in the demodulator circuit (Faulkner & Briffa, 1998) and investigated the stability conditions of the Cartesian circuit (Faulkner & Briffa, 1996). The study provides a detailed analysis of the Cartesian feedback circuit stability conditions, as well as recommendations for transmitter design. Phase shift circuit correction methods were also investigated (Faulkner, 2000). As mentioned earlier, one of the main advantages of a polar transmitter is its higher power efficiency due to the use of constant amplitude linearization. Attempts have been made to adapt the modulated power source to the Cartesian transmitter, thus increasing its power efficiency (Briffa & Faulkner, 1993). A hybrid Cartesian and feedforward linearization circuit has been proposed to reduce the effects of noise in the feedback circuit (J. Li et al., 2018). A similar hybrid was also described (Ock et al., 2015). Much attention has been paid to the

integrated implementation of the Cartesian transmitter using CMOS, for example, by Fakhrutdinov et al. (2020) and J. Li et al. (2017, 2018).

Table 1.2 presents the results obtained by the feedback linearization methods. The data was selected based on the date of publication (publication made no earlier than 2010), the feedback used, the results achieved, and the completeness of the description of the results. Table 1.2 contains both fully integrated and discrete power amplifier implementations.

The highest achieved PAE was 28%. In this work, the authors propose an integrated feedback amplifier with a reduced overall group delay, which is achieved by applying feedback only to the last stage of the amplifier. The feedback is implemented using separate circuits: a differential amplifier for phase distortions and a transconductance modulation amplifier to compensate for amplitude distortions. The phase feedback circuit maintains the phase difference between the input and output constant by regulating the gate voltages of the transistors. The amplitude feedback regulates the operating point of the transistors and, thus, maintains a constant gain. The authors propose this method as an alternative to Cartesian and polar feedback because it does not require an oscillator and can work with signals at the RF frequency without the need to transfer them back to the baseband. The authors managed to obtain a −40 dBc adjacent channel leakage ratio.

Table 1.3. Feedback method results (created by the author)

Source	Output Power, dBm	Efficiency, %	ACLR (lowest), dBc	Carrier Frequency, MHz	Bandwidth, MHz
(Ishihara et al., 2010)	15	13.2	−38.4	2000	10
(Kousai et al., 2012)	27.1	28 (PAE)	−40	1880	5
(Ock et al., 2015)	16.6	N/A	−33.8	2400	1.4
(J. Li et al., 2017)	14.1	N/A	−35	2	2
(J. Li et al., 2019)	21.4	22.3	−49	10000	4

The highest value of side harmonics attenuation (−49 dBc), which also meets the goal set in sub-6 GHz 5G networks, was achieved using Cartesian feedback. In this work, in addition to the standard feedback, a reference signal path is used, which subtracts the main signal from the feedback signal, thus leaving only the

distortions generated by the amplifier. In this way, the authors partially solve the dilemma of the feedback signal power: a higher feedback signal power results in larger nonlinear distortions in the feedback, and a lower signal value results in a decrease in the signal-to-noise ratio. A reference signal suppresses the power of the feedback signal by subtracting the unnecessary part from it, leaving only the necessary information about the distortions generated by the main amplifier.

1.2.3. Predistortion

The concept of the predistortion linearization, which is similar to every great scientific idea, is simple to understand: an inverse transmission characteristic circuit, receiving an undistorted signal at the output, is connected to an amplifier with a nonlinear transmission characteristic, as shown in Figure 1.8. For a long time, this method coexisted with the feedforward and feedback methods but saw very limited application. As far as can be deduced from the records, the active research of predistortion methodologies began in the 1980s (Bateman et al., 1988; Holz, 1984; Lenz, 1981; Stewart & Tusuriba, 1988). Many research papers at that time investigated analog predistortion circuits, but with the rapid development of digital processors, more and more attention was paid to digital predistortion methods (Faulkner et al., 1990; Feher, 1989). Finally, today, digital predistortion is arguably the most popular and widely studied linearization method.

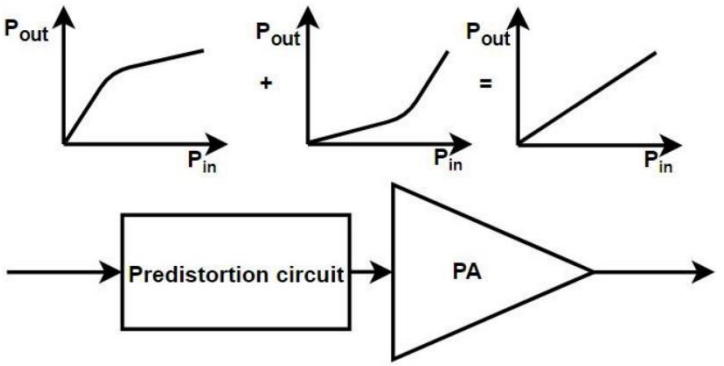

Fig. 1.8. Predistortion linearization conceptual diagram (created by the author)

Together with the relatively simple implementation, the main advantage of predistortion is that it potentially allows compensation for nonlinear distortions in the entire signal bandwidth, as it, ideally, completely compensates for the nonlinearity of the amplifier under any operating conditions. Usually, it is practically impossible to achieve full compensation of nonlinearity. In reality, the optimal

relationship must be found between the implementation complexity and the obtained linearity performance. The arising difficulties become apparent from a more detailed examination of the method's operation. Predistortion challenges can be split into two main research topics: the creation of an accurate power amplifier model and the design of the circuit with the required transmission characteristic. The easiest solution is to measure the transmission characteristic of the power amplifier under the selected operating conditions and design a compensating analog circuit accordingly. In the simplest case, this compensating analog circuit is a Schottky diode (Sun et al., 1999; Yamauchi et al., 1996) connected in series to the circuit, setting its operating point so that the nonlinear signal distortions generated by this diode compensate for the distortions generated by the power amplifier. This is an almost cost-free solution, but it can provide only limited compensation: an improvement by several dB ACLR at most. As in the case described above, the natural drift of the power amplifier parameters changes the form of its transmission characteristic. To achieve better results in nonlinear distortion suppression, adaptive predistortion methods are used, similar to the case of feedforward.

The simplest way to implement the adaptation algorithm is by working with a digital signal form. Consequently, more sophisticated algorithms, which are impractical to implement in analog, can be used in the digital domain. This has led to the widespread use of digital adaptation algorithms. Figure 1.9 (adapted from Braithwaite (2011)) shows an operational diagram of an adaptive digital predistortion transmitter. In the general case, the sampling of the analog signal $x(t)$ can be included in the scheme, but in this case, it was omitted from consideration. The input signal $x(n)$ is fed to the DPD and coefficient estimation blocks. Depending on the adaptation algorithm used, only $x(n)$ or $x_{\mathrm{DPD}}(n)$ input signals may be fed to the coefficient estimation circuit. The distorted signal is then transferred to a digital-to-RF converter, after which the signal is fed to the power amplifier. Part of the output signal is demodulated, digitized, and transmitted to a coefficient estimation circuit, which changes the DPD coefficients according to the difference between the received input and output signals.

The presented circuit and its variants have become the most widely used methods of linearization. The success of adaptive DPD is explained by the fact that, when using adaptive digital predistortion models, it is possible to achieve the linearity parameters of the feedforward while having self-regulation properties similar to feedback circuits. Additionally, in the case of DPD, the stability problem that arises in the case of feedback linearization does not have to be solved. The change of the predistortion circuit is relatively slow compared to the signal envelope change and depends on the rate of change of circuit working conditions.

The feedback used by DPD allows the predistortion circuit to be adapted depending on the change in operating conditions. Energy-efficient and fast processors available today allow for extremely accurate models to be calculated and, therefore, to significantly reduce nonlinear distortions. New challenges arise together with the benefits offered. The main DPD problems can be classified into the following groups: accuracy of analog/RF components in the transmission and feedback paths, data converters (ADC and DAC), digital hardware for transmission characteristic generation, and algorithms for controlling that hardware. These problems have been extensively reviewed by Braithwaite (2011) and Wood (2017), so the discussion will be brief.

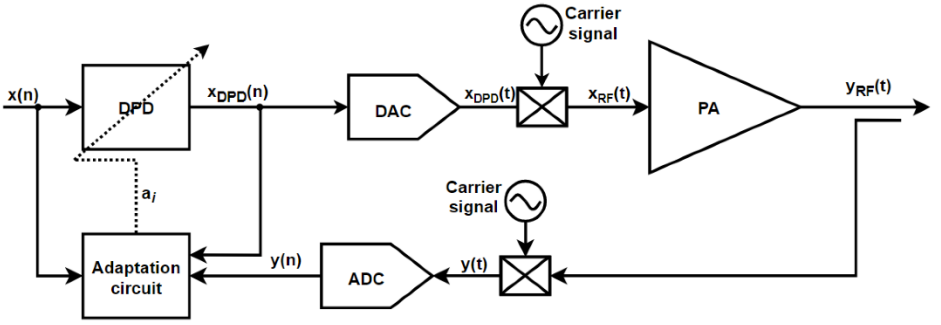

Fig. 1.9. Adaptive predistortion linearization operational diagram (created by the author)

When addressing the DPD architecture, the investigation must focus on the adaptation and/or learning system, which will meet the requirements of a particular task. Depending on whether amplifiers with memory are modeled (i.e., when the output signal value depends on both current and past input signal values) or without it (signal output value depends only on the current input value), several DPD training algorithms have been described in the literature. One of the earliest adaptive digital linearization methods for memoryless amplifiers has been described by Cavers (1990). These kinds of methods are applicable when working with relatively low-power amplifiers. However, when considering high-power amplifiers, memory effects occur and have a significant effect on the linearization results. Therefore, the most commonly used implementations include algorithms of direct (Beltagy et al., 2019; Zhou & DeBrunner, 2007) and indirect (Ding et al., 2002; Eun & Powers, 1997; Yu et al., 2019) training, all of which evaluate the memory effects of the amplifier. An overview of other, less commonly used methods is provided in (Psaltis et al., 1988). Structural diagrams of indirect and direct learning algorithms are presented in Figure 1.10 (adapted from Zhou & DeBrunner (2007)).

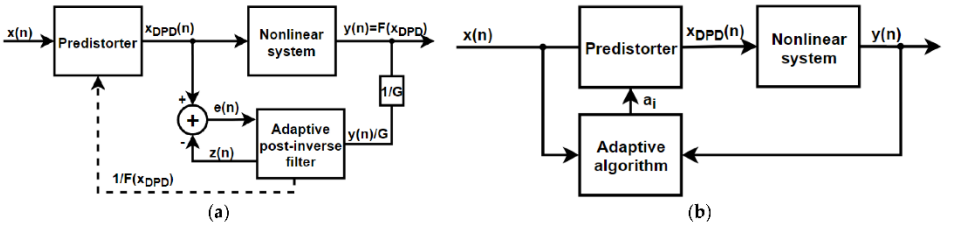

Fig. 1.10. (a) Indirect learning architecture, (b) direct learning architecture (created by the author)

Using an indirect learning architecture allows for obtaining the inverse transfer characteristic of a nonlinear system. Signal $x(n)$ is fed to the control system (in the studied case, the predistorter circuit), which is identical to the adaptive post-inverse filter in the observation path. The resulting signal $x_{\mathrm{DPD}}(n)$ is fed to the input of the nonlinear system and to the comparator. Normalized nonlinear system output $\frac{y(n)}{G}$ is fed to the post-inverse filter, whose output $z(n)$ is then compared to the predistorter's output $x_{\mathrm{DPD}}(n)$. Convergence is reached when the error signal $e(n)$ is equal to 0, i.e., $x_{\mathrm{DPD}}(n) = z(n)$. This ensures that the inverse transfer function is obtained in the adaptive post-inverse filter, and the output of the nonlinear system $y(n) = G \times x(n)$. Indirect learning can be applied to power amplifier linearization. In the literature, the resulting circuit is called a *self-tuning regulator* (STR), as shown in Figure 1.11. It should be noted that there are two versions of STR in the literature: the first evaluates an amplifier's transfer characteristic by comparing its input and output signals and then inverts it to use as a DPD function. However, in the case of amplifiers with significant memory effects, the inversion operation can be difficult to implement. The second STR version is based on an indirect learning architecture and needs no additional inversion operation. Its implementation is shown in Figure 1.11. The post-distortion module is added, whose input is PA's output signal $y(n)$. This module adapts the variable nonlinear function $G[y(n)]$ to achieve $G[y(n)] = z(n) = x_{DPD}(n)$. When convergence is achieved, the resulting function $G[y(n)]$ will be the inverted power amplifier transfer function and can be used as a DPD function. Although this method solves the inversion problem, other problems arise: the inverse function G is undefined in the amplifier saturation region, and the comparison $G[y(n)] = x_{DPD}(n)$ requires a higher bandwidth than when comparing it to the input signal $x(n)$, since the DPD algorithm extends the $x(n)$ spectrum by adding higher frequency components to it (Braithwaite, 2011).

Different from indirect, the direct learning method compares the output signal $y(n)$ with the input signal $x(n)$. In this case, the adaptive algorithm tries to reach the condition when $y(n) = x(n)$ by changing the values of the coefficients a_i (Fig. 1.10 **(b)**). In this case, a function inversion is not required either. Direct learning greatly reduces the complexity of the modeling systems with memory, as there is no need to use an additional post-distortion module. The implementation of this architecture for power amplifier linearization is called a *model reference adaptive system* (MRAS). A block diagram of MRAS is shown in Figure 1.12. The main disadvantage of this structure is that it is suitable for use only when the nonlinearity of $y(t)$ is relatively small, because the adaptation algorithm uses a first-order approximation (Braithwaite, 2011).

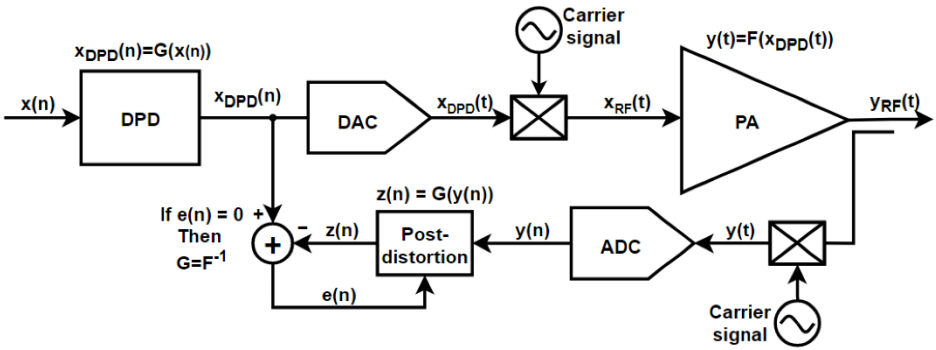

Fig. 1.11. STR transmitter (created by the author)

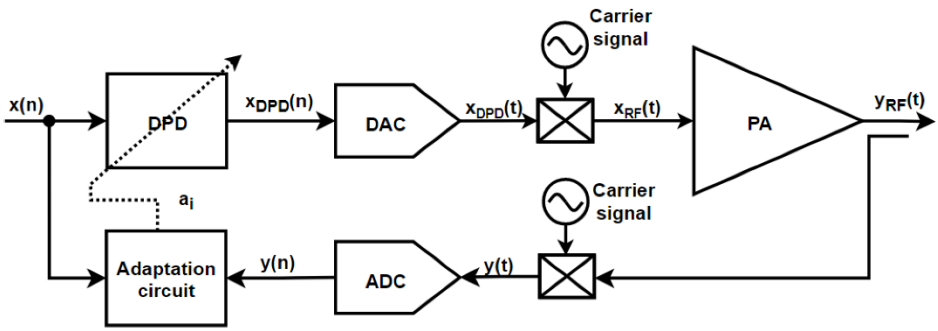

Fig. 1.12. MRAS transmitter (created by the author)

A hybrid of these algorithms is possible, the block diagram of which is shown in Figure 1.13. In this case, both STR and MRAS linearization methods are used

to mitigate the deficiencies of both. STR linearization compensates for most of the nonlinear distortions, while MRAS corrects those small distortions due to memory effects that STR failed to linearize. Because both systems work with different datasets (MRAS with $x(n)$ and $y(n)$ and STR with $x_{STR}(n)$ and $y(n)$), stability problems do not arise in such structures. STR correction factors are independent of MRAS correction, and MRAS correction follows STR factor correction (Braithwaite, 2011).

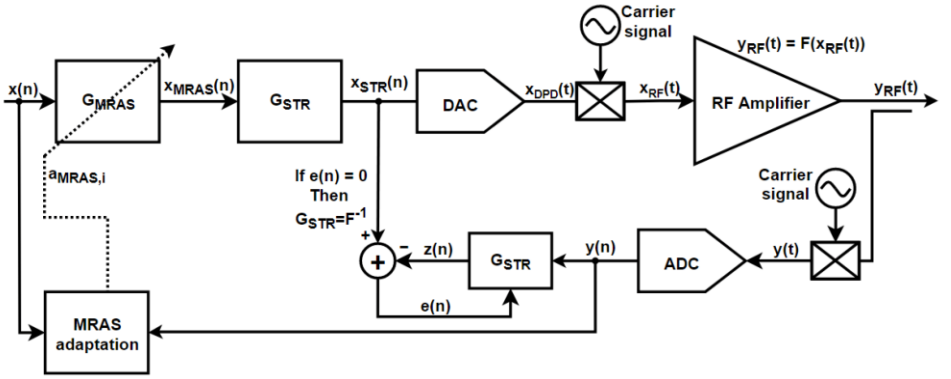

Fig. 1.13. MRAS-STR transmitter (created by the author)

Another important question for DPD is the mathematical apparatus chosen for amplifier modeling. Here, a dilemma arises: in general, the more detailed (and at the same time more accurate) mathematical model is chosen, the more time and energy it will take to calculate this model, thus reducing the energy efficiency and increasing the hardware cost. Furthermore, depending on the mathematical model used, the predistortion block adds additional spectral components to the input signal that extend the spectral width of the input signal up to seven times (Wood, 2017). This means that to avoid aliasing, the predistorted input and distorted output signals must be sampled several times at the Nyquist sampling rate. For this reason, the sampling rates of modern DPD systems range from a few hundred MS/s to several GS/s.

The simplest known modeling method is a look-up table. The table stores the inverted values of the amplifier's AM/AM and AM/PM characteristics. When using adaptive DPD, the table values change according to a change in operational conditions. The change occurs after gathering a set of the output signal values of the amplifier. To increase the accuracy, every value is sampled a certain number of times. Subsequently, the average of every set is taken and inverted. In this way, every input signal value is paired with a corresponding averaged and inverted predistorter value, generating a table of values. The most common types of LUT methods are described in (Muhonen et al., 2000). A simple look-up table does not

allow for evaluating the effects of the amplifier's memory effects. It is most commonly used where nonlinear distortions are relatively small. Although there are ways to apply infinite impulse response filters in look-up table system feedback, they can also be applied to the linearization of amplifiers with memory (Gilabert et al., 2008).

In applications where high precision is required, polynomial approximation of a nonlinear system is used. In modeling systems without memory, the polynomial given in (1.4) is often used. More complex models are needed when evaluating memory effects. The so-called Volterra series was described in the second half of the last century (Benedetto et al., 1979). This is a general mathematical model for describing nonlinear systems. Using Volterra (or any other) polynomial approximation, one attempts to interpolate the collected samples of discrete (in the studied case, power amplifier output) values to get a mathematical approximation of the power amplifier transfer function. The accuracy of the approximation depends on the chosen model, the degree of the polynomials, and, in the Volterra series case, the depth of memory. It is important to choose the correct degree of the polynomial. The problem with the Volterra series is that when the order of the polynomial and the depth of its memory grow, the number of computations increases exponentially (Ding, 2004). This makes the application of the Volterra series impractical in real-time systems. To solve this problem, a series of simplifications for the Volterra series have been proposed that sacrifice part of the accuracy but propose a significant reduction in the number of calculated coefficients. The best known and most widely used simplifications are the Wiener model, the Hammerstein model, the Wiener–Hammerstein model, the memory polynomial model, and the general memory polynomial model. A detailed description of the mathematical apparatus of these models can be found in the research by Morgan et al. (2006). Many additional behavioral models have been described by Ghannouchi et al. (2015a).

As mentioned above, the signal spectrum expands when using DPD linearization. Depending on the frequency of the signal used, the ADC and DAC speeds must follow suit to satisfy the Nyquist requirement. For high-frequency input signals, the ADC and DAC energy consumption increases significantly. To avoid aliasing, the input signal requires oversampling three to seven times. The exact value of oversampling depends on the order of nonlinearity that is compensated for in the predistortion circuit. A higher oversampling value allows for the compensation of the higher nonlinearity order. For example, a 20 MHz single-carrier LTE signal expands to 60 MHz–140 MHz. This means that ADC/DAC with a sampling frequency of 280 MHz is required to linearize the 20 MHz signal (Wood, 2017). In the case of a 100 MHz LTE-A signal (Ghosh et al., 2010), the signal spectrum expands up to 500 MHz–700 MHz and requires converters with speeds from 1 GS/s to 1.4 GS/s (Hu & Boumaiza, 2016). The power consumption

of these converters becomes a major barrier to higher efficiency, especially when one considers lower-power wireless transmitters as opposed to base station deployments. Along with high sampling frequencies, the ADC and DAC have stringent requirements for accuracy and spectral efficiency. For example, for a GSM mask, the spurious-free dynamic range of the converters utilized must be -86 dBc (Wood, 2017). Higher accuracy always requires additional cost and reduces the efficiency of DPD implementations in relatively low-power and low-cost applications.

When it comes to the analog/RF architecture of a DPD transmitter, one of the key issues is the choice between a real-IF and a complex-IF signal architecture. Architectures with two parallel mixers, driven using the same local oscillator whose phase is offset by 90° to one of them, are considered to be complex-IF. A single mixer architecture is considered to be real-IF. Today, one of the most common solutions is a complex-IF transmitter and a real-IF observer receiver (although there are also cases of complex-IF observer receivers) (Wood, 2017). An operational diagram of such a structure is shown in Figure 1.14.

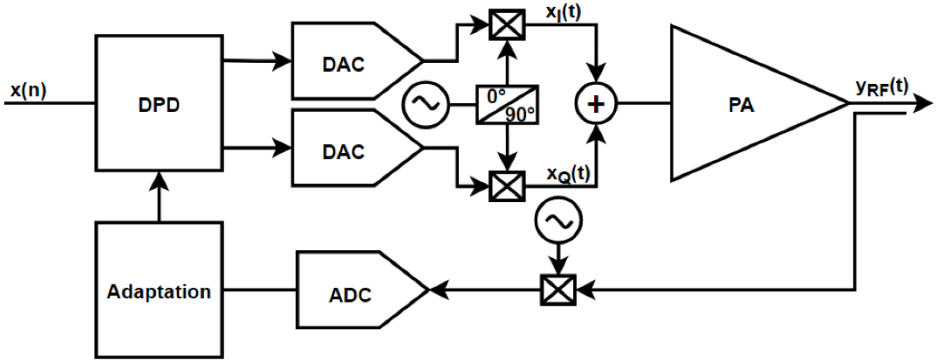

Fig. 1.14. Mixed complex/real transmitter (created by the author)

The complex-IF signal architecture offers a higher bandwidth and several other advantages, but, as may be seen in Figure 1.14, requires two separate DACs and a quadrature modulator for its implementation. There are also distortions due to the imbalance of the I and Q components, which are frequency-dependent and cause problems in broadband signals. Transmission characteristic distortions due to errors in DAC, modulators, and filters are ultimately compensated by the DPD. So, from this viewpoint, it is only essential to ensure the required bandwidth of the circuit. The situation is quite different in the observer receiver circuit. The distortions created here are inseparable from the distortions created by the power amplifier. For this reason, the DPD circuit adds unnecessary signal components

that are not related to the errors generated by the power amplifier. The ADC and the entire observer circuit should be the most accurate part of the transmitter, should not have any memory effects, and should exceed the accuracy of all other components of the circuit by at least 10 dB (Wood, 2017). Such components are quite expensive, which is one of the reasons for the popularity of the real-IF observer receiver architecture.

Table 1.3 presents the results of research on predistortion linearization over the past decade. This is not a full list, as it is impossible to list all the results achieved. In selecting the data, the authors deliberately tried to select studies from different applications, so that it may be possible to evaluate broad application opportunities, as well as blind spots.

Table 1.4. Predistortion method results (created by the author)

Source	Output Power, dBm	PAE, %	ACLR (lowest), dBc	Carrier Frequency, MHz	Bandwidth, MHz
(Bondar et al., 2010)	15	51	−42	880	0.2
(Gilabert et al., 2020)	26.3	18.7 (η)	−40	900	200
(Tian et al., 2015)	37.5	45	−48.1	1890	40
(Jung et al., 2013)	23.3	8	−43.5	1950	5
(Wang et al., 2017)	46	34.6	−40	2140	20
(Wolf et al., 2016)	35	29.8	−45.9	2650	16
(Rostomyan et al., 2018)	16.4	15.2	−28.8	15000	200
(Ali et al., 2019)	9.8	18.2	−30	28000	340
(Tsai et al., 2011)	7	N/A	−21*	60000	5

The predistortion method has a wider application than any other linearization method discussed. Predistortion is applied at carrier frequencies from less than 1 GHz to more than 60 GHz. The range of linearized power stretches from 7 dBm to 46 dBm. Linearized channel bandwidths are from less than 1 MHz to 200–300 MHz. These operational ranges arise from the data collected. It should be noted that these are not the only possible ranges of values, since predistortion

techniques can and are applied at other operational conditions. This demonstrates the versatility and universal character of predistortion linearization. The lower the frequencies used, and the higher the power, the more efficient and frequent is the use of digital linearization. In cases where low-power amplifiers are used, digital linearization becomes too expensive, and analog predistortion linearization is used. In higher carrier frequencies and wider channels, there is also still a tendency toward analog solutions, although there are exceptions(Gilabert et al., 2020). Predistortion linearization is a go-to technique when it comes to traveling wave tube (TWT) amplifiers, which are used in satellite communications (Bremenson et al., 1980; Bremenson & Lombard, 1975; Whartenby & Wolkstein, 1985).

1.2.4. Summary on Linearization Methods

Looking at the dynamics of today's linearization research, it is safe to say that predistortion in general, and DPD in particular, is and, due to its versatility, will be the most widely used linearization technique in the near future. Ongoing research on learning architectures and approximation algorithms, and development of faster and more efficient ADCs, DACs, and digital processors, make DPD an increasingly attractive linearization technique. However, this still does not facilitate the discussion about the redundancy of other methodologies. Predistortion now faces a big problem: low-power and/or battery-powered transmitters. On the one hand, digital predistortion is (or at least will be in the very near future) a methodology that requires excessive energy consumption, especially when it comes to broadband standards such as LTE-A. On the other hand, the level of linearization proposed by analog predistortion is often insufficient to meet the 3GPP standard requirement of −45 dBc radiated to other channels. Feedforward is unlikely to be superior in this respect to DPD, as the need for additional active elements at low power again greatly reduces efficiency. Thus, feedback remains, which is a good option for applications where the required channel bandwidths do not exceed 5–10 MHz. On the other hand, other linearization techniques have already been proposed, such as generating part of the fundamental power with a more linear amplifier (Hu & Boumaiza, 2016). There is a whole series of studies, for example (Bulusu et al., 2014; H. Li et al., 2011; Zayani et al., 2019), trying to reduce the so-called Crest factor, which aims to substantially relax the requirements for amplifier linearity.

Currently, at higher powers (base station level), according to the data collected, feedforward can still compete with DPD; this can be seen by comparing the data in Table 1.1 and Table 1.3. From this data, one can conclude that feedforward can meet and exceed the −45 dBc ACLR requirement. Adaptive feedforward often is a viable alternative to DPD in the case of working with broadband signals, since DPD also faces the problem of expensive ADC and DAC converters

at high frequencies. Other research directions include attempts to combine analog RF linearization with lower frequency DPD linearization (Gumber & Rawat, 2017; Xie et al., 2018). Additionally, one of the main hurdles in 5G networks should be introduced – MIMO (multiple input multiple output) and mMIMO (massive MIMO) (S. Yang & Hanzo, 2015). These systems present additional challenges for amplifier linearization: additional transmission channels and parasitic interactions between them. To the best of the authors' knowledge, currently, the main method of linearization in these systems is DPD (X. Liu et al., 2020). This further encourages the research and development of all components that comprise a DPD system, from the hardware used to the mathematical models and algorithms implemented.

Digital predistortion is a predominantly researched linearization method to date. Not only that, but it is also the most versatile, with the widest range of applications. As mentioned above, DPD design tasks may be split into two broad categories: a replication of PA's transfer characteristic (i.e., creating a model of a PA) and a design of the DPD transmitter circuit. This dissertation will be focused on the former category.

Replicating PA's transfer characteristic is commonly achieved using behavioral modeling. There are quite a few modeling approaches: Volterra, Memory Polynomial, General Memory Polynomial, Wiener, Hammerstein, Wiener-Hammerstein, etc. All of them differ in the mathematical form but are similar in the aspect that the resulting model is generally applicable only to conditions under which it was extracted. In the context of PA modeling, extraction conditions include: natural parameters, such as the temperature at which measurements were taken; the form of the excitation signal used. Generally, in lower power applications, it is not practical to include adaptive coefficient estimation into the operation of the transmission circuit. Therefore, more versatile behavioral modeling approaches are desired.

1.3. Behavioral Modeling

A PA model needed for DPD linearization can be extracted in several different ways. Three modeling methods are known in the literature: physical, equivalent, and behavioral (Steve C. Cripps, 2006). Physical models are built using device physics and fabrication geometries. Equivalent models translate device physics into analogous circuit elements. Behavioral models use abstract equations to fit the device's input and output measurements.

Equivalent or physics-based PA models attempt to describe device behavior using semiconductor physics and circuit-level representations. Although such

models offer strong predictive capabilities across a wide range of operating conditions, they are typically computationally expensive and require detailed knowledge of device parameters. This complexity limits their applicability in real-time digital transmitters, where computational efficiency is a critical requirement.

Behavioral modeling provides an effective alternative by representing the PA as a black-box system whose behavior is inferred directly from measured input–output data. By focusing on reproducing the externally observable characteristics of the PA rather than its internal physical structure, behavioral models achieve a balance between accuracy and computational complexity. This makes them particularly well-suited for DPD applications, where models must be trained efficiently, updated as operating conditions change, and executed in real time on digital hardware platforms.

Some behavioral modeling techniques were mentioned in the section about DPD linearization, including Volterra series–based models and their simplified variants. While the Volterra framework offers a theoretically complete description of nonlinear systems with memory, its practical use is limited by the rapid growth in the number of parameters. As a result, reduced-complexity structures such as the memory polynomial and generalized memory polynomial models have become widely adopted. These models retain the essential nonlinear and memory effects relevant to RF PAs while enabling efficient coefficient estimation through linear parameter formulations.

The accuracy of a behavioral model is inherently tied to the operating conditions under which the model is identified. Behavioral models are typically extracted for specific signal characteristics and operational conditions. While this specialization enables high accuracy within the trained region, it also limits the model's predictive capability outside those conditions. Understanding and addressing this trade-off between accuracy and generalization is a central challenge in behavioral modeling and forms a key motivation for the work presented in this thesis.

Key operating conditions influencing PA behavior include input power level, modulation format, signal bandwidth, peak-to-average power ratio, temperature, supply voltage, and carrier frequency. Variations in these parameters alter the effective nonlinearities and memory effects exhibited by the PA, leading to model mismatch. In the context of DPD, such a mismatch manifests as reduced linearization performance, increased spectral regrowth, and degraded error vector magnitude, often necessitating frequent model retraining or adaptation.

This operating-condition dependence presents a challenge for practical transmitter systems, particularly in modern wireless standards that demand flexibility and dynamic reconfiguration. Frequent model updates increase system complexity, computational load, and calibration time. Consequently, there is strong motivation to develop behavioral modeling techniques that can generalize across a

broader range of operating conditions while preserving the simplicity and efficiency required for real-time implementation. Among the various parameters affecting model validity, carrier frequency variation is especially critical and forms a central focus of this dissertation.

This dissertation aims to specifically investigate the effect of carrier-frequency variation on behavioral model accuracy and propose a model that can operate across a wide range of frequencies. It is universally acknowledged that a change in carrier frequency has a significant impact on the PA model accuracy. Research trying to account for these effects (J. Liu et al., 2004; Zhao et al., 2017) is conducted. Authors (Zhao et al., 2017) proposed a Time Delay Neural Network Model, which is trained on baseband data from several carrier frequencies. Earlier modeling approaches were also focused on data collection across different carrier frequencies (Launay et al., 2002). But the increase in model training data increases the model's computational complexity. In very low power applications, such as Narrow Band Internet of Things or Low Power Wide Area Network, the priority will always be with lower complexity. To use digital linearization methods in these applications, ways must be found to simplify the model calculations and/or extend their usability beyond the range at which they were extracted.

Although many PA architectures are designed to operate over wide frequency ranges, their electrical characteristics are shaped by frequency-dependent effects such as matching network responses, device parasitics, bias circuitry, and package-level resonances. These factors result in variations in gain, phase response, nonlinear distortion, and memory effects as the carrier frequency changes, even when all other operating conditions remain constant.

From a behavioral modeling perspective, carrier-frequency variation introduces a systematic change in the PA input–output relationship. A model extracted at one frequency may no longer accurately capture the amplifier behavior at another, leading to increased modeling error and reduced linearization performance when used in DPD systems. Conventional behavioral models are typically extracted and optimized for a fixed carrier frequency, limiting their usefulness in frequency-agile systems.

Modern wireless communication standards increasingly rely on flexible spectrum usage, including dynamic spectrum allocation, carrier aggregation, and multi-band operation. In such scenarios, frequent switching of carrier frequency is required, making repeated model extraction impractical due to measurement time, computational cost, and system downtime. These constraints motivate the development of behavioral modeling techniques capable of generalizing across a range of carrier frequencies, enabling accurate PA characterization and linearization over a wide operating band without the need for exhaustive retraining at every frequency point.

1.4. Conclusions of the First Chapter and Formulation of the Dissertation Tasks

1. Power amplifier linearization techniques can be broadly separated into three groups: feedforward, feedback, and predistortion. To date, the predominant and most useful method of linearization is digital predistortion.

2. Digital predistortion linearization uses a mathematical model of the amplifier. The model is usually extracted using the behavioral modeling characterization technique.

3. The main drawback of the behavioral modeling is its accuracy only under the conditions that are similar to those under which it was extracted. Specifically, the model extracted at one carrier frequency cannot be applied to another carrier frequency without losing accuracy.

The following hypothesis is being tested:

- The frequency-dependent modeling error can be determined by characterizing the power amplifier with the same excitation signal across a range of carrier frequencies. The resulting error can be reduced by applying a form of model parametrization.

The following tasks should be completed to conduct this research:

1. To develop a characterization system that allows the collection of excitation and response data sets for power amplifier modeling.
2. To investigate and propose metrics for power amplifier modeling error caused by carrier frequency variation.
3. To examine experimentally the impact of excitation signal characteristics on power amplifier modeling error caused by carrier frequency variation.
4. To propose methods for reducing power amplifier response modeling error caused by carrier frequency variation.

2

Methodology for Power Amplifier Behavioral Model Extraction

This chapter investigates behavioral model extraction for power amplifiers. It introduces a dedicated measurement setup and describes the development of automated measurement setup. Particular attention is given to practical challenges in configuration and synchronization, which are analyzed in detail. The chapter also examines numerical procedures for model extraction and proposes a parametric modeling method. The results presented in this chapter were reported at the Institute of Radioelectronics of Riga Technical University (Borel, A. Power Amplifier Modeling and Linearization) and subsequently published in a journal article (Borel et al., 2025).

During the preparation of this thesis AI tools were used for translation and text clarity improvement.

2.1. Design of a Measurement Setup

As established earlier, some input excitation and the ability to capture the power amplifier's output response are needed to create a behavioral model of a power amplifier. Both requirements may be achieved using several different measurement devices and techniques. The exact measurement setup depends heavily on the type and order of modeled nonlinearities.

2.1.1. Design of the Excitation Signal

The order of a nonlinearity refers to a number k in the (2.1) series expansion.

$$y(t)=\sum_{k=1}^{K}a_k x^k(t), \tag{2.1}$$

here, $y(t)$ is the response, $x^k(t)$ – excitation and a_k – the weight of the corresponding series term. Attaining a behavioral model of a PA means solving (2.1) for a_k. The value of a_k is proportional to the amount of nonlinear distortion produced by the PA. The latter depends on an operating zone of the PA. Operating deep in the nonlinear zone, close to saturation, leads to higher nonlinear distortion and, consequently, higher a_k. To drive the PA deeper into the nonlinear operating zone, an excitation signal needs to have higher average power. Specific average power values depend on the modeled PA parameters, but the general conclusion is as follows: to model a higher order nonlinearity, the input excitation signal needs to have an appropriate average power level, which would drive the PA sufficiently deep into saturation. Sufficiently deep here means that, for example, if one desires to characterize 5th-order nonlinearity of the PA, they should ensure that $x(t)$ has high enough average power so that $x^5(t)$ would be discernible from the noise floor.

The second aspect of the excitation signal is its content. Say the excitation for (2.1) is a harmonic function $A\cos(\omega t)$, assuming 5th-order nonlinearity is modeled, thus K = 5 is substituted into equation (2.1):

$$y(t)=\sum_{k=1}^{5}a_k A^k cos^k(\omega t), \tag{2.2}$$

using trigonometric identities (2.2) can be rewritten as:

$$\begin{aligned} y(t)&=\left[a_1 A+\frac{3a_3A^3}{4}+\frac{10a_5A^5}{16}\right]\cos(\omega t)+\ldots \\ \ldots&+\frac{a_2A^2}{2}\cos(2\omega t)+\left[\frac{a_3A^3}{4}+\frac{5a_5A^5}{16}\right]\cos(3\omega t)+\ldots \\ \ldots&+\frac{a_4A^4}{8}\cos(4\omega t)+\frac{a_5A^5}{16}\cos(5\omega t)+\left(\frac{a_2A^2}{2}+\frac{3a_4A^4}{8}\right). \end{aligned} \tag{2.3}$$

From (2.3), it can be deduced that an exciting nonlinear PA with a single tone harmonic creates even and odd harmonics at frequencies $n\omega$ $(n=1,2,3...)$, a DC offset, and a gain compression at a fundamental frequency ω. In RF applications,

even and odd harmonics are sufficiently far away from a fundamental frequency and, generally, can be filtered out, just like a DC offset. Their evaluation is not as important as the behavior of the PA around fundamental frequency ω. Single tone test gives no information about PA behavior around the frequency ω and thus is generally insufficient for PA behavioral modeling applications.
To evaluate the impact of PA nonlinearity around fundamental frequency ω, a sum of two harmonic tones may be used:

$$x(t) = A_1 \cos(\omega_1 t) + A_2 \cos(\omega_2 t). \tag{2.4}$$

This time, assume $K = 3$.

$$\begin{aligned} y(t) &= \sum_{k=1}^{3} a_k (A_1 \cos(\omega_1 t) + A_2 \cos(\omega_2 t))^k = \dots \\ \dots &= a_1 \left(A_1 \cos(\omega_1 t) + A_2 \cos(\omega_2 t) \right) + \dots \\ \dots &+ a_2 (A_1 \cos(\omega_1 t) + A_2 \cos(\omega_2 t))^2 + \dots \\ \dots &+ a_3 \left(A_1 \cos(\omega_1 t) + A_2 \cos(\omega_2 t) \right)^3, \end{aligned} \tag{2.5}$$

opening brackets and applying some basic trigonometry gives:

$$\begin{aligned} y(t) &= a_1 \left[A_1 \cos(\omega_1 t) + A_2 \cos(\omega_2 t) \right] + \dots \\ \dots &+ a_2 \left[\frac{A_1^2 + A_2^2}{2} + \frac{A_1^2}{2} \cos(2\omega_1 t) + \frac{A_2^2}{2} \cos(2\omega_2 t) + A_1 A_2 \cos\left((\omega_1 - \omega_2) t \right) \right] + \dots \\ \dots &+ a_3 \left[\frac{3A_1^3}{4} \cos(\omega_1 t) + \frac{3A_2^3}{4} \cos(\omega_2 t) + \frac{A_1^3}{4} \cos(3\omega_1 t) + \dots \right. \\ \dots &+ \frac{A_2^3}{4} \cos(3\omega_2 t) + \frac{3A_1^2 A_2}{2} \left(\frac{\cos\left((2\omega_1 + \omega_2) t \right)}{2} + \frac{\cos\left((2\omega_1 - \omega_2) t \right)}{2} \right) + \dots \\ \dots &+ \left. \frac{3A_1 A_2^2}{2} \left(\frac{\cos\left((2\omega_2 + \omega_1) t \right)}{2} + \frac{\cos\left((2\omega_2 - \omega_1) t \right)}{2} \right) \right]. \end{aligned} \tag{2.6}$$

In addition, to gain compression, DC offset, even and odd harmonics (2.6) response demonstrates signal components with frequencies $\omega_1 \pm \omega_2$, $2\omega_1 \pm \omega_2$ and $2\omega_2 \pm \omega_1$. The frequencies of the original tones modulate each other; therefore, these components are referred to as *intermodulation distortions (IMD)*. Depending on the order of nonlinearity that causes them, they are numbered IMD_2, IMD_3, etc. Continuing (2.6) calculations for higher K values would produce

higher-order intermodulation components, such as IMD_4, IMD_5, and so on. In practice, however, IMD_3 products are of the utmost interest, since their impact on an amplifier's linearity is most notable. This is because IMD_3 products are too close to the fundamental frequencies to be filtered out. The presence of IMD_3 is degrading the overall accuracy of a modulation as well as causing signal leakage into adjacent channels.

Figure 2.1 shows an example of the nonlinearity effect on the transferred signal spectrum. The IMD_3 products $2\omega_1 - \omega_2$ and $2\omega_2 - \omega_1$, together with IMD_5 products $3\omega_1 - 2\omega_2$ and $3\omega_2 - 2\omega_1$ are creating regrowth of the original signal to adjacent frequency bands. A similar effect may be observed with a modulated signal. There are no effective ways of filtering these intermodulation products; the only way to mitigate their impact on signal quality is to use some sort of linearization technique on the PA. Measuring the power level of intermodulation products allows us to get an idea about nonlinear behavior around the fundamental frequency.

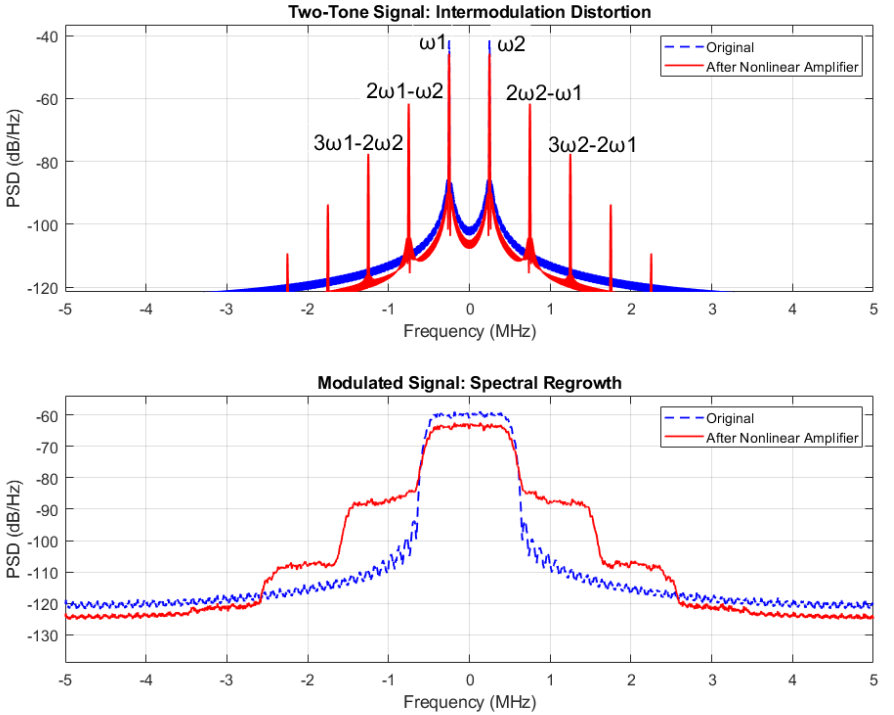

Fig. 2.1. Example of the nonlinearity effect on a two-tone signal and a modulated signal

The two-tone test described here is a viable way to get an estimation of the PA nonlinear behavior, and it may be conducted with basic equipment such as an arbitrary waveform generator and a spectrum analyzer.

Looking again at (2.1), it may be seen that the instantaneous value of the response depends only on the current instantaneous value of the excitation signal. This behavior type is referred to as a *static* or *memoryless* behavior. In addition to a static, a PA also displays a *dynamic* behavior. The dynamic behavior of a PA means that its instantaneous output value depends not only on the current, but also on the previous input values. In Section 1, it was referred to as the *memory effects* of an amplifier. To incorporate the dynamic behavior of a PA, more complex models than (2.1) are required; some of them were mentioned in Section 1.

The memory effects of power amplifiers originate from heating and cooling of a transistor junction and electrical effects in its biasing and matching networks (Ghannouchi et al., 2015b). To understand thermal memory effects, it should be noted that the gain and the phase shift introduced by the transistor amplifier are temperature dependent. The rise in junction temperature leads to a decrease in gain and phase shift, and vice versa: falling temperature leads to a gain and phase shift increase. The junction temperature follows the power envelope of the input signal. Signal power transition from low to high leads to junction temperature transition in the same direction. The same is true for the reverse case: signal power transition from high to low leads to a decrease in junction temperature. The problem here is the inertia of the junction temperature, which results in the trailing of the junction heating/cooling from the signal power rising/falling. This, in turn, means that the same signal power values will get amplified and phase shifted by different amounts depending on the current junction temperature, which itself is the result of previous signal power values: this is a memory effect by definition. Given the fact that junction temperature will change more slowly than the rate of change of the signal envelope, the thermal memory usually impacts lower frequency (below 1 MHz) signal components (Ghannouchi et al., 2015b).

Electrical memory effects are caused by varying envelope, fundamental, or second harmonic impedances at different modulation frequencies (Vuolevi et al., 2001). This can be understood by comparing the (2.1) model to the actual transistor amplifier. Equation 2.1 treats a transistor amplifier as a single-stage device, whose output directly corresponds to its input. Authors (Vuolevi et al., 2001) propose to model a PA as a two-stage device, where distortions created in the first stage are then transferred as an input to a second stage, where they become a cause of higher-order distortions. The nonlinearities may be viewed as a current source, which means that the shape of the voltage envelope is determined by the node impedances of the amplifier. These node impedances include matching network impedance, bias network impedance, and load impedance (Ghannouchi et al.,

2015b). These impedances exhibit frequency-dependent behavior. To limit impedance-related memory behavior of the amplifier, constant node impedances over the signal modulation range need to be ensured. The normalization of the signal impedance over a given frequency range becomes more difficult as the said range increases. This makes electrical memory effects more dominant in signals with modulation bandwidths exceeding 1−2 MHz.

One of the effects produced by the amplifier's memory is the asymmetry between positive and negative IMD_3 components. The magnitude of these components and the difference between them are reported to be dependent on the frequency spacing of the two tones in (2.4). This means that a two-tone test may indeed be used to quantify the memory effects of the amplifier.

A natural extension to the two-tone test is a multi-tone test, where the number of tones in (2.4) is increased depending on the needs of a characterization. Typically, a multi-tone test tries to estimate a PA response to a modulated signal. For this purpose, the overall bandwidth of a multi-tone signal is chosen to be similar to the bandwidth of the modulated signal. The number of tones is chosen according to a desired frequency resolution. The main difficulty in designing a multi-tone signal is choosing the magnitude and phase of the tones. Remley (2003) demonstrated that different tone magnitude and phase settings may overestimate or underestimate PA nonlinear behavior. The best results may be achieved if the multi-tone signal's PAPR and probability density function are closely matched to those of the wideband modulated signal.

A wideband modulated signal is defined as a signal whose bandwidth is significantly larger than the coherence bandwidth of the channel through which it is transmitted. A coherence bandwidth defines a range of frequencies over which the frequency-selective fading is approximately flat, meaning every frequency component is attenuated evenly. Wideband signal frequency components, therefore, are subjected to different attenuation values, which creates additional difficulties when modeling a PA response to such excitation. Even with most precautions taken, there will be some discrepancy between multi-tone characterization and the actual wideband modulated signal characterization results.

2.1.2. Design of the Physical Test Bench

To produce a digitally modulated signal, which would excite both static and dynamic PA behaviors, a Vector Signal Generator (VSG) can be used. Additionally, a basic spectrum analysis is insufficient in this case, since it provides information only about the magnitude of the response. Digital modulation schemes, such as QPSK and QAM, modulate the amplitude and the phase of the carrier. To successfully demodulate the information from a digitally modulated carrier, a Vector Signal Analyzer is the most convenient choice. Having that in mind, a structure

of the test bench is proposed in Figure 2.2. This structure is similar to those proposed earlier (Chang et al., 2024; X. Liu et al., 2024).

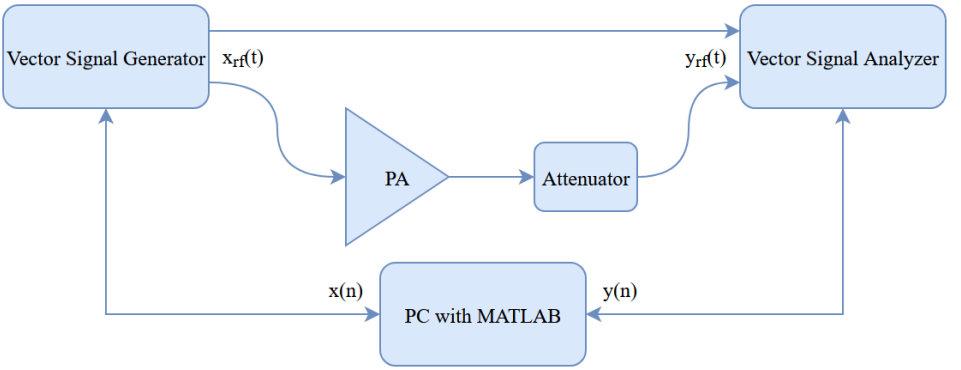

Fig. 2.2. Structure of the proposed test bench

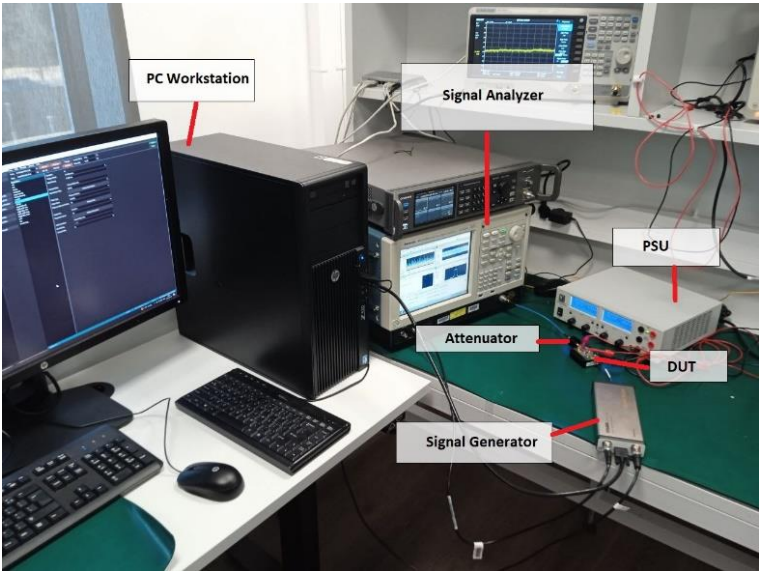

Fig. 2.3. Photo of the proposed test bench

The structure consists of a device under test (DUT) signal path and a direct signal path. SignalHound VSG60A is used for signal generation, and Tektronix RSA5106A is used for signal analysis. Both the VSG and VSA are connected to a PC running MATLAB software. For a given baseband excitation signal $x(n)$, multiple measurements are conducted while varying the carrier frequency of

$x_{RF}(t)$. The direct signal path from the VSG to the VSA allows for comparing baseband versions of $x_{RF}(t)$ and $y_{RF}(t)$, effectively comparing the amplifier's input and output. For each excitation signal $x(n)$, a set of signals is obtained:

$$x_{CF_1}(n), y_{CF_1}(n), x_{CF_2}(n), y_{CF_2}(n), \ldots x_{CF_l}(n), y_{CF_l}(n). \qquad (2.7)$$

The measured excitation and response signals are then used to extract the behavioral model of the PA. The attenuator in the signal path ensured that the VSA would not be damaged or run into saturation during measurements. Figure 2.3 demonstrates the physical measurement setup.

Several problems need to be addressed to accurately characterize a PA with this setup. First, the calibration of the power level accuracy: to know the exact power level at the input of the PA, VSG power level settings should be calibrated. The main reason for the discrepancy between the programmatically set VSG power level and the power that PA "sees" at its input is the losses at the interconnecting cables. Failing to account for these losses will lead to less accurate characterization of the PA response.

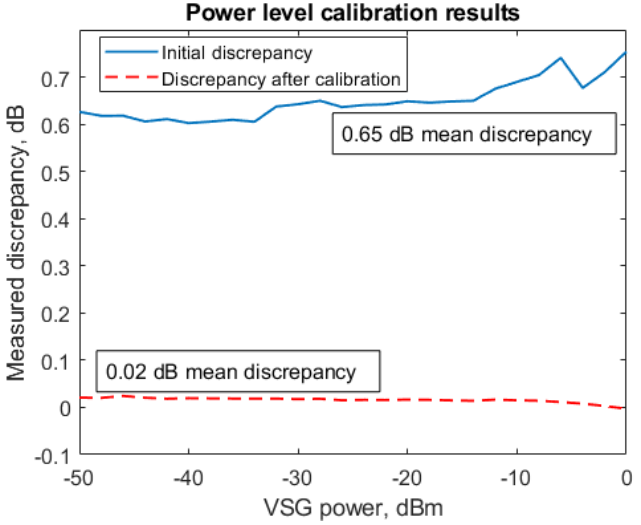

Fig. 2.4. VSG power-level calibration results

To mitigate the impact of the interconnecting cable losses, the VSG is connected directly to the RSA. A CW sweep with different average power levels is performed, measuring the received power for every case at the RSA. The discrepancy between the set VSG and measured VSA values is then saved to the PC memory. A second CW sweep is performed, considering the difference measured

the first time. For example, if the initial measurement has shown −1 dB discrepancy, during the calibration measurement, the VSG average power is increased by 1 dB compared to the nominal to compensate for it. The results of the calibration procedure are given in Figure 2.4. Before the calibration, the average measured discrepancy reached ~0.65 dB. Calibration lowers the average discrepancy to ~0.015 dB.

Measurements in Figure 2.4 are valid only for a single carrier frequency at which they were taken, because of the non-flat frequency response of the interconnecting cables. To ensure more accurate power settings at every frequency, the frequency calibration of the measurement setup is performed. First, the frequency sweep is performed in a desired frequency range. The attenuation values obtained are stored in a PC memory. Using these values, power compensation coefficients are calculated for every measured frequency value. The second frequency sweep is performed to check the results. This procedure allows for improving the flatness of the frequency response from ~0.8 dB over a 2−4 GHz range before calibration to ~0.06 dB after. The graph of the frequency response before and after the calibration is given in Figure 2.5.

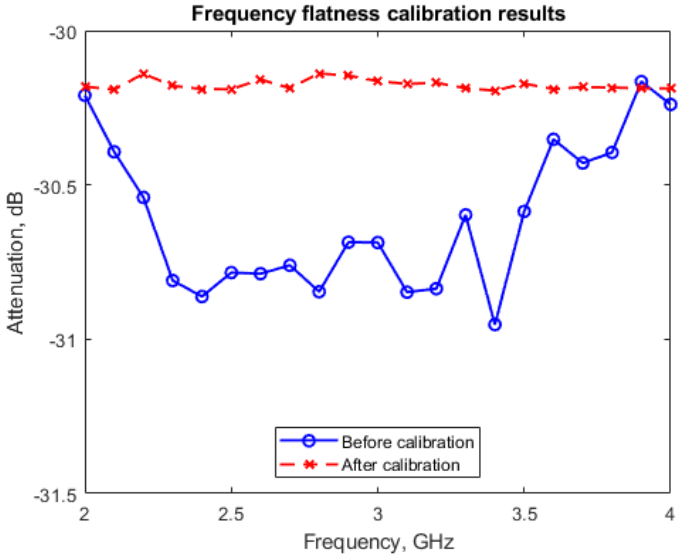

Fig. 2.5. Signal path frequency response flatness calibration results

Both calibrated results should be compared to the measurement accuracy of the instruments used. In the present case, both VSG and VSA have a ±0.5 dB amplitude uncertainty as reported by manufacturers, which determines the overall measurement uncertainty to ~±0.7 dB. In both cases, the measured discrepancy in

power level settings and the measured flatness over the frequency range are below this uncertainty. This means that there is no significant effect of the calibration on the measurement.

Another important aspect of the model extraction setup is the time delay compensation. The main reason for a time delay between excitation and response signals is the time it takes for a signal to propagate through a PA. In the proposed setup, the excitation and response signals are measured separately and are not time-aligned. Figure 2.6 shows the comparison between time delay compensated and non-compensated signal characteristics. It is evident that a time delay has a detrimental impact on the results of the characterization. An increase in time delay leads to an increase in AM/AM characteristics spread, similar to severe memory effects. This is because the time misaligned characterization process assigns the dependency of the output sample n on the input sample $n - t_d$, where t_d represents the time delay in samples, when there is no such dependency in reality.

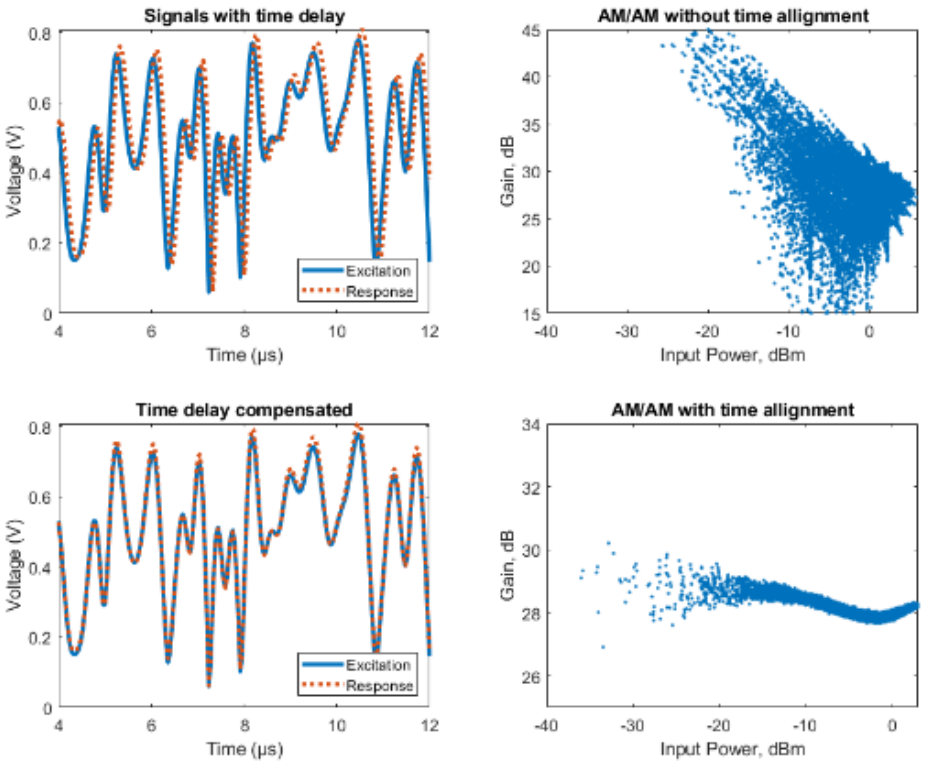

Fig. 2.6. Time delay impact between excitation and response signals

To estimate a delay between two signals, *x* and *y*, a cross-covariance between them may be calculated:

$$C_{xy}(d)=\begin{cases}\sum_{n=0}^{N-d-1}\left(x(n+d)-\bar{x}\right)\left(y^{*}(n)-\bar{y}^{*}\right) \text{ for } d\geq 0\\ \sum_{n=0}^{N-d-1}\left(x^{*}(n-d)-\bar{x}^{*}\right)\left(y(n)-\bar{y}\right) \text{ for } d<0\end{cases}, \tag{2.8}$$

here, N stands for number of samples of the two signals, x^{*} and y^{*} are the complex conjugates of the x, and y, $\bar{x}$ and $\bar{y}$ are the averages of the waveforms *x* and *y*, and are defined as:

$$\begin{cases}\bar{x}=\frac{1}{N}\sum_{n=0}^{N-1}x(n)\\ \bar{y}=\frac{1}{N}\sum_{n=0}^{N-1}y(n)\end{cases}. \tag{2.9}$$

(2.8–2.9) calculate a cross-covariance value for every possible delay value d in signal samples. Maximal cross-covariance corresponds to an actual delay value in samples. The resolution of the time delay is limited to a sample length in seconds, which is equal to the reciprocal of the sample rate. For example, for a sample rate of 20 MHz, the time resolution is equal to 50 ns. To get a better time resolution, signal oversampling may be used. It is also worth noting that (2.8) can be simplified by removing the subtraction of signal averages. In that case, cross-correlation can be calculated, which includes the DC component estimation.

To extract the actual signal power values from the measured data, a power adjustment needs to be performed. Usually, the signal values from a VSA are received in the form of IQ samples. The extraction of the voltage magnitude and phase from them is straightforward and done with basic linear algebra procedures. After that, the power adjustment formula is used:

$$y_{\text{adj}}(t)=10\log_{10}\left(\frac{y^{2}(t)}{0.001\times Z_{\text{ref}}}\right)+A, \tag{2.10}$$

here, $y_{\text{adj}}(t)$ stands for adjusted signal value in dBm, Z_{ref} is a reference impedance (typically 50 Ohm), $y^{2}(t)$ squared voltage magnitude obtained from IQ samples, A – signal path attenuation value in dB.

2.2. Numerical Procedures of the Power Amplifier Behavioral Model Extraction

2.2.1. Model Extraction Technique

As discussed earlier, the model presented in (2.1) can only capture static PA behavior, which will not represent PA response to a wideband modulated signal used in modern communication networks. To capture static and dynamic PA behavior, different models must be applied. Commonly used models were mentioned in Section 1. One of the most common PA models is a Memory Polynomial, which is a simplification of the Volterra series:

$$y(n)=\sum_{k=1}^{K}\sum_{m=0}^{M}a_{km}x(n-m)\left|x(n-m)\right|^{k-1}, \tag{2.11}$$

here, $y(n)$ represents the n-th sample of the response signal, M is the memory depth of the polynomial function, K – the degree of the polynomial function, and $x(n-m)$ is the excitation signal's sample delayed by the memory depth. A comparison of (2.1) and (2.11) shows that the latter incorporates the dependency of the current response signal's sample not only on the current, but also on several previous excitation signal samples. This allows for incorporating both static and dynamic behaviors into the model.

A memory polynomial is one of the possible dynamic model formulations. In general, a different model may be selected, depending on the needs of a design. For example, a memory polynomial can be generalized by incorporating cross terms from leading and lagging signal envelope components:

$$\begin{aligned} y_{\mathrm{GMP}}(n)&=\textstyle\sum_{k=1}^{K}\sum_{m=0}^{M}a_{k\,m}x(n-m)\left|x(n-m)\right|^{k-1}+\ldots\\ \ldots&+\textstyle\sum_{k=2}^{K_b}\sum_{p=1}^{P}\sum_{m=0}^{M_b}b_{m\,k\,p}x(n-m)\left|x(n-m-p)\right|^{k-1}+\ldots\\ \ldots&+\textstyle\sum_{k=2}^{K_c}\sum_{q=1}^{Q}\sum_{m=0}^{M_c}c_{m\,k\,q}x(n-m)\left|x(n-m+q)\right|^{k-1}\end{aligned}, \tag{2.12}$$

here, the second and third polynomial functions represent the lagging and leading envelope values. Even though the M_b, K_b, M_c, K_c terms are, generally, much smaller than M and K (Ghannouchi et al., 2015b), the complexity of the model, meaning the number of coefficients that need to be calculated, increases significantly compared to the basic MP in (2.11). In general, more complex models should lead to more accurate modeling results. However, the GMP model increases model accuracy compared to the MP only when strong memory effects

are present. In cases of low or moderate memory effects, MP is more computationally efficient and provides similar results to GMP. For the purposes of the present dissertation, where power amplifiers with moderate powers (1−2W) are investigated, the memory polynomial model is an optimal choice.

To fit measured data into the MP model, the following calculations are performed. For n observed samples, a system of linear equations can be written for (2.11):

$$\begin{aligned} y(1) &= a_{10}x(1) + a_{11}x(0) + \ldots + a_{KM}x(1-M)\left|x(1-M)\right|^{K-1} \\ y(2) &= a_{10}x(2) + a_{11}x(1) + \ldots + a_{KM}x(2-M)\left|x(2-M)\right|^{K-1} \\ y(n) &= a_{10}x(n) + a_{11}x(n-1) + \ldots + a_{KM}x(n-M)\left|x(n-M)\right|^{K-1} \end{aligned}, \qquad (2.13)$$

the system can be reformulated into the matrix multiplication form:

$$Y = X \times A, \qquad (2.14)$$

where the output vector Y is defined as a set of measured response values:

$$Y = \begin{pmatrix} y(1) \\ y(2) \\ \vdots \\ y(n) \end{pmatrix}, \qquad (2.15)$$

model coefficient vector A defined as:

$$A = \begin{pmatrix} a_{10} \\ a_{11} \\ \vdots \\ a_{KM} \end{pmatrix}, \qquad (2.16)$$

And measured excitation is grouped into the input vector X, commonly referred to as a regression matrix, and is defined as:

$$X = \begin{pmatrix} x(1) & \ldots & x(1-M) & x(1)^2 & \ldots & x(1-M)^2 & \ldots & x(1-M)^K \\ x(2) & \ldots & x(2-M) & x(2)^2 & \ldots & x(2-M)^2 & \ldots & x(2-M)^K \\ \vdots & \ddots & \vdots & \vdots & \ddots & \vdots & \ddots & \vdots \\ x(n) & \ldots & x(n-M) & x(n)^2 & \ldots & x(n-M)^2 & \ldots & x(n-M)^K \end{pmatrix}, \qquad (2.17)$$

here, samples are grouped into blocks by nonlinearity powers and memory taps. The system in (2.13) presents an overdetermined case, where no exact solution can be found. Instead, a solution may be found by minimizing the residual mean-squared error:

$$e = \frac{1}{2}Y - XA^2 = \frac{1}{2}\left[XA - Y\right]^T \left[XA - Y\right]. \tag{2.18}$$

Minimization is done by taking the partial derivative of the (2.18) with respect to A (coefficient vector) and equating it to zero:

$$\frac{\partial}{\partial A}e = \frac{\partial}{\partial A}Y - XA^2 = X^T\left[XA - Y\right] = 0, \tag{2.19}$$

this gives an expression for the coefficients vector A:

$$A = \left[X^T X\right]^{-1} X^T Y. \tag{2.20}$$

Expression $\left[X^T X\right]^{-1} X^T$ is known as a matrix X left pseudo-inversion. Equation (2.20) is suitable in a case where the coefficient estimation process is done once from a set batch of data. When considering online coefficient estimation, the inefficiency arising from matrix multiplication and inversion in (2.20) becomes an obstacle. In those cases, a recursive least squares estimation algorithm is preferred. After obtaining the a_{km} coefficients of the (2.11), the model's output can be compared to the actual characterization data to determine the modeling error.

2.2.2. Model Error Estimation

The model error is estimated by comparing the data from the actual measurement to the prediction obtained by the extracted behavioral model. To quantify the resulting discrepancy, several metrics are used. One of the most common is the *normalized mean squared error* (NMSE), which is defined as:

$$NMSE = \frac{\frac{1}{N}\sum|e|^2}{\frac{1}{N}\sum|y|^2}, \tag{2.21}$$

here, e is the difference between the measurement and model prediction taken sample by sample. The formula takes the average of this error and normalizes it by the power level of the response signal.

2.2.3. Signal Acquisition Parameters

Results of the characterization process can be correct only when excitation and response signals are measured adequately, without losing any critical signal information. To ensure this, the measurement parameters of the instruments should be set to capture all important signal features.

The spectral regrowth, caused by a nonlinear response of the amplifier, increases the bandwidth of the signal by 7−10 times. This requires an appropriate increase to the receiver's bandwidth (RB). Given the symbol rate SR of the excitation signal, RB in Hz, is given by:

$$RB = 10 \times SR, \tag{2.22}$$

for example, a 1 MHz symbol rate requires 10 MHz observer bandwidth to fully capture the regrown signal spectrum, produced by the PA. In case a set of discrete measurements takes place, the receiver needs to be configured for a fixed record length, so that the same sets of data can be later compared against each other. For a given number of bits *N*, the record length can be calculated:

$$RL = \frac{N}{MO} \times \frac{1}{SR}, \tag{2.23}$$

here, RL is the record length in seconds, MO – modulation order, i.e., how many bits can be transmitted in a modulation symbol, $\frac{1}{SR}$ − the reciprocal of the symbol rate gives the symbol length in seconds. Record length is typically limited by the amount of the receiver's internal memory. Larger record length allows for capturing a wider range of PA behaviors and getting more representative models, but also leads to increased measurement time and takes a large amount of storage space.

To avoid signal clipping due to the saturation of the receiver's ADC, a correct reference power level should be selected. Reference power level, for most VSA's, is the maximal power level expected by the receiver. Too large a discrepancy between the actual maximal signal power and the reference level leads to characterization errors, similar to those shown in Figure 2.6. For a system with a power amplifier and an attenuator a reference level in dBm is given by:

$$ref = P_{\text{avg}} + G + PAPR - A, \tag{2.24}$$

here, P_{avg} is the average excitation signal power, G is expected gain of the PA, $PAPR$ is the peak to average power ratio of the excitation signal, A – the value of the attenuator in dB.

PAPR in Equation 2.24 is an important signal characteristic. As mentioned before, this parameter describes the ratio between peak signal values and their average values. Different *PAPR* values impact the results of the characterization, meaning that the model extracted for 3 dB *PAPR* will not accurately reflect the amplifier's response to the signal with *PAPR* equal to 6 dB. *PAPR* is generally controlled by the modulation scheme and by the transmitter's shaping filter parameters.

2.3. Considerations for Carrier Frequency Effects Modeling

The model formulation provided above in (2.11−2.20) does not explicitly reference carrier frequency in any of its terms. Instead, the carrier frequency is implied implicitly, since the characterization data sets *x* and *y* are baseband data, demodulated from a carrier with a particular frequency. A question arises: how well would a model, extracted at a given carrier frequency, hold up on the data extracted at a different carrier frequency? This question received very limited consideration in the subject literature.

It is known that every amplifier has a frequency-dependent behavior, and that behavioral model should be extracted under conditions resembling those of the actual operation. There are, however, cases where the transmission system operates across a range of carrier frequencies, choosing one or another depending on the situation in the network, in particular, cognitive radio. In these applications, behavioral modeling should either include characterization from multiple carrier frequencies at once, which would make the model computationally less efficient, or use a model extracted at one carrier frequency in all cases. The latter would result in some model accuracy degradation. Depending on the severity of model performance degradation, one would choose between two evils: higher complexity or higher modeling errors.

2.3.1. Direction of the Model Error Investigation

It is expected that the error of a model would increase as it is applied further from the conditions from which it was extracted. Having that in mind, it is still important to understand how parameters of the model, characteristics of a PA, and properties of an excitation signal will impact the rate of the model degradation. Parameters of every PA are unique. Different manufacturing technologies, materials, temperature profiles, architectures, power levels, and operation conditions – all contribute to the behavior of the PA. This is the reason why behavioral model-

ing is generally performed on a case-by-case basis. In cases where carrier frequency varies, the same spread of operational parameters between different PA models should be expected. Some of them will have higher sensitivity to said change, some lower: the actual sensitivity of a particular PA can be determined only after concrete evaluation.

Consider the measurement setup in Figure 2.2. It is designed to characterize a DUT under a set of experiments, where the only variable in the measurement setup is the carrier frequency of the signal. Say there is an excitation signal and a response of the DUT:

$$y_{f_1}(t) = F_{f_1}\left[x_{f_1}(t)\right], \tag{2.25}$$

here, $y_{f_1}(t)$ is the baseband response of the DUT, extracted at the carrier frequency f_1, $x_{f_1}(t)$ is the baseband excitation signal for the DUT, extracted at a carrier frequency f_1, and $F_{f_1}[\ ]$ is the transfer function of the DUT at a frequency f_1, which is being identified. Data from this measurement is then used to identify a PA model utilizing the procedure described in Section 2.2.1.

$$z_{f_1}(t) = P_{f_1}\left[x_{f_1}(t)\right], \tag{2.26}$$

here, $z_{f_1}(t)$ is the system's response to excitation $x_{f_1}(t)$, predicted by the polynomial model P_{f_1}. The discrepancy between the actual response $y_{f_1}(t)$ and the model's prediction $z_{f_1}(t)$ can then be calculated and quantified using the metric described in Section 2.2.2.

$$e_{f_1} = y_{f_1}(t) - z_{f_1}(t). \tag{2.27}$$

This produces the modeling error at a carrier frequency f_1.

To evaluate the prediction at a different carrier frequency, an additional measurement is taken:

$$y_{f_2}(t) = F_{f_2}\left[x_{f_2}(t)\right], \tag{2.28}$$

here, all the terms of the equation have the same meaning as in Equation 2.25, the only difference being the carrier frequency of the excitation signal. Instead of identifying new model coefficients, those from Equation 2.26 are used to evaluate the model error again:

$$z_{f_2}(t) = P_{f_1}\left[x_{f_2}(t)\right], \tag{2.29}$$

the error:

$$e_{f_2} = y_{f_2}(t) - z_{f_2}(t). \tag{2.30}$$

There are a few things that need to be addressed. First, performing the calibration procedures ensures that there is no noticeable difference between $x_{f_1}(t)$ and $x_{f_2}(t)$ after demodulation. This means that since the same polynomial function P_{f_1} is employed, there will be no noticeable difference between $z_{f_1}(t)$ and $z_{f2}(t)$ – the same excitation provides the same response of the model. Meaning that the difference between e_{f_1} and e_{f_2} is decided entirely by the difference between $y_{f_1}(t)$ and $y_{f_2}(t)$:

$$\begin{aligned} e_{f_1} - e_{f_2} &= \left(y_{f_1}(t) - z_{f_1}(t)\right) - \left(y_{f_2}(t) - z_{f_2}(t)\right) = \ldots \\ \ldots &= y_{f_1}(t) - y_{f_2}(t) + z_{f_2}(t) - z_{f_1}(t) \cong \ldots \\ \ldots &\cong y_{f_1}(t) - y_{f_2}(t). \end{aligned} \tag{2.31}$$

The difference between $y_{f_1}(t)$ and $y_{f_2}(t)$ is determined, in one part, by the individual frequency response of the measured PA. To draw any general conclusions from this part's evaluation, a large set of different amplifiers should be tested. The said set should contain PAs with diverse architectures, manufacturing technologies, and so on. This kind of test goes beyond the scope of the present dissertation.

Another part that determines the difference between two responses is the distance between points f_1 and f_2 on the frequency axis. It is logical to assume that a larger distance between these two points will lead to a larger error discrepancy. The one case where this may not be strictly true is the case with a non-flat frequency response of the amplifier. Consider the two frequency responses in Figure 2.7. The figure presents two frequency responses: a flat, drawn with a dashed line, and a non-flat (in this case, it has the form of a sinusoid for illustration) drawn with a solid line. Three separate frequency points f_1, f_2, f_3 are selected, their position matches the position of the positive and negative peaks of the sinusoidal frequency response. Let's say a model is extracted from the data gathered at the carrier frequency f_1. Utilizing the procedure described in Equations 2.25−2.31,

the differences $e_{f_1} - e_{f_2}$ and $e_{f_1} - e_{f_3}$ are calculated. For an amplifier with a frequency response resembling a flat line, there is no reason to believe that inequality:

$$\left| e_{f_1} - e_{f_2} \right| < \left| e_{f_1} - e_{f_3} \right|, \tag{2.32}$$

would not hold in general. Equal linear gain ensures that only the frequency-dependent nonlinear and memory-related PA behaviors are contributing to the error difference. The impact of those behaviors tends to become more severe as the distance between the model extraction point and the model application point increases. For example, Section 2.1.1 discusses the contribution of the amplifier's node impedance mismatch on the memory effects. Impedance mismatch, modeled at f_1 will be more similar to impedance mismatch, modeled at f_2, than that of f_3, since the impedances at f_1 will be closer to impedances at f_2.

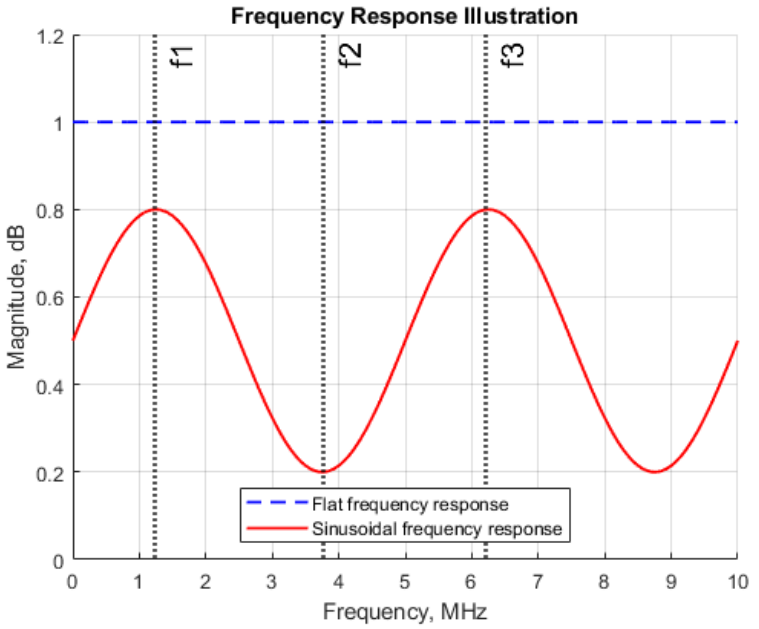

Fig. 2.7. Frequency response impact on the modeling accuracy

In cases of the sinusoidal response, however, there is no such guarantee. The linear gain difference between points f_1 and f_2 will produce additional error proportional to the value of the said difference. If the linear gain difference is large enough, it can outweigh the contribution of nonlinear and memory effects. The

resulting error may be closer to that of f_3, since the linear gain at f_1 is approximately equal to that at f_3. To reduce the effects of the linear distortion, some form of gain normalization may be employed.

Finally, the difference between the amplifier's responses at different carrier frequencies may be determined by the characteristics of the excitation signal $x_{f_1}(t)$. It was established in Section 2.1.1 that depending on the form of the $x_{f_1}(t)$, different types of nonlinear behaviors can be excited, including: different orders of nonlinearities, static and/or dynamic behavior. To the best of the author's knowledge, there are no experiments done to evaluate this aspect of the PA behavioral modeling. Together with an average signal power, characteristics such as signal PAPR and modulation bandwidth may also have an impact on the error produced by the carrier frequency change.

The metric, which would allow for evaluating the impact described above, is the frequency error rate of change:

$$FE_{\text{roc}} = \frac{\left| e_{f_\text{n}} - e_{f_\text{k}} \right|}{\left| f_n - f_k \right|}, \tag{2.33}$$

here, e_{f_n} and e_{f_k} are modeling errors in dB, produced at frequencies f_n and f_k, respectively, FE_{roc} frequency error rate of change, measured in dB/Hz. This metric allows for the evaluation of how fast the frequency-dependent error increases with every Hz of change in carrier frequency. For example, NMSE values of −44 dB and −33 dB are measured at frequency points 3.6 GHz and 3.7 GHz, respectively. This would provide:

$$FE_{\text{roc}} = \frac{\left| -33 \text{ dB} - (-44 \text{ dB}) \right|}{\left| 3.6 \text{ GHz} - 3.7 \text{ GHz} \right|} \cong 0.11 \frac{\text{dB}}{\text{MHz}}. \tag{2.34}$$

The measurement would be taken at some excitation signal configuration. Controlled change in the characteristic of the excitation signal would allow for checking the impact of said characteristic on the rate of change of the error. This would allow for drawing a general conclusion about the influence of the excitation signal characteristics on the performance of the PA behavioral model over a range of carrier frequencies.

2.3.2. Method of Decreasing Modeling Error

To improve the MP model's from Equation 2.11 performance across varying carrier frequencies, a parametrization technique is proposed:

$$y_{\mathrm{PMP}}(n, f_c) = \sum_{k=0}^{K-1} \sum_{m=0}^{M-1} p_{km}(f_c)\, x(n-m)\left|x(n-m)\right|^k. \tag{2.35}$$

where the conventional frequency-independent coefficients a_{km} are replaced with frequency-dependent functions $p_{km}(f_c)$. These parametric functions are derived through the following methodological steps:

Conduct N measurements at distinct carrier frequencies f_c, obtaining corresponding excitation-response pairs:

$$\left\{x_{CF_1}, y_{CF_1}\right\}, \left\{x_{CF_2}, y_{CF_2}\right\}, \ldots \left\{x_{CF_N}, y_{CF_N}\right\}. \tag{2.36}$$

For each dataset, extract an MP model, yielding N coefficient sets:

$$\mathrm{A}(f_{c_0}) = \begin{pmatrix} a_{00} \\ a_{01} \\ \vdots \\ a_{km} \end{pmatrix}, \quad \mathrm{A}(f_{c_1}) = \begin{pmatrix} b_{00} \\ b_{01} \\ \vdots \\ b_{km} \end{pmatrix}, \quad \ldots \mathrm{A}(f_{c_N}) = \begin{pmatrix} c_{00} \\ c_{01} \\ \vdots \\ c_{km} \end{pmatrix}. \tag{2.37}$$

Apply interpolation to generate continuous coefficient functions:

$$\begin{cases} p_{00}(f_c) = F_{int}\left[\left(a_{00}; f_{c_0}\right), \left(b_{00}; f_{c_1}\right) \ldots \left(c_{00}; f_{c_N}\right)\right] \\ p_{01}(f_c) = F_{int}\left[\left(a_{01}; f_{c_0}\right), \left(b_{01}; f_{c_1}\right) \ldots \left(c_{01}; f_{c_N}\right)\right] \\ \vdots \\ p_{km}(f_c) = F_{int}\left[\left(a_{km}; f_{c_0}\right), \left(b_{km}; f_{c_1}\right) \ldots \left(c_{km}; f_{c_N}\right)\right]. \end{cases} \tag{2.38}$$

The method assumes sufficiently smooth PA behavior across the operational bandwidth (i.e., there are no resonances or other reasons for sharp behavior changes). Under this condition, the *parametrical memory polynomial* (PMP) model can accurately predict amplifier behavior at arbitrary frequencies within the characterized range, including untested frequencies between measurement points.

Several interpolation methods exist for approximating functions from discrete data points. The simplest approach, linear interpolation, constructs piecewise linear connections between points. While computationally efficient, this method yields non-smooth functions that often poorly approximate the underlying relationship unless an impractically large number of points is used. For applications requiring accurate modeling of physical processes, the polynomial interpolation is generally more suitable. This method generates a smooth polynomial function

when given at least $k \times m+1$ data points, producing a continuous representation of the form:

$$p_{km}(f_c) = \varphi_0 + \varphi_1 f_c + \varphi_2 f_c^2 + \ldots + \varphi_{(k\times m)} f_c^{(k\times m)}, \tag{2.39}$$

where $[\varphi_0 \ldots \varphi_{(k\times m)}]$ is an array of polynomial coefficients, obtained from solving a system of linear equations:

$$\begin{cases} a_{00} = \varphi_0 + \varphi_1 f_{c_0} + \varphi_2 f_{c_0}^2 + \ldots + \varphi_{(k\times m)} f_{c_0}^{(k\times m)} \\ b_{00} = \varphi_0 + \varphi_1 f_{c_1} + \varphi_2 f_{c_1}^2 + \ldots + \varphi_{(k\times m)} f_{c_1}^{(k\times m)} \\ \vdots \\ c_{00} = \varphi_0 + \varphi_1 f_{c_N} + \varphi_2 f_{c_N}^2 + \ldots + \varphi_{(k\times m)} f_{c_N}^{(k\times m)} \end{cases}. \tag{2.40}$$

The solution of this system of equations can be computationally optimized through established techniques such as Lagrange interpolation or Newton's divided difference method (W. Y. Yang et al., 2020). However, this polynomial interpolation approach suffers from a fundamental limitation: the solution becomes increasingly unstable as the number of data points increases. This instability stems from the higher-order terms required in Equation 2.39 when interpolating more points, leading to severe oscillations known as Runge's phenomenon. In practice, polynomial interpolation remains reliable only for modest numbers of points (typically 8–10), and in some cases, oscillatory artifacts may appear even with fewer interpolation points.

To circumvent the instability associated with high-order polynomials, the proposed method employed cubic spline interpolation (W. Y. Yang et al., 2020). This technique partitions the dataset into subintervals and fits a unique cubic polynomial to each segment. The resulting composite function achieves global smoothness by enforcing continuity in both the first and second derivatives at the connecting knots between adjacent splines. The complete set of spline functions was subsequently determined by solving a system of linear equations derived from these continuity conditions and the specified boundary conditions.

The implementation of the PMP in Equation 2.35 involves two critical design considerations: first, the number of interpolated frequency points and their distribution across the frequency axis. The first aspect is conceptually straightforward; a higher number of points generally yields a more accurate approximation of the underlying coefficient functions. However, this improved accuracy comes at the cost of increased measurement overhead and greater computational complexity. To explore this trade-off, PMP performance across several approximation orders

(i.e., different numbers of points) should be evaluated. Second, the optimal distribution of these selected points along the frequency band should be considered. While a uniform (linear) distribution is the most intuitive starting point, its performance can be compared against more sophisticated sampling strategies. Specifically, this work will contrast the results from a uniform distribution with those achieved using a Chebyshev node distribution, which is designed to minimize interpolation error by concentrating points near the boundaries of the interval.

The performance of the proposed PMP model is evaluated using a frequency-averaged normalized mean square error metric. For each carrier frequency within the considered band, the NMSE is first computed in the linear domain by comparing the model output with the corresponding measured PA output. These frequency-dependent NMSE values are then averaged across the entire carrier frequency range, and the resulting average NMSE is finally expressed in decibels. This procedure yields a single scalar metric that represents the expected modeling error power over the investigated frequency interval. Assuming N discrete frequencies are measured:

$$e_{\text{avg}} = 10 \times \log_{10}\left(\frac{1}{N} \sum_{f_c=1}^{N} e(f_c) \right). \tag{2.41}$$

The proposed PMP model is specifically designed to improve frequency generalization relative to conventional single-frequency memory polynomial models. Consequently, its performance cannot be fully characterized by pointwise NMSE at individual frequencies alone. The frequency-averaged NMSE metric directly quantifies the ability of the model to maintain low error across the entire band, rather than excelling only near the extraction frequencies. A reduction in the averaged NMSE therefore indicates a genuine improvement in model robustness with respect to carrier-frequency variation, rather than a localized gain in accuracy.

2.3.3. Overall Review of the Measurement and Modeling Process

Figure 2.8 depicts a schematic of the modeling setup design. Rectangular boxes represent the input information; the hexadecimal boxes represent the output information.

The modeling process starts with the selection of the order of the non-linearity and the type of behavior modeled. The latter includes static and/or dynamic modeling. These parameters determine the general setup of the measurement. After the selection of the general measurement setup, a calibration procedure needs

to be performed. A calibration is performed for a selected range of frequencies and signal powers.

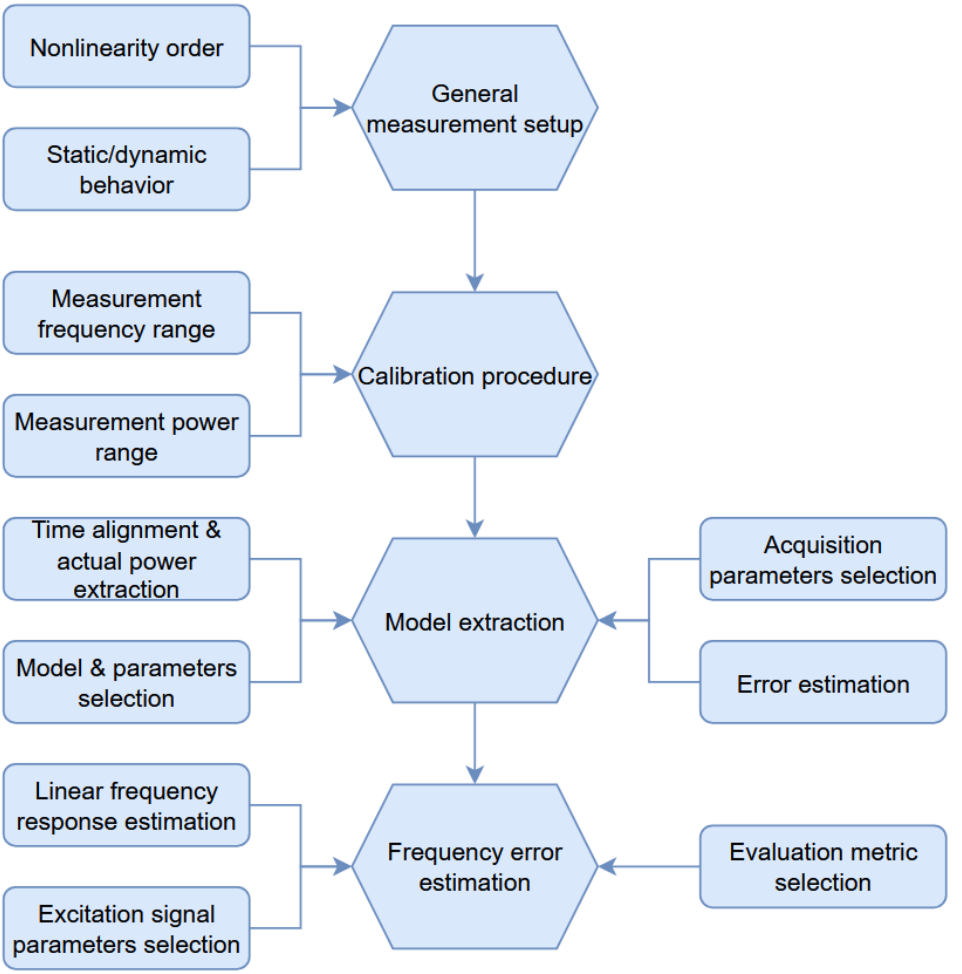

Fig. 2.8. Proposed workflow for model's frequency error estimation

After the calibration, data acquisition for model extraction may begin. First, adequate acquisition parameters must be determined. Then, a model type and its parameters need to be chosen, depending on the type of nonlinearity modeled. Before extracting the model coefficients, time alignment and actual power value extraction must be performed; this process is sometimes referred to as data de-embedding. After that, the model parameters can be extracted and their predictions

compared to actual data to estimate modeling error using an appropriate metric. The extracted coefficients are then used to assess applicability to data from different carrier frequencies. To isolate nonlinear and memory-dependent behavior, the linear frequency response should be estimated and compensated for. General conclusions can be drawn by evaluating frequency error dependence on different excitation signal forms.

2.4. Conclusions of the Second Chapter

1. The type of measurement setup used for PA characterization is determined by the type and order of the nonlinearity being characterized. The higher the order of the nonlinearity, the higher the average power of the excitation signal is needed. The type of nonlinearity – static or dynamic – determines the form of the excitation signal. Dynamic nonlinearities require wideband modulated signals as an excitation for power amplifiers.
2. The accuracy of the measurement setup proposed is evaluated by performing specific calibration procedures. Power level discrepancy calibration displays 0.65 dB mean discrepancy. Frequency response flatness calibration displays ~0.8 dB mean flatness over the measured range. These discrepancies are below the measurement uncertainty of the used instruments; therefore, they have no noticeable impact on the overall measurement accuracy.
3. The frequency error rate of change characteristic allows for generalizing and comparing behaviors of different power amplifiers across different carrier frequency ranges, since it considers not initial modeling accuracy, but the ability of the model to keep its accuracy over a given carrier frequency range.
4. The PMP model generalizes conventional memory polynomial modeling by parameterizing the coefficients as functions of carrier frequency, theoretically enabling accurate PA modeling across a wide frequency range without retraining. Its performance is assessed using a frequency-averaged NMSE metric.

3

Investigating Carrier Frequency Change Impact on the Power Amplifier Model's Accuracy

This section focuses on experimental evaluation of the modeling error, arising due to change in carrier frequency. The error is evaluated while varying the excitation signal's configuration. Finally, the proposed PMP technique is experimentally validated, its limitations are discussed. The materials presented in this chapter were published in Borel et al. (2025).

3.1. Design of the Experiment

3.1.1. Object of the Experiment

The experiments were conducted using the QPA9942 power amplifier. This is a high-efficiency InGaP/GaAs HBT technology transistor amplifier. Its operational frequency is 3300–3800 MHz as reported by the manufacturer. The PAE of the device is reported to be ~25% around +28 dBm output power. The frequency range is inside the 5G FR−1, and the amplifier is tuned to work around ~1W of the output power. These specifications agree with the scope of the present dissertation. The amplifier is also reported to be "ready for linearization", meaning

that in its default state, it is not linearized. The wide operational frequency range is also critical to the goal of the present work. The manufacturer does not provide any details on the internal structure of the device, except for the fact that it is a 3-stage device. The amplifier is tested using a development board provided by the manufacturer.

The actual operating parameters may differ from those provided by the manufacturer for a plethora of reasons. To understand the performance of the device in concrete conditions, used in this experiment, some basic measurements were conducted. First, the dependency of the gain on the output power values, and the dependency of the PAE on the output power values were measured. To conduct these measurements, the setup shown in Figure 3.1 was used.

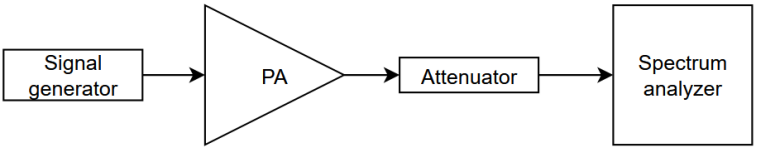

Fig. 3.1. Measurement setup for evaluation of gain and PAE

The setup consists of a signal generator, a spectrum analyzer, an attenuator, and the PA. A range of CW signals with known power levels is sent to the PA while measuring output power with a spectrum analyzer. Actual output power values in decibels can be calculated knowing the power reduction produced by the attenuator and interconnection cables:

$$P_{\text{out}} = P_{\text{SA}} + A, \tag{3.1}$$

where A stands for the overall attenuation of the measurement setup, P_{SA} is the power level measured at the spectrum analyzer, P_{out} is the power level at the output of the PA. The efficiency of the amplifier is evaluated knowing the total DC power consumed by the device:

$$PAE = \frac{P_{\text{out}} - P_{\text{in}}}{I_{\text{DC}} \times V_{\text{DC}}} \times 100\%, \tag{3.2}$$

where I_{DC} and V_{DC} are supply current and supply voltage values, respectively, which were recorded during the measurement. The gain is calculated by subtracting the input power value in dBm from the output power value in dBm. All measurements are conducted on a single frequency. The results of the measurement are presented in Figure 3.2.

The efficiency curve, as expected, is rising along with the value of the output power. At +28 dBm output power, measured PAE is around 27−28%, which is

higher than reported by the manufacturer. The discrepancy may be caused by the spread of the PAE depending on the temperature of the amplifier. The gain dependency on the output power level shows the nonlinear behavior of the amplifier. The swing of the gain in the measured power range reaches about 1 dB.

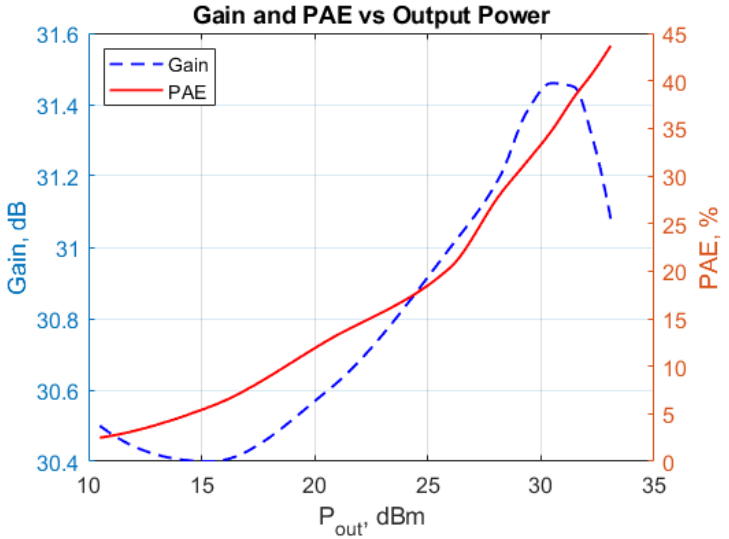

Fig. 3.2. PA gain and PAE dependency on the output power

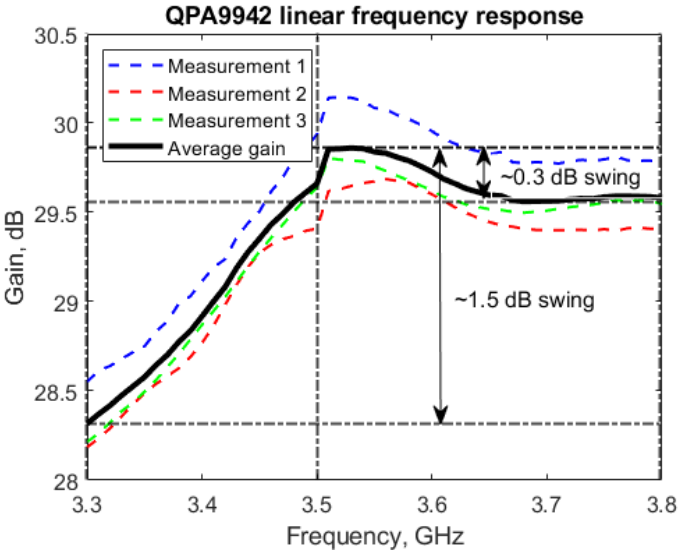

Fig. 3.3. Frequency-dependent gain of the PA

To evaluate PA gain dependence on the frequency, the same setup as shown in Figure 3.1 is used. This time, the frequency of the CW signal is being changed. The measurement was taken across the whole operational bandwidth of the PA, 3300–3800 MHz. The measurement step was 10 MHz. The input signal's average power was −15 dBm. This ensures that the results are dominated by the linear PA gain, without noticeable impact of the nonlinear components. The results of the measurement are presented in Figure 3.3. The figure presents four different curves. Curves 1, 2 , and 3 are obtained from three separate measurements, taken at different times. A considerable difference between measurements may be observed. This happens because of the unstable temperature conditions. Since there was no possibility to create an experimental environment with stable temperature conditions, the average frequency-dependent gain curve is used as a representation of the PA operation. It is calculated by averaging the results of three previous measurements.

The overall gain swing in the case of the calculated average curve is ~1.54 dB. For the most part, it is caused by the gain in the 3.3−3.5 GHz frequency range. In this range, the gain has an approximately positive linear dependency on the frequency. Range 3.5−3.8 exhibits less frequency-dependent behavior. In this range, the gain swing reaches about 0.3 dB. Section 2.3 discusses the possible impact of the non-flat gain response of the PA on its model's accuracy across different frequencies. The impact of the presented response on the measurements, along with suggested ways to mitigate it, will be shown in later sections.

3.1.2. Excitation Signal Design

Section 2.3 discusses the necessity to test the model's frequency-dependent accuracy with different excitation signal parameters, such as modulation bandwidth, average power level, and PAPR. Here, the particularities of excitation sequence design are discussed.

The first aspect of the signal that needs to be discussed is its length and bit content. Larger signal length allows for capturing a wider range of PA behaviors, but also slows down the measurement process. Literature on the subject usually mentions signal lengths ranging from 10k points to 100−500k points. In the presented case, there were no considerations for choosing one signal length over another. It was important only to keep it consistent during all measurements to ensure the comparability between the results. The same goes for the bit content. There are no widely used standard test bit sequences, although different bit sequences produce signals with different power density functions that have an impact on the resulting model accuracy. To remove the impact of different signal lengths and bit sequences on the results, all the measurements are conducted with the same sequence. It has a length of 4096 QAM16 constellation symbols. At the

receiver, every symbol of the constellation is represented by 8 points. This gives a total of 32768 points per measurement.

The sequence length in seconds is determined by the symbol rate of the measurement. Since one of the goals of the experiment is to check the behavior of the signals with different modulation bandwidths, the time span it takes to transmit the sequence differs, but the same sequence is always transmitted. Let's say the symbol rate set in the VSG is 1 MHz. This creates a signal at the output of the VSG with a length in seconds equal to 4096/1 MHz = 4.096 ms. Lowering the symbol rate will increase the signal length in seconds, but the bit content of the signal will not change.

The average signal power setup is trivial and does not require additional discussion. The third aspect of the signal – PAPR, requires some attention. Signal PAPR is decided, firstly, by the modulation used. In general, a higher modulation order (i.e., a higher number of bits represented by 1 modulation symbol) produces signals with higher PAPR. Also, different bit sequences produce signals with different PAPR values. Since our experiment is designed to use the same bit sequence with the same modulation scheme, the PAPR of the signal should be constant across all measurements, assuming all other parameters of the VSG stay constant. The PAPR is also impacted by the form of the shaping filter of the VSG. Controlling the steepness of said filter controls the output signal's PAPR. This allows for using the same signal sequence as in the tests above, allowing for the reduction of the number of unknowns, which could have an impact on the results of the experiment.

3.1.3. Model Parameters

The obtained measurement results are used to identify polynomial model coefficients with the procedure described in Section 2.2. The following question arises: What order of the polynomial to use? There are no general recommendations except for the fact that the use of higher-order functions should lead to higher model accuracy up to some point. Together with accuracy comes an increase in computational costs. Also, there is the risk of overfitting the model by selecting higher polynomial and memory degrees. The overfitted model may perform well under training data but fail completely on different data sets.

In the presented experiment, polynomial function orders are determined empirically, by computing functions with every possible combination of polynomial degree and memory depth up to a given number and then evaluating the mean error of said functions over the testing frequency range. Mean values were calculated for all possible combinations of memory lengths and polynomial degrees up to 8. Further calculations were unnecessary, as the error had largely

stabilized beyond this point. For the selected dataset, the model's NMSE is stable at K = 6, M = 1.

3.1.4. Measurement Conditions

To examine the PA behavior under a wide range of conditions, a total of twelve measurements were taken. Their parameters are listed in Table 3.1. The measurements are split into three groups, each containing four data sets. The groups are formed depending on the parameter of the excitation signal that is being changed for every measurement. There are three parameters, whose impact is being investigated: average power, modulation bandwidth, and PAPR. Two out of three parameters are constant in every group, while one is being changed. The modulation bandwidth setting is determined by the capabilities of the available VSG and VSA. Maximal 2 MHz modulation bandwidth allows for the evaluation of the dynamic PA behavior, while a 10 kHz signal excites mainly the static behavior. Two intermediate frequencies, 0.1 MHz and 1 MHz, are also tested to see possible variations in modeling accuracy. Power levels −1 dBm and −3 dBm are set so that the PA would be driven near the saturation point for optimal efficiency. Lower power levels allow for evaluating the PA at a further off saturation point. The power levels are set sufficiently far apart so they would not overlap, considering the ±0.5 dBm power level accuracy reported in the datasheet of the VSG. The PAPR setting variation is determined by the roll-off filter setting limits.

Every measurement consists of several sub-measurements taken over a range of carrier frequencies. The range of carrier frequencies is chosen to cover the whole operational bandwidth of the QPA9942, 3300−3800 MHz. The measurement step was chosen to match the one used when characterizing the frequency response of the amplifier, 10 MHz. This gives 51 unique data sets for every measurement of each group. One of these sub-measurements is chosen as training data for model extraction. The other 50 sub-measurements serve as validation data for model coefficients. NMSE is calculated for every sub-measurement. The resulting errors are then plotted against the carrier frequency at which they were extracted. The following question may arise: What sub-measurement should be used as a model training data? Since it is expected that the differences in linear gains at different carrier frequencies will have an impact on the resulting error magnitude, it seems logical to use a sub-measurement whose linear gain matches most closely to gains at other sub-measurement points. In the presented case, Figure 3.3. suggests that a sub-measurement located in the middle, between 3500−3800 MHz, should be used, as the linear gain in this range is much more stable than the gain in the range 3300−3500 MHz. This is a starting point for the experiment results presentation.

Table 3.1. Measurement conditions

	Meas. No.	Modulation bandwidth, kHz	Avg. input signal power, dBm	PAPR, dB
Group I	1	1000	−1±0.5	6.4±0.05
	2	1000	−3±0.5	6.4±0.05
	3	1000	−5±0.5	6.4±0.05
	4	1000	−8±0.5	6.4±0.05
Group II	1	10	−3±0.5	6.4±0.05
	2	100	−3±0.5	6.4±0.05
	3	1000	−3±0.5	6.4±0.05
	4	2000	−3±0.5	6.4±0.05
Group III	1	1000	−3±0.5	7±0.05
	2	1000	−3±0.5	5.9±0.05
	3	1000	−3±0.5	5.5±0.05
	4	1000	−3±0.5	4.6±0.05

Repeated measurements for the purpose of estimating statistical dispersion were not performed. This decision was primarily motivated by the practical duration of the measurement procedure, as each measurement requires a significant amount of time due to signal generation, acquisition, and subsequent data processing. Repeating the measurements for statistical analysis would therefore considerably increase the total experimental time without providing a proportional benefit. Moreover, research in the field of behavioral modeling typically focuses on evaluating modeling accuracy rather than achieving extremely high absolute measurement precision, as the primary objective is to assess the ability of models to reproduce amplifier behavior rather than to perform metrological characterization of the device.

Another limitation of the experimental setup was the inability to maintain fully controlled environmental conditions, particularly with respect to the amplifier temperature. To mitigate the influence of thermal variations, the device under test was preheated prior to the measurement campaign to ensure operation in a thermally stabilized state. Furthermore, all measurements were conducted consecutively on the same day to minimize environmental drift and maintain comparable operating conditions throughout the dataset acquisition.

3.2. Results of the Experiment

3.2.1. Group I Results

Figure 3.4 presents the results of Group I. The model was trained using data from 3.55 GHz and 3.65 GHz.

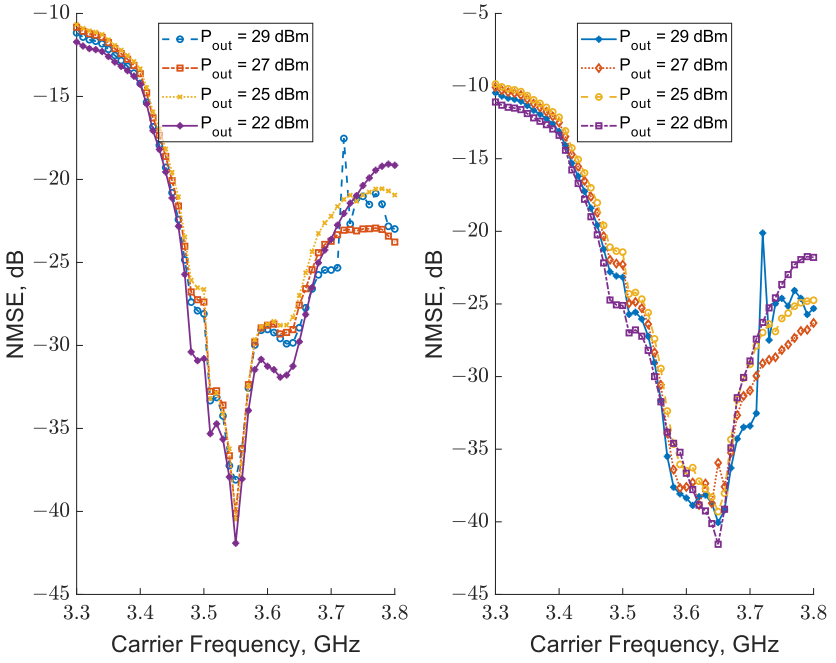

Fig. 3.4. Group I NMSE dependency on the carrier frequency for the model extracted at 3.55 GHz and 3.65 GHz

In both cases, NMSE is smallest near the model extraction frequency. The error increases as the frequency gap between the extraction frequency and the sub-measurement frequency increases. Tables 3.2−3.3 list error value swings as well as rates of change of errors. There is a considerable difference between model performance at 3.8 GHz and 3.3 GHz. One of the reasons for this may be the difference in linear gain that was discussed before. Another reason may be the distance between the 3.65 GHz and 3.3 GHz points, which is equal to 350 MHz, while the distance from 3.65 GHz to 3.8 GHz is just 150 MHz. The result comparison shows that moving the model extraction point to 3.55 GHz did not affect NMSE significantly at any measured point compared to the 3.65 GHz case.

Table 3.2. Group I measurement results when the model is extracted at 3.65 GHz

Avg. input, dBm	NMSE at 3.65 GHz, dB	NMSE at 3.3 GHz, dB	NMSE at 3.8 GHz, dB	NMSE ROC, dB/MHz
−1	−40.0	−10.46	−25.31	0.0914
−3	−35.9	−10.08	−26.3	0.0691
−5	−39.3	−9.85	−24.75	0.0906
−8	−41.5	−11.09	−21.79	0.1093

Table 3.3. Group I measurement results when the model is extracted at 3.55 GHz

Avg. input, dBm	NMSE at 3.55 GHz, dB	NMSE at 3.3 GHz, dB	NMSE at 3.8 GHz, dB	NMSE ROC, dB/MHz
−1	−38.09	−11.17	−22.98	0.0841
−3	−40.12	−10.83	−23.77	0.0913
−5	−40.47	−10.66	−20.93	0.0987
−8	−41.92	−11.72	−19.14	0.1059

This conclusion is supported by the data given in Tables 3.2−3.3. In fact, the results stayed relatively close in both cases. The form of the error curves in Figure 3.4 is also similar. In both cases, the left part of the curve reaches significantly higher values. This corroborates the assumption that differences in linear gain at different carrier frequencies significantly affect resulting model errors. The correlation between average excitation signal power and the frequency error rate of change reaches −0.99 for the 3.55 GHz model data. This indicates a strong negative correlation. But when the model extraction frequency is moved to 3.65 GHz, the correlation drops to −0.64, which indicates a much weaker correlation.

3.2.2. Group II Results

The results of group II are analyzed under the same assumptions as Group I, so they won't be repeated. Figure 3.5 shows the results acquired for both frequencies. Table 3.4 displays the numerical values. Curves are similar to those of Group I. The smallest modeling error is observed at the extraction frequency. The value of the error increases as the gap between extraction and sub-measurement frequency increases. The rate of increase of the error is in the same order as displayed in Tables 3.2−3.3. Different from the case above, a strong correlation between modulation bandwidth and error rate of change can be observed. Increasing modulation bandwidth seems to increase the error rate of change. The correlation for both

3.55 GHz and 3.65 GHz reaches 0.93 and 0.99. Contrary to the previous case, a strong correlation is observed at both extraction frequencies. Also, a significant error value oscillation can be observed in the graph of 2 MHz NMSE. It is difficult to pinpoint a reason for such oscillation.

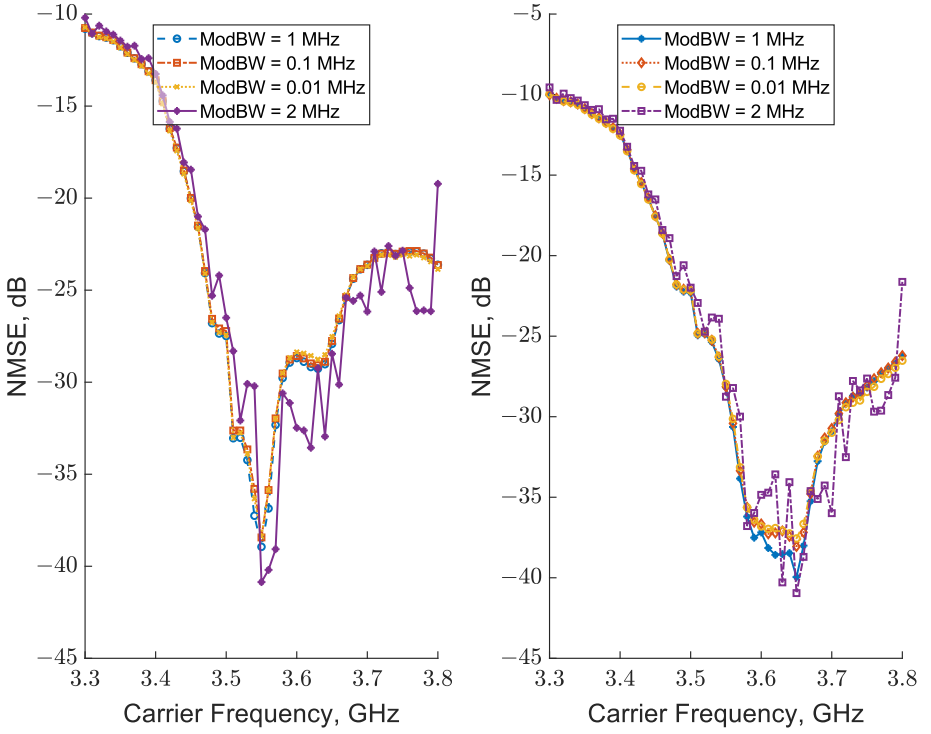

Fig. 3.5. Group II NMSE dependency on carrier frequency for the model extracted at 3.55 GHz and 3.65 GHz

Table 3.4. Group II measurement results when the model is extracted at 3.65 GHz

Mod. BW, MHz	NMSE at 3.65 GHz, dB	NMSE at 3.3 GHz, dB	NMSE at 3.8 GHz, dB	NMSE ROC,dB/MHz
2	−40.95	−9.55	−21.63	0.1093
1	−39.96	−10.05	−26.23	0.0885
0.1	−38.06	−10.01	−26.23	0.0796
0.01	−37.56	−9.96	−26.52	0.0762

Table 3.5. Group II measurement results when the model is extracted at 3.55 GHz

Mod. BW, MHz	NMSE at 3.55 GHz, dB	NMSE at 3.3 GHz, dB	NMSE at 3.8 GHz, dB	NMSE ROC dB/MHz
2	−40.86	−10.12	−19.23	0.1046
1	−38.94	−10.79	−23.63	0.0869
0.1	−38.43	−10.76	−23.63	0.0849
0.01	−38.38	−10.72	−23.86	0.0843

The differences between Tables 3.4−3.5 resemble the differences between Tables 3.2−3.3. The slight decrease in error accuracy at 3.3 GHz is balanced by an increase in error at 3.8 GHz. The shape of the curves stayed approximately the same for both extraction frequencies.

3.2.3. Group III Results

The final set of measurements was conducted while changing the PAPR of the excitation signal. The model extraction and error evaluation were performed using the same procedure as in Sections 3.2.1−3.2.2. The resulting error curves are given in Figure 3.6. Numerical values are provided in Tables 3.6−3.7.

Table 3.6. Group III measurement results when the model is extracted at 3.65 GHz

PAPR dB	NMSE at 3.65 GHz, dB	NMSE at 3.3 GHz, dB	NMSE at 3.8 GHz, dB	NMSE ROC dB/MHz
7.00	−40.24	−9.97	−26.21	0.0900
5.90	−40.30	−9.89	−26.33	0.0900
5.51	−40.74	−10.02	−26.55	0.0912
4.59	−41.05	−9.87	−23.89	0.1018

Table 3.7. Group III measurement results when the model is extracted at 3.55 GHz

PAPR dB	NMSE at 3.65 GHz, dB	NMSE at 3.3 GHz, dB	NMSE at 3.8 GHz, dB	NMSE ROC dB/MHz
7.00	−40.67	−10.72	−23.54	0.0941
5.90	−41.17	−10.67	−23.32	0.0967
5.51	−41.34	−10.78	−23.74	0.0963
4.59	−41.02	−10.62	−20.65	0.1015

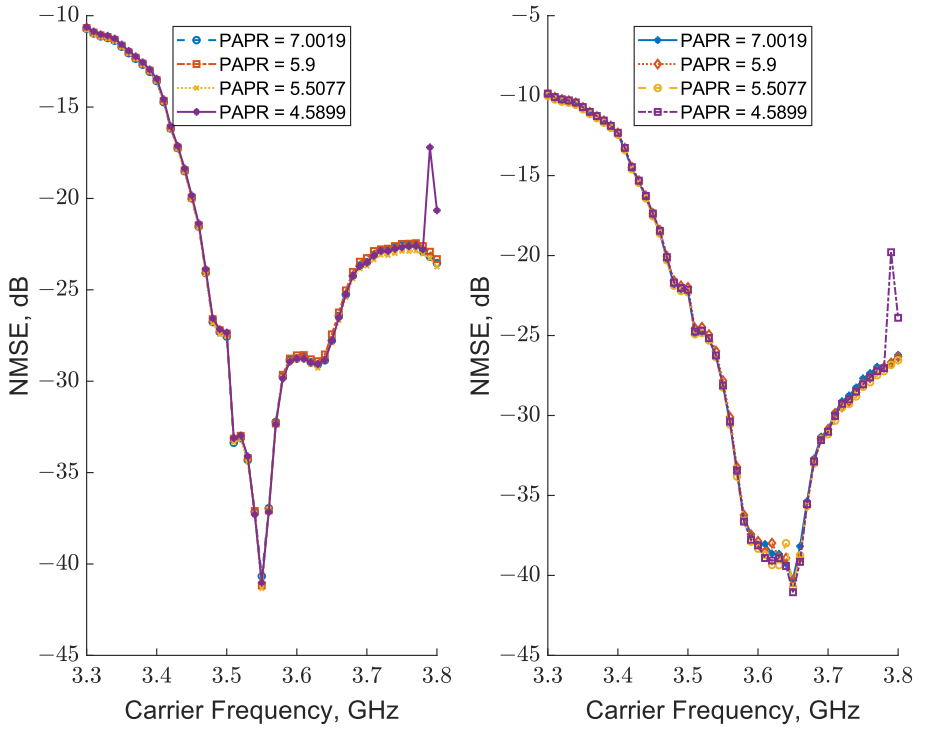

Fig. 3.6. Group III NMSE dependency on carrier frequency for the model extracted at 3.55 GHz and 3.65 GHz

Figure 3.6 shows that changing the PAPR of the excitation signal has the least impact on the model's accuracy over a range of carrier frequencies compared to previous measurements. General tendencies are similar to those reported for Groups I and II. Modeling error keeps increasing while moving away from the model extraction frequency. The correlation between the model's frequency error rate of change and PAPR is −0.93 and −0.81 for models extracted at 3.55 GHz and 3.65 GHz. The correlation for the 3.55 GHz model is strong, but moving the frequency extraction point reduces the correlation, similar to the case of Group I measurements. Also, it can be observed that the shapes of the error curves are much more similar to each other than in the cases of Groups I and II. Moving the extraction frequency from 3.65 GHz to 3.55 GHz yielded the same results as in previous cases: a slight error drop at 3.3 GHz and a slight error increase at 3.8 GHz.

3.3. Parametric Memory Polynomial Modeling Results

A single set of measurements from Group I was used to test the modeling technique proposed in Section 2.3.2.

To select a model structure, an evaluation similar to one described earlier was conducted. The difference being that this NMSE was evaluated for a single data set at the edges of the operating range of the PA: 3.3 and 3.8 GHz. The results are presented in Figure 3.7.

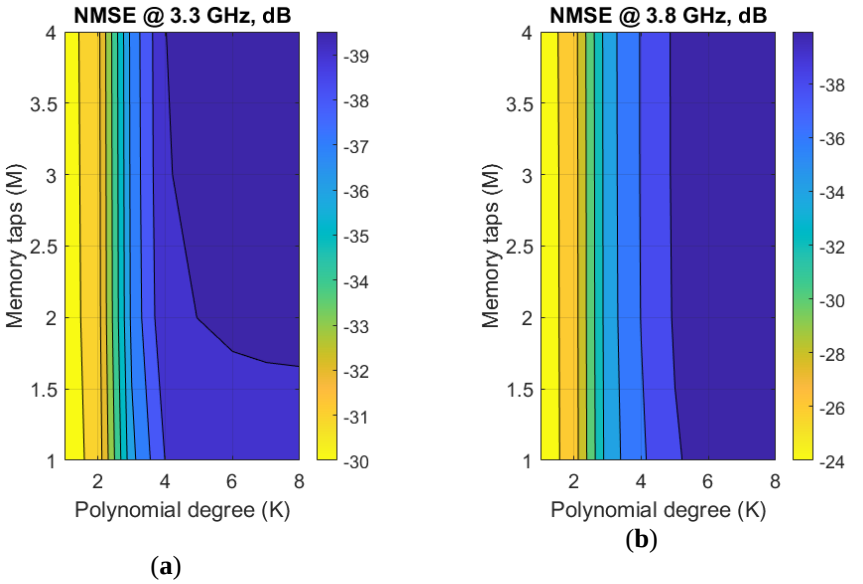

(**a**) (**b**)

Fig. 3.7. Modeling error with different M and K (a) for MP at 3.3 GHz, (b) for MP at 3.8 GHz

Figure 3.7 reveals that the optimal model order is frequency-dependent, and a memory depth of M = 2 is required at 3.3 GHz to capture significant memory effects. A memory depth of M = 1 suffices at 3.8 GHz, indicating quasi-static operation. A fixed structure (K = 5, M = 2) was selected as it represents the lowest common order that minimizes error across both frequencies. This results in a standard MP model with 10 coefficients and a parametric MP model requiring 10 continuous functions, $p_{km}(f_c)$.

Figure 3.8 presents the AM/AM and AM/PM characteristics of the PA measured at four distinct carrier frequencies. The results demonstrate that PA's behavior is significantly influenced by the carrier frequency. This dependence affects

not only the signal gain but also the phase relationship, a phenomenon likely attributable to the frequency-sensitive parasitic inductances and capacitances inherent to the PA's architecture.

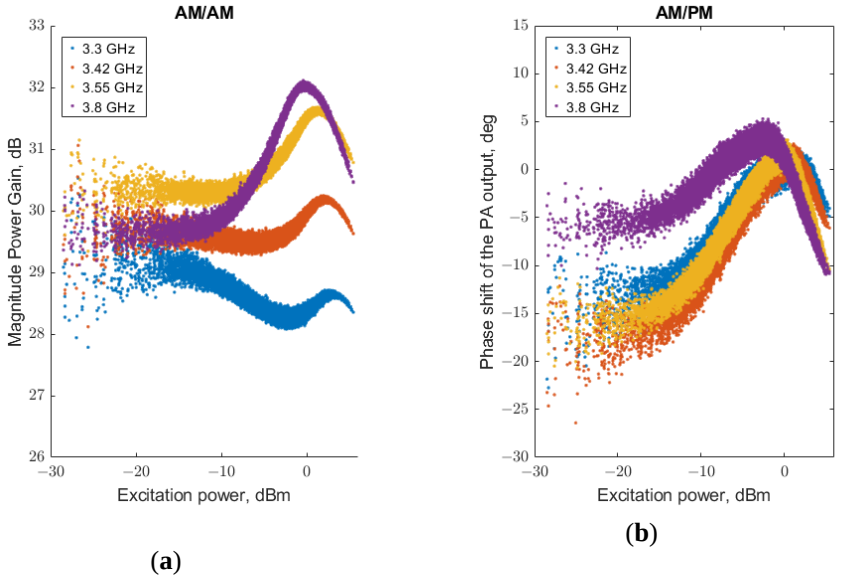

(**a**) (**b**)

Fig. 3.8 AM/AM (a), AM/PM (b) characteristics of the QPA9942 at 4 different carrier frequencies

To establish a performance baseline for comparison with the proposed PMP model, a standard MP model was extracted from a dataset at a single frequency. This model was then applied to data from different frequencies. The results of this baseline experiment are presented in Figure 3.10.

For a quantitative assessment of model performance across the frequency band, the average NMSE using Eq. (2.43) was computed for each test case. The resulting average error values for each single-frequency model are displayed in Figure 3.9. The analysis reveals that the model extracted at 3.3 GHz yields the largest average error across the band, while the model from 3.55 GHz yields the smallest error. This indicates that a single model extracted at 3.55 GHz performs, on average, approximately 9 dB better over the entire operational bandwidth than one extracted at 3.3 GHz.

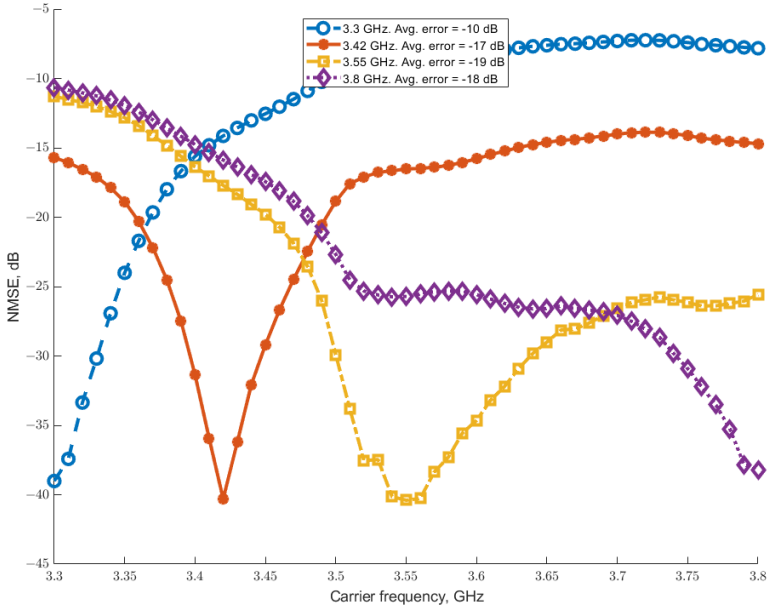

Fig. 3.9 Performance of the MP model, extracted at different carrier frequencies, over a range of carrier frequencies

A comparison of these modeling results with the transfer characteristics in Figure 3.8 elucidates the reason for this discrepancy. The AM/AM characteristic at 3.3 GHz exhibits a significantly lower average gain and a different shape compared to the response at 3.55 GHz. This suggests that the behavioral characteristics of the PA at 3.55 GHz are more representative of its average behavior across the operational bandwidth. Consequently, the 3.55 GHz response is selected as the baseline for subsequent comparison.

Figure 3.10 presents a performance comparison between the baseline single-frequency model and four PMP models. The PMP models were constructed using 3, 5, 7, and 11 interpolation points, distributed uniformly across the 3.3–3.8 GHz frequency range (with each point rounded to the nearest measured frequency value).

The results demonstrate a notable reduction in modeling error across the entire carrier frequency band compared to the baseline. The PMP model derived from 3 points achieves an average error reduction of approximately 14 dB. Increasing the interpolation order to 7 and 11 points yields further improvements, reducing the average error by 18 dB and 20 dB, respectively, relative to the baseline.

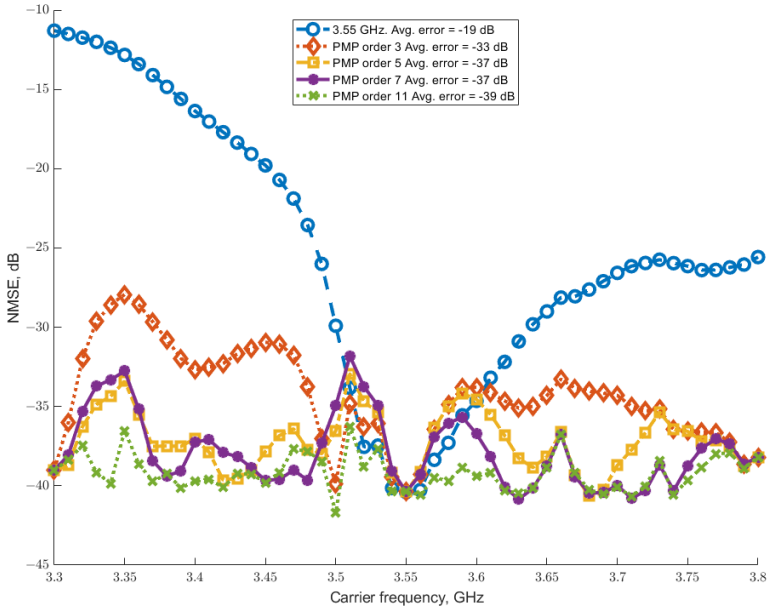

Fig. 3.10. Different order parametric MP performance over a range of carrier frequencies

To evaluate the impact of node distribution on modeling accuracy, the interpolation points were also allocated according to the Chebyshev node distribution. For the frequency range of 3.3–3.8 GHz, which is represented by measurement indices 1 through 51, the *k*-th node index (for $k = 0, 1, \ldots N$), is given by the formula:

$$f_k = round\left(\frac{51-1}{2}\cos\left(\frac{2N+1-2k}{2(N+1)}\pi\right)+\frac{1+51}{2}\right). \tag{3.4}$$

This distribution yields a higher density of nodes near the boundaries of the interpolation interval. Figure 3.11 compares the average NMSE achieved using a uniform (linear) point distribution against that of the Chebyshev distribution. The results demonstrate similar performance trends for both methods. The Chebyshev distribution exhibits a disadvantage at intermediate approximation orders. This finding indicates that the specific selection of interpolation points has an impact on the overall modeling error. For optimal performance, frequencies should be sampled across the entire operational bandwidth linearly.

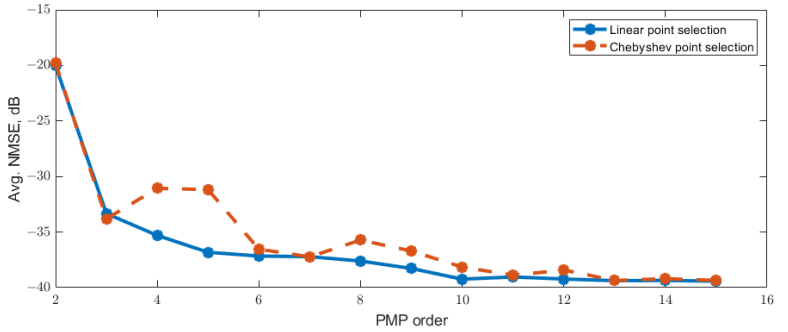

Fig. 3.11. Error dependency on the approximation order

Figure 3.11 also reveals a saturation effect in the modeling error, where its sensitivity to increases in approximation order diminishes. This phenomenon can be explained by examining the frequency-dependent behavior of the MP model coefficients, as illustrated in Figure 3.12, as well as initial model fitting accuracy across the band. Figure 3.12 shows the 6 continuous functions, $p_{km}(f_c)$, derived using 7 interpolation points, against the discrete coefficient values a_{km},b_{km}…c_{km} obtained from extracting standard MP models from all 51 individual datasets. The first row of Figure 3.12 displays three parameter functions from the first memory tap of the MP model. The second row displays three parameter functions from the second memory tap.

A visual analysis shows that the coefficients associated with the first memory tap (m = 0) are accurately captured by the smooth interpolating functions. In contrast, the coefficients of the second memory tap (m = 1) exhibit a poorer fit. This discrepancy arises because the underlying values of these higher-order coefficients demonstrate a more erratic, non-smooth dependence on frequency. The root cause of the non-smooth behavior observed is difficult to isolate. However, the most plausible explanation aligns with the phenomenon illustrated in Figure 3.7: the power amplifier exhibits different behavioral regimes at different carrier frequencies. Specifically, certain frequencies show noticeable memory effects, while at others, the PA operates in a quasi-static manner.

This frequency-dependent shift in dynamics presents a challenge for a fixed-model structure. The standard memory polynomial model, with its predetermined memory depth, is applied uniformly across all frequencies. Consequently, at frequencies where memory effects are pronounced, the second tap coefficients accurately capture real physical behavior. In contrast, at frequencies where the PA response is essentially static, these same coefficients lack a strong underlying physical correlation. Without sufficient excitation for these terms, the least square

error estimation process produces unstable and noisy solutions, manifesting as the observed non-smooth trajectories in the coefficient curves.

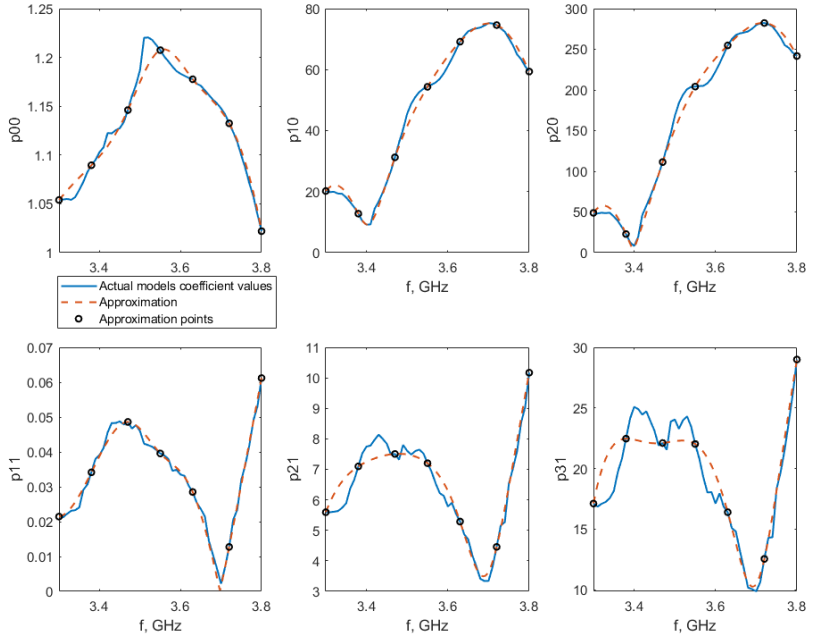

Fig. 3.12. p_{km} comparison against actual values of MP coefficients

The limitation of employing a fixed model structure is further illustrated in Figure 3.13, which depicts the performance of the PMP model trained on 11 nodes (marked by blue squares). The resulting model exhibits an oscillatory error across the frequency band. This oscillation is a direct consequence of the inherent variation in the accuracy of the underlying single-frequency MP models used for training.

As evidenced in the figure, the initial MP models demonstrate different levels of performance at their respective extraction frequencies; for instance, the model at 3.5 GHz achieves an NMSE of −41.7 dB, while the model at 3.35 GHz only achieves −36.5 dB. Since the parametric model is derived from these discrete points, their residual errors become anchor points that the PMP must interpolate, thereby propagating the initial inaccuracies into the continuous frequency-dependent function. This performance discrepancy arises because the chosen fixed model structure (K = 5, M = 2) is inherently better suited to characterizing the PA's behavior at some frequencies (e.g., 3.5 GHz) than at others (e.g., 3.35 GHz).

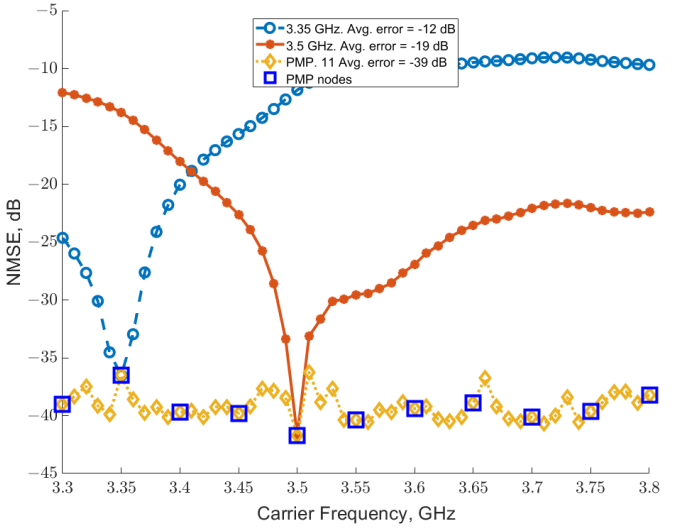

Fig. 3.13. Effect of the residual MP modeling error on the PMP accuracy

The saturation observed in Figure 3.11 is also attributable to the fitting errors of the initial single-frequency MP models. The mean NMSE of the 11 frequency points used for training, as shown in Figure 3.13, is −39.4 dB. This value aligns closely with the asymptotic limit of the PMP's performance in Figure 3.11. The parametrization process cannot surpass the average accuracy of the models upon which it is based, as it operates solely on their coefficients rather than on the original measurement data. The PMP's performance is, therefore, bounded by the quality of the initial MP estimations.

The fitted dependence of the frequency-averaged modeling error on the interpolation order is given in Figure 3.14. It was approximated using an exponential decay model of the form:

$$y = -38.6 + 140.8e^{-1.02x} \tag{3.5}$$

The obtained fit demonstrates a high level of agreement with the calculated data, as indicated by the coefficient of determination $R^2 = 0.969$. This confirms that the selected function adequately captures the observed error reduction trend. The fitted curve exhibits a clear asymptotic behavior, where the modeling error rapidly decreases for low interpolation orders and gradually stabilizes as the number of interpolation points increases. The asymptotic limit of the function approaches approximately −38.6 dB. This again confirms that further increasing the interpo-

lation order beyond a certain point does not significantly improve the overall accuracy, as the total error becomes dominated by the intrinsic modeling error of the underlying memory polynomial representation rather than the interpolation process itself.

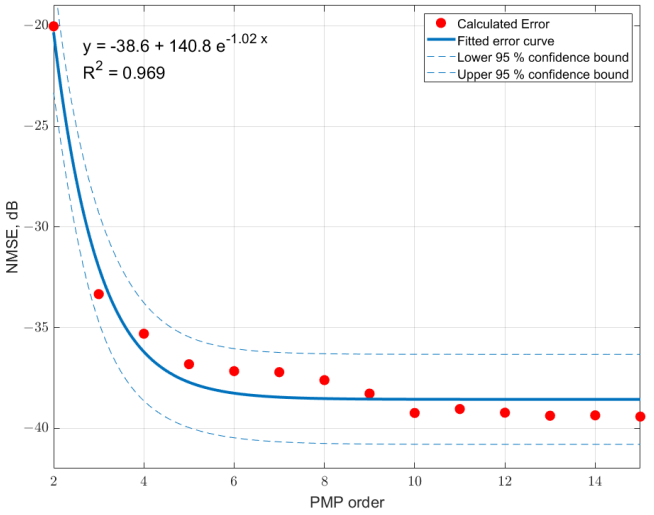

Fig. 3.14. Fitted error curve with 95% confidence bounds

Given that the accuracy of the proposed PMP model is contingent upon both the initial single-frequency MP model fitting accuracy and the error introduced by spline interpolation, it is instructive to analyze the contribution of each component separately.

Figure 3.15 illustrates this relationship by comparing the performance of the 11th-order PMP model against the fitting error of all initial MP models. The initial fitting error (represented by the dotted line) was determined by evaluating each of the 51 standard MP models exclusively at their own extraction frequency. The mean error of 51 standard MP models is determined to be −39.5. As expected, the PMP error curve intersects these points precisely at the anchor frequencies and exceeds them in the intervening regions, demonstrating the additive effect of interpolation error. The asymptotic limit of −38.6 determined in Figure 3.14 is approximately 1 dB higher than the mean error of 51 separate MP models. This is to be expected, as the limit of the interpolated model performance is still limited by the maximum achievable interpolation accuracy. After a certain number of points, adding additional interpolation points does not improve the overall model accuracy.

To isolate the interpolation error, Figure 3.15 shows the difference between the PMP error and the initial MP fitting error for approximation orders ranging from 2 to 15. This analysis reveals that the interpolation error component diminishes rapidly. This indicates that for orders ≥10, the overall PMP error is dominated almost entirely by the initial MP fitting inaccuracy, confirming that the interpolation itself reaches a plateau with a sufficient density of anchor points.

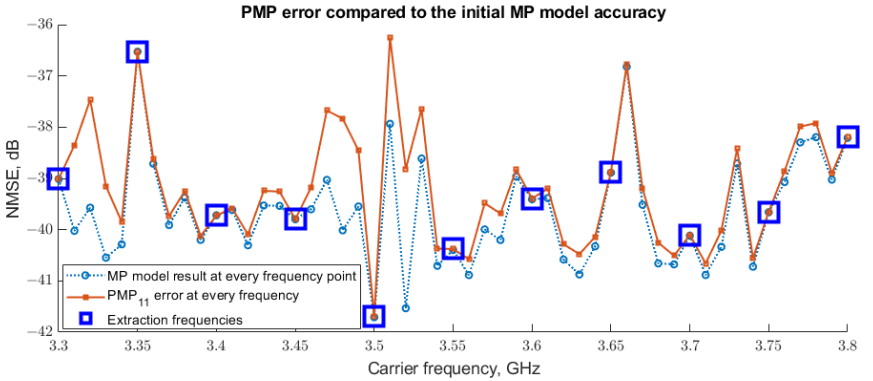

Fig. 3.15. PMP performance comparison to the initial model fitting over the frequency range

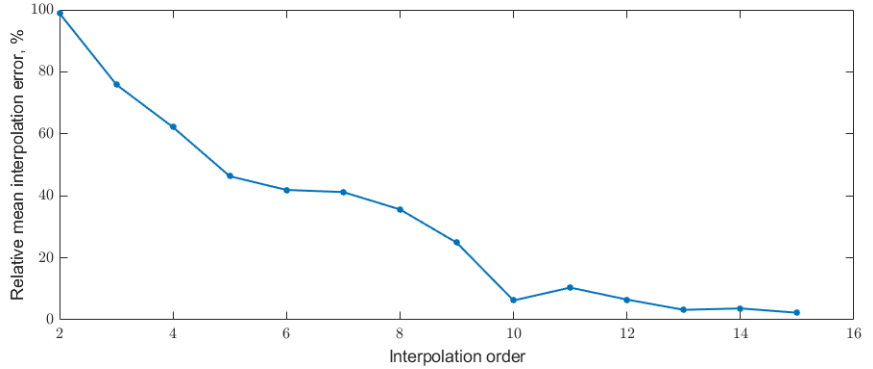

Fig. 3.16. Interpolation error percentage in the overall PMP model error

The standard MP model extracted at 3.55 GHz achieves an NMSE of approximately -40.4 dB at its extraction frequency. As illustrated in Figure 3.15, the PMP model derived from eleven frequencies nearly replicates this level of performance across the entire 3.3–3.8 GHz band, significantly improving frequency generalization. However, the result is not ideal, as evidenced by the oscillation in the

NMSE curve. This oscillation is in part caused by the coefficient interpolation error, as shown in Figure 3.12. The second part of this oscillation is directly attributable to the inherent discrepancy in the fitting accuracy of the initial single-frequency MP models across the operational band, as demonstrated by the varying error levels at the anchor points in Figure 3.13. The parametric model's ability to generalize is fundamentally constrained by the quality and consistency of these underlying local approximations.

This irregularity in the coefficient trajectories may suggest that the memory effects were not uniformly or sufficiently excited across the entire measurement bandwidth. This insufficient excitation could lead to instability and fluctuations in the LSE solution used for coefficient extraction. As initially demonstrated in Figure 3.7, the DUT exhibits both dynamic and quasi-static behavior under the identical excitation signal, depending on the carrier frequency. This mixed dynamic and quasi-static behavior poses a challenge for frequency-adaptive modeling, as the same excitation may activate different nonlinear mechanisms at different frequencies. Had the PA's behavior been consistently dynamic or consistently quasi-static across the band, the irregular, non-smooth nature of the coefficient curves would likely be far less severe or even non-existent. Furthermore, a more consistent behavioral response from the power amplifier across the operational frequency band would likely lead to a more uniform accuracy among the initial single-frequency MP models. This uniformity would, in turn, provide a more stable foundation for the parametric interpolation, likely enhancing the overall performance and predictive capability of the PMP model by eliminating the erratic coefficient behavior caused by the current performance discrepancies. As demonstrated in Figures 3.15−3.16, the interpolation error introduced by the parametric method effectively diminishes to a negligible level once the approximation order reaches ten. Beyond this point, the overall error of the PMP model is dominated solely by the inherent inaccuracy of the initial single-frequency MP models. These discrepancies in the initial model fitting are a direct consequence of the fundamental variance in the power amplifier's behavioral characteristics across the operational frequency band. Consequently, any further significant improvement in the overall PMP accuracy must be achieved by reducing this initial modeling discrepancy, rather than by increasing the interpolation order.

An important assumption underlying the proposed parametrization technique is that the power amplifier exhibits reasonably smooth behavioral characteristics across its operational bandwidth. This assumption of continuity validates the use of a uniform (linear) node distribution, as it minimizes the risk of missing significant nonlinear irregularities between the interpolation points. However, should the PA's response contain sharp discontinuities, this approach would be insufficient. In such scenarios, accurately capturing the PA's behavior would necessitate a substantially denser distribution of frequency nodes. Alternatively, an optimal

sampling strategy would require prior knowledge of the irregularity locations to place interpolation points strategically and ensure they are adequately captured by the model.

Considering the real-time deployment of the model, the proposed PMP modeling approach introduces a moderate increase in computational overhead during an offline training stage, while maintaining minimal runtime cost during deployment. Specifically, the training stage requires extracting N memory polynomial models, each using M input-output samples and producing P coefficients. This involves solving N least-squares regression problems, each with a computational complexity of $O(MP^2+P^3)$, resulting in an overall cost of $O(NMP^2+NP^3)$. Once the MP models are obtained, spline interpolation is performed for each of the P coefficients across the N frequency points to obtain frequency-dependent coefficient functions. For the calculation of the splines, this step is computationally efficient, with a total complexity of $O(PN)$, and it is performed only once. During online operation, the model requires evaluating these P spline functions at the current carrier frequency, which involves evaluating a cubic polynomial per coefficient and has negligible overhead $O(P)$. Therefore, the added computational cost of the proposed PMP technique is confined to the offline training phase, while its runtime complexity remains comparable to that of a standard memory polynomial model, allowing for possible integration into real-time digital predistortion systems.

The proposed parametric MP model is particularly suited for practical deployment in Low-Power Wide-Area Networks, such as Narrow Band Internet of Things and Long Range Wide Area Networks. These applications are characterized by their use of lower bandwidth transmissions and a critical requirement for long-range, energy-efficient communication. Devices in these networks must often operate across multiple fragmented frequency bands to connect to different gateways or adhere to regional regulations. The PMP's ability to provide a single, pre-trained model that generalizes across a wide frequency range, without the need for retraining or a bank of models, directly addresses this need for frequency agility.

3.4. Conclusions of the Third Chapter

1. Modeling error at a particular carrier frequency depends on the distance between said frequency and model extraction frequency, as well as the difference in linear gains between these two frequencies.
2. Modeling error rate of change did not show correlation for both tested frequencies on the excitation signal average power level and peak to average power level. Modeling error rate of change did, however, correlate

with the modulation bandwidth of the excitation signal, with the correlation coefficient 0.93 for the 3.55 GHz model and 0.99 for the 3.65 GHz model. An increase in excitation signal modulation bandwidth from 0.01 MHz to 2 MHz produced an increase in modeling error rate of change from 0.08 dB/MHz to 0.11 dB/MHz based on NMSE.

3. PMP model dependence of interpolation order was shown to fit an asymptotic exponential saturation function with a coefficient of determination R^2=0.96. Two main sources of PMP modeling error are interpolation error and initial model fitting error. The former is significantly reduced by an increasing number of interpolation points. An increase in interpolation points from 2 to 10 reduces the interpolation error ratio to the entire modeling error by ~90%. The initial model fitting error may be reduced only by reducing the underlying errors of the MP models used for interpolation.

General Conclusions

1. When a behavioral model extracted at one carrier frequency is applied at other carrier frequencies, the modeling error increases; this phenomenon is referred to as frequency-dependent modeling error. This error can be characterized using metrics describing its rate of change with respect to carrier frequency and the average modeling error over the analyzed frequency range. These metrics enable comparison of different behavioral models in terms of their generalization capability with respect to carrier frequency.
2. The modulation bandwidth of the excitation signal exhibits a direct correlation with the rate of change of frequency-dependent modeling error, with a correlation coefficient of 0.93 for the 3.55 GHz model and 0.99 for the 3.65 GHz model. Increasing the modulation bandwidth from 10 kHz to 2 MHz resulted in an increase in the error variation rate from 0.08 dB/MHz to 0.11 dB/MHz.
3. No significant correlation was observed between the average power of the excitation signal and the rate of change of frequency-dependent modeling error, nor was it detected only at one of the analyzed carrier frequencies. Similarly, no correlation was found between the peak-to-average power ratio of the excitation signal and the rate of change of the modeling error.

4. The average error of the proposed parameterized memory polynomial model follows an inverse exponential saturation function with respect to the interpolation order. It was determined that the average modeling error of the parameterized model using 11 interpolation points reaches −39 dB, which is equivalent to the average error obtained by separately extracting models at each carrier frequency. This indicates that the accuracy of the proposed method over a wide carrier frequency range is comparable to that of individually calibrated models for each frequency.
5. The total modeling error of the parameterized approach consists of two main components: interpolation error and baseline model fitting error. The interpolation error decreases significantly as the number of interpolation points increases; increasing the number of points from 2 to 10 reduces the relative contribution of interpolation error to the total modeling error by approximately 90%. The baseline model fitting error can only be reduced by improving the accuracy of the memory polynomial models used for interpolation.

References

Ali, S. N., Agarwal, P., Gopal, S., & Heo, D. (2019). Transformer-Based Predistortion Linearizer for High Linearity and High Modulation Efficiency in mm-Wave 5G CMOS Power Amplifiers. *IEEE Transactions on Microwave Theory and Techniques*, *67*(7), 3074–3087. https://doi.org/10.1109/TMTT.2019.2914900

Ballesteros, E., Perez, F., & Perez, J. (1988). Analysis and Design of Microwave Linearized Amplifiers Using Active Feedback. *IEEE Transactions on Microwave Theory and Techniques*, *36*(3), 499–504. https://doi.org/10.1109/22.3541

Barzdenas, V., & Navickas, R. (2009). The Design Aspects for Ultra Low-Power, Low-Noise 90 nm CMOS Charge Sensitive Amplifier for the Active Pixel Detector. *ACTA PHYSICA POLONICA A*, *115*(6). https://doi.org/10.12693/APhysPolA.115.1139

Bateman, A., Wilkinson, R. J., & Marvill, J. D. (1988). The application of digital signal processing to transmitter linearisation. In *8th European Conference on Electrotechnics, Conference Proceedings on Area Communication* (p.p. 64–67). https://doi.org/10.1109/EURCON.1988.11105

Beltagy, Y., Mitran, P., & Boumaiza, S. (2019). Direct Learning Algorithm for Digital Predistortion Training Using Sub-Nyquist Intermediate Frequency Feedback Signal. *IEEE Transactions on Microwave Theory and Techniques*, *67*(1), 267–277. https://doi.org/10.1109/TMTT.2018.2873331

Benedetto, S., Biglieri, E., & Daffara, R. (1979). Modeling and performance evaluation of nonlinear satellite links-a volterra series approach. *IEEE Transactions*

on Aerospace and Electronic Systems, *AES-15*(4), 494–507. https://doi.org/10.1109/TAES.1979.308734

Bennett, T. J., & Clements, R. F. (1974). Feedforward—an alternative approach to amplifier linearization. *Radio and Electronic Engineer*, *44*(5), 257–262. https://doi.org/10.1049/ree.1974.0067

Black, H. S. (1977). Inventing the negative feedback amplifier: Six years of persistent search helped the author conceive the idea "in a flash" aboard the old Lackawanna Ferry. *IEEE Spectrum*, *14*(12), 55–60. https://doi.org/10.1109/mspec.1977.6501721

Bondar, D., Lopez, N. D., Popovic, Z., & Budimir, D. (2010). Linearization of high-efficiency power amplifiers using digital baseband predistortion with iterative injection. *2010 IEEE Radio and Wireless Symposium, RWW 2010 - Paper Digest*, 148–151. https://doi.org/10.1109/RWS.2010.5434184

Braithwaite, R. N. (2008). Positive feedback pilot system for second loop control in a feedforward power amplifier. *IEEE Transactions on Circuits and Systems I: Regular Papers*, *55*(10), 3293–3305. https://doi.org/10.1109/TCSI.2008.923272

Braithwaite, R. N. (2011). General principles and design overview of digital predistortion. In F.-L. Luo (Ed.), *Digital Front-End in Wireless Communication and Broadcasting* (pp. 143–191). Cambridge University Press. https://doi.org/10.1017/CBO9780511744839.007

Braithwaite, R. N. (2015). A Comparison for a Doherty power amplifier linearized using digital predistortion and feedforward compensation. *2015 IEEE MTT-S International Microwave Symposium, IMS 2015*, 0–3. https://doi.org/10.1109/MWSYM.2015.7166827

Braithwaite, R. N., & Khanifar, A. (2013). High efficiency feedforward power amplifier using a nonlinear error amplifier and offset alignment control. *IEEE MTT-S International Microwave Symposium Digest*, *2*(2), 21–24. https://doi.org/10.1109/MWSYM.2013.6697336

Bremenson, C., & Lombard, D. (1975). Linearization of a satellite transmission channel in a time division multiple access system. In *3rd International Conference on Digital Satellite Communications* (pp. 144–151).

Bremenson, C., Palazo, M., & Neyer, R. (1980). Linearizing TWT amplifiers in satellite transponders, systems aspects and practical implementation. In *8th Communications Satellite Systems Conference* (pp. 80–89). https://doi.org/10.2514/6.1980-484

Briffa, M., & Faulkner, M. (1993). Dynamically biased cartesian feedback linearization. In *IEEE Vehicular Technology Conference* (pp. 672–675). https://doi.org/10.1109/VETEC.1993.508781

Bulusu, S. S. K. C., Shaiek, H., Roviras, D., & Zayani, R. (2014). Reduction of PAPR for FBMC-OQAM systems using dispersive SLM technique. In *2014 11th International Symposium on Wireless Communications Systems, ISWCS 2014 - Proceedings* (p.p. 568–572). https://doi.org/10.1109/ISWCS.2014.6933418

Cavers, J. K. (1990). Amplifier Linearization Using a Digital Predistorter with Fast Adaptation and Low Memory Requirements. *IEEE Transactions on Vehicular Technology*, *39*(4), 374–382. https://doi.org/10.1109/25.61359

Cavers, J. K. (1995). Adaptation Behavior of a Feedforward Amplifier Linearizer. *IEEE Transactions on Vehicular Technology*, *44*(I), 31–40. https://doi.org/10.1109/25.350267

Chang, Z. H., Zhang, Y., & Chen, H. C. (2024). Dynamic LSTM for 5G Signal Power Amplifier Behavioral Model. *IEEE Microwave and Wireless Technology Letters*, *34*(6), 683–686. https://doi.org/10.1109/LMWT.2024.3382888

Cho, K. J., Kim, J. H., & Stapleton, S. P. (2005). A highly efficient doherty feedforward linear power amplifier for W-CDMA base-station applications. *IEEE Transactions on Microwave Theory and Techniques*, *53*(1), 292–300. https://doi.org/10.1109/TMTT.2004.839341

Choi, H., Jeong, Y., Kim, C. D., & Kenney, J. S. (2010). Efficiency enhancement of feedforward amplifiers by employing a negative group-delay circuit. *IEEE Transactions on Microwave Theory and Techniques*, *58*(5 PART 1), 1116–1125. https://doi.org/10.1109/TMTT.2010.2045576

Dawson, J. L., & Lee, T. H. (2004). *Feedback linearization of RF power amplifiers*. Kluwer Academic Publishers.

Denny, H. W. (1970). *Linearization Techniques for Broadband Transistor Amplifiers*. 1–10. https://doi.org/10.1109/isemc.1970.7565371

Ding, L. (2004). Digital Predistortion of Power Amplifiers for Wireless Applications. In *School of Electrical and Computer Engineering*. Georgia Institute of Technology.

Ding, L., Zhou, G. T., Morgan, D. R., Ma, Z., Kenney, J. S., Kim, J., & Giardina, C. R. (2002). Memory polynomial predistorter based on the indirect learning architecture. *Conference Record / IEEE Global Telecommunications Conference*. https://doi.org/10.1109/glocom.2002.1188221

Eun, C., & Powers, E. J. (1997). A new volterra predistorter based on the indirect learning architecture. *IEEE Transactions on Signal Processing*, *45*(1), 223–227. https://doi.org/10.1109/78.552219

Fakhrutdinov, R. R., Zavyalov, S. A., Murasov, K. V., & Liashuk, A. N. (2020). Integrated cartesian feedback with automatic phase adjustment and power amplifier. *International Conference of Young Specialists on Micro/Nanotechnologies and Electron Devices, EDM*. https://doi.org/10.1109/EDM49804.2020.9153504

Faulkner, M. (2000). An automatic phase adjustment scheme for RF and cartesian feedback linearizers. *IEEE Transactions on Vehicular Technology*, *49*(3), 956–964. https://doi.org/10.1109/25.845112

Faulkner, M., & Briffa, M. A. (1996). Stability analysis of Cartesian feedback linearisation for amplifiers with weak nonlinearities. *IEE Proceedings - Communications*, *143*(4), 212–218. https://doi.org/10.1049/ip-com:19960614

Faulkner, M., & Briffa, M. A. (1998). Amplifier linearisation using RF feedback and feedforward techniques. *IEEE Transactions on Vehicular Technology*, *47*(1), 209–215. https://doi.org/10.1109/25.661047

Faulkner, M., Mattson, T., & Yates, W. (1990). Adaptive linearisation using predistortion. In *40th IEEE Conference on Vehicular Technology* (p.p. 35–40). https://doi.org/10.1109/VETEC.1990.110292

Feher, K. (1989). A New Generation of 90 Mb/s Systems: Bandwidth efficient, field tested 16-QAM. *IEEE Transactions on Broadcasting*, *35*(1), 23–30. https://doi.org/10.1109/11.18762

Ghannouchi, F. M., Hammi, O., & Helaoui, M. (2015a). *Behavioral Modeling and Predistortion of Wideband Wireless Transmitters*. Wiley. https://doi.org/10.1002/9781119004424

Ghannouchi, F. M., Hammi, O., & Helaoui, M. (2015b). *Behavioral Modeling and Predistortion of Wideband Wireless Transmitters*. Willey. https://doi.org/10.1002/9781119004424

Ghosh, A., Ratasuk, R., Mondal, B., Mangalvedhe, N., & Thomas, T. (2010). LTE-advanced: Next-generation wireless broadband technology. *IEEE Wireless Communications*, *17*(3), 10–22. https://doi.org/10.1109/MWC.2010.5490974

Gilabert, P. L., Cesari, A., Montoro, G., Bertran, E., & Dilhac, J. M. (2008). Multi-lookup table FPGA implementation of an adaptive digital predistorter for linearizing RF power amplifiers with memory effects. *IEEE Transactions on Microwave Theory and Techniques*, *56*(2), 372–384. https://doi.org/10.1109/TMTT.2007.913369

Gilabert, P. L., Vegas, D., Ren, Z., Montoro, G., Perez-Cisneros, J. R., Ruiz, M. N., Si, X., & Garcia, J. A. (2020). Design and Digital Predistortion Linearization of a Wideband Outphasing Amplifier Supporting 200 MHz Bandwidth. In *2020 IEEE Topical Conference on RF/Microwave Power Amplifiers for Radio and Wireless Applications, PAWR 2020* (p.p. 46–49). https://doi.org/10.1109/PAWR46754.2020.9035997

Gokceoglu, A., Ghadam, A., & Valkama, M. (2012). Steady-state performance analysis and step-size selection for LMS-adaptive wideband feedforward power amplifier linearizer. *IEEE Transactions on Signal Processing*, *60*(1), 82–99. https://doi.org/10.1109/TSP.2011.2169254

Gumber, K., & Rawat, M. (2017). A Modified Hybrid RF Predistorter Linearizer for Ultra Wideband 5G Systems. *IEEE Journal on Emerging and Selected Topics in Circuits and Systems*, *7*(4), 547–557. https://doi.org/10.1109/JETCAS.2017.2754422

Holz, W. (1984). An IF-Predistorter for TWTA-Linearization in 16 QAM Digital Radio. In *1984 14th European Microwave Conference* (p.p. 543–548). https://doi.org/10.1109/EUMA.1984.333375

Hu, Y., & Boumaiza, S. (2016). Power-Scalable Wideband Linearization of Power Amplifiers. *IEEE Transactions on Microwave Theory and Techniques*, *64*(5), 1456–1464. https://doi.org/10.1109/TMTT.2016.2550039

Ishihara, H., Hosoya, M., Otaka, S., & Watanabe, O. (2010). A 10-MHz signal bandwidth cartesian loop tansmitter capable of off-chip PA linearization. *IEEE Journal of Solid-State Circuits*, *45*(12), 2785–2793. https://doi.org/10.1109/JSSC.2010.2075290

Jung, Y., Fritzin, J., Enqvist, M., & Alvandpour, A. (2013). Least-squares phase predistortion of a +30 dBm class-D outphasing RF PA in 65 nm CMOS. *IEEE Transactions on Circuits and Systems I: Regular Papers*, *60*(7), 1915–1928. https://doi.org/10.1109/TCSI.2012.2230507

Kang, S., Baek, D., & Hong, S. (2017). A 5-GHz WLAN RF CMOS Power Amplifier with a Parallel-Cascoded Configuration and an Active Feedback Linearizer. *IEEE Transactions on Microwave Theory and Techniques*, *65*(9), 3230–3244. https://doi.org/10.1109/TMTT.2017.2691766

Kang, S., Sung, E. T., & Hong, S. (2018). Dynamic Feedback Linearizer of RF CMOS Power Amplifier. *IEEE Microwave and Wireless Components Letters*, *28*(10), 915–918. https://doi.org/10.1109/LMWC.2018.2861881

Katz, A., Wood, J., & Chokola, D. (2016). The Evolution of PA Linearization: From Classic Feedforward and Feedback Through Analog and Digital Predistortion. *IEEE Microwave Magazine*, *17*(2), 32–40. https://doi.org/10.1109/MMM.2015.2498079

Kenington, P. B. (1992). Efficiency of feedforward amplifiers. *IEE Proceedings, Part G: Circuits, Devices and Systems*, *139*(5), 591–593. https://doi.org/10.1049/ip-g-2.1992.0091

Kenington, P. B. (2000). *High Linearity RF Amplifier Design*. Artech House. https://doi.org/10.1049/ic:20000145

Kousai, S., Onizuka, K., Yamaguchi, T., Kuriyama, Y., & Nagaoka, M. (2012). A 28.3 mW PA-closed loop for linearity and efficiency improvement integrated in a + 27.1 dBm WCDMA CMOS power amplifier. *2012 IEEE International Solid-State Circuits Conference*, *47*(12), 2964–2973. https://doi.org/10.1109/JSSC.2012.2217833

Launay, F., Wang, Y., Toutain, S., Barataud, D., Nebus, J. M., & Quere, R. (2002). Nonlinear amplifier modeling taking into account HF memory frequency. *IEEE MTT-S International Microwave Symposium Digest*, *2*, 865–868. https://doi.org/10.1109/MWSYM.2002.1011767

Lenz, S. (1981). Linearization of Radio-Relay Transmitters by a Predistortion Upconverter. *1981 11th European Microwave Conference*, 209–214. https://doi.org/10.1109/EUMA.1981.332924

Li, H., Jiang, T., & Zhou, Y. (2011). An improved tone reservation scheme with fast convergence for PAPR reduction in OFDM systems. *IEEE Transactions on Broadcasting*, *57*(4), 902–906. https://doi.org/10.1109/TBC.2011.2169622

Li, J., Shu, R., & Gu, Q. J. (2017). A fully-integrated cartesian feedback loop transmitter in 65nm CMOS. *IEEE MTT-S International Microwave Symposium Digest*, 103–106. https://doi.org/10.1109/MWSYM.2017.8058770

Li, J., Xu, Z., & Gu, Q. J. (2019). A 21dBm-OP1dB 20.3%-Efficiency -131.8dBm/Hz-Noise X-Band Cartesian-Error-Feedback Transmitter with Fully Integrated Power Amplifier in 65nm CMOS. *Digest of Technical Papers - IEEE International Solid-State Circuits Conference*, 452–454. https://doi.org/10.1109/ISSCC.2019.8662474

Li, J., Xu, Z., Hong, W., & Gu, Q. J. (2018). A Low-Noise Cartesian Error Feedback Architecture. *IEEE Transactions on Circuits and Systems I: Regular Papers*, *65*(3), 1133–1142. https://doi.org/10.1109/TCSI.2017.2761394

Li, P., Song, Z., Lin, J., Wei, M., Guo, F., Jia, W., Wang, Z., & Chi, B. (2016). A reconfigurable digital polar transmitter with open-loop phase modulation for Sub-GHz applications. *IEEE International Symposium on Industrial Electronics*, *2016-Novem*, 1158–1161. https://doi.org/10.1109/ISIE.2016.7745058

Liu, J., Arslan, H., Dunleavy, L. P., Webster, A., & Paviol, J. (2004). Impact of carrier frequency dependent power amplifier behavior on 802.11a WLAN system. In *Conference Proceedings - 7th European Conference on Wireless Technology, ECWT2004* (p.p. 289–292).

Liu, J., Cao, C., Li, Y., Tan, T., Chen, D., Huang, Z., & Li, X. (2019). A broadband CMOS high efficiency power amplifier with large signal linearization. In *Asia-Pacific Microwave Conference Proceedings, APMC*, *2019-Decem*(1) (1155–1157). https://doi.org/10.1109/APMC46564.2019.9038796

Liu, X., Lv, G. sheng, Wang, D. han, Chen, W. hua, & Ghannouchi, F. M. (2020). Energy-efficient power amplifiers and linearization techniques for massive MIMO transmitters: a review. *Frontiers of Information Technology and Electronic Engineering*, *21*(1), 72–96. https://doi.org/10.1631/FITEE.1900467

Liu, X., Zhai, J., Zhang, Z., Ning, D., Chen, P., & Yu, C. (2024). High-Precision Digital Predistortion for Sub-6-GHz GaN Power Amplifiers Excited by a Signal with 400-MHz Modulation Bandwidth. *IEEE Microwave and Wireless Technology Letters*, *34*(5), 552–555. https://doi.org/10.1109/LMWT.2024.3372025

Macchiarella, G., Iommi, R., Galli, S., & Delzanno, A. (2004). Study and experiment of a novel class of error envelope feedback linearizers. In *European Microwave Conference*, *2* (p.p. 1057–1060).

Morgan, D. R., Ma, Z., Kim, J., Zierdt, M. G., & Pastalan, J. (2006). A generalized memory polynomial model for digital predistortion of RF power amplifiers. *IEEE Transactions on Signal Processing*, *54*(10), 3852–3860. https://doi.org/10.1109/TSP.2006.879264

Muhonen, K. J., Kavehrad, M., & Krishnamoorthy, R. (2000). Look-up table techniques for adaptive digital predistortion: a development and comparison. *IEEE Transactions on Vehicular Technology*, *49*(5), 1995–2002. https://doi.org/10.1109/25.892601

Ock, S., Song, H., & Gharpurey, R. (2015). A Cartesian feedback-feedforward transmitter IC in 130nm CMOS. *Proceedings of the Custom Integrated Circuits Conference*, *2015-Novem*, 31–34. https://doi.org/10.1109/CICC.2015.7338483

Parsons, K. J., & Kenington, P. B. (1994). The Efficiency of a Feedforward Amplifier with Delay Loss. *IEEE Transactions on Vehicular Technology*, *43*(2), 407–412. https://doi.org/10.1109/25.293658

Perez, F., Ballesteros, E., & Perez, J. (1985). Linearisation of microwave power amplifiers using active feedback networks. *Electronics Letters*, *21*(1), 9–10. https://doi.org/10.1049/el:19850006

Petrovic, V., & Gosling, W. (1979). Polar-loop transmitter. *Electronics Letters*, *15*(10), 286–288. https://doi.org/10.1049/el:19790204

Pothecary, N. (1999). *Feedforward Linear Power Amplifiers*. Artech House.

Psaltis, D., Sideris, A., & Yamamura, A. A. (1988). A Multilayered Neural Network Controller. *IEEE Control Systems Magazine*, *8*(2), 17–21. https://doi.org/10.1109/37.1868

Raab, F. H., Asbeck, P., Cripps, S., Kenington, P. B., Popović, Z. B., Pothecary, N., Sevic, J. F., & Sokal, N. O. (2002). Power amplifiers and transmitters for RF and microwave. *IEEE Transactions on Microwave Theory and Techniques*, *50*(3), 814–826. https://doi.org/10.1109/22.989965

Remley, K. A. (2003). Multisine excitation for ACPR measurements. *IEEE MTT-S International Microwave Symposium Digest*, *3*, 2141–2144. https://doi.org/10.1109/MWSYM.2003.1210586

Rostomyan, N., Jayamon, J. A., & Asbeck, P. M. (2018). 15 GHz Doherty Power Amplifier with RF Predistortion Linearizer in CMOS SOI. *IEEE Transactions on Microwave Theory and Techniques*, *66*(3), 1339–1348. https://doi.org/10.1109/TMTT.2017.2772785

Seidel, H., Beurrier, H. R., & Friedman, A. N. (1968). Error-Controlled High Power Linear Amplifiers at VHF. *Bell System Technical Journal*, *47*(5), 651–722. https://doi.org/10.1002/j.1538-7305.1968.tb00057.x

Smith, A. M., & Cavers, J. K. (1998). A Wideband Architecture for Adaptive Feedforward Linearization. In *IEEE Vehicular Technology Conference* (p.p. 2488–2492). https://doi.org/10.1109/VETEC.1998.686207

Steve C. Cripps. (2006). *RF Power Amplifiers for Wireless Communications* (2nd ed.). Artech House.

Stewart, R. D., & Tusuriba, F. F. (1988). Predistortion Linearisation of Amplifiers for UHF Mobile Radio. In *1988 18th European Microwave Conference* (p.p. 1017–1022). https://doi.org/10.1109/EUMA.1988.333943

Sun, J., Li, B., & Chia, Y. W. M. (1999). A Novel CDMA power amplifier for high efficiency and linearity. In *IEEE Vehicular Technology Conference* (p.p. 2044–2047). https://doi.org/10.1109/vetecf.1999.797296

Tian, T., Zhao, Y., Dou, Y., Yu, C., & Qiu, J. (2015). A novel concurrent tri-band digital predistortion for broadband signals. In *European Microwave Week 2015:*

“Freedom Through Microwaves”, EuMW 2015 - Conference Proceedings; 2015 45th European Microwave Conference Proceedings, EuMC (p.p. 1136–1139). https://doi.org/10.1109/EuMC.2015.7345968

Tsai, J. H., Wu, C. H., Yang, H. Y., & Huang, T. W. (2011). A 60 GHz CMOS power amplifier with built-in pre-distortion linearizer. *IEEE Microwave and Wireless Components Letters*, *21*(12), 676–678. https://doi.org/10.1109/LMWC.2011.2171929

Vasjanov, A., & Barzdenas, V. (2016). 74 Original scientific paper MIDEM Society 0.18 μm CMOS power amplifier architecture comparison for a wideband Doherty configuration. *Journal of Microelectronics, Electronic Components and Materials*, *46*(2), 74–79.

Vasjanov, A., & Barzdenas, V. (2018). A Review of Advanced CMOS RF Power Amplifier Architecture Trends for Low Power 5G Wireless Networks. *Electronics,7*(11). https://doi.org/10.3390/ELECTRONICS7110271

Vasjanov, A., & Barzdenas, V. (2020). 0.13 μm CMOS Traveling-Wave Power Amplifier with On- and Off-Chip Gate-Line Termination. *Electronics*, *9*(1). https://doi.org/10.3390/ELECTRONICS9010133

Vuolevi, J. H. K., Rahkonen, T., & Manninen, J. P. A. (2001). Measurement technique for characterizing memory effects in RF power amplifiers. *IEEE Transactions on Microwave Theory and Techniques*, *49*(8), 1383–1389. https://doi.org/10.1109/22.939917

Wang, S., Hussein, M. A., Venard, O., & Baudoin, G. (2017). Impact of the normalization gain of digital predistortion on linearization performance and power added efficiency of the linearized power amplifier. In *European Microwave Week 2017: “A Prime Year for a Prime Event”, EuMW 2017 - Conference Proceedings; 47th European Microwave Conference, EuMC 2017* (p.p. 1050–1053). https://doi.org/10.23919/EuMC.2017.8231026

Whartenby, J. C., & Wolkstein, H. J. (1985). Predistortion Linearizer Using GaAs Dual-Gate MESFET for TWTA and SSPA Used in Satellite Transponders. *IEEE Transactions on Microwave Theory and Techniques*, *33*(12), 1479–1488. https://doi.org/10.1109/TMTT.1985.1133243

Wolf, N., Heinrich, W., & Bengtsson, O. (2016). A Novel Model for Digital Predistortion of Discrete Level Supply-Modulated RF Power Amplifiers. *IEEE Microwave and Wireless Components Letters*, *26*(2), 146–148. https://doi.org/10.1109/LMWC.2016.2517445

Wood, J. (2014). *Behavioral Modeling and Linearization of RF Power Amplifiers*. Artech House.

Wood, J. (2017). System-level design considerations for digital pre-distortion of wireless base station transmitters. *IEEE Transactions on Microwave Theory and Techniques*, *65*(5), 1880–1890. https://doi.org/10.1109/TMTT.2017.2659738

Xiang, Y. B., & Wang, G. M. (2009). Doherty power amplifier with feedforward linearization. In *APMC 2009 - Asia Pacific Microwave Conference 2009* (p.p. 1621–1624). https://doi.org/10.1109/APMC.2009.5384357

Xie, X., Hui, M., Liu, T., & Zhang, X. (2018). Hybrid linearization of broadband radio-over-fiber transmission. *IEEE Photonics Technology Letters*, *30*(8), 692–695. https://doi.org/10.1109/LPT.2018.2812745

Xu, K. (2021). Silicon electro-optic micro-modulator fabricated in standard CMOS technology as components for all silicon monolithic integrated optoelectronic systems *. *Journal of Micromechanics and Microengineering*, *31*(5), Article 054001. https://doi.org/10.1088/1361-6439/abf333

Yamauchi, K., Mori, K., Nakayama, M., Itoh, Y., Mitsui, Y., & Ishida, O. (1996). A novel series diode linearizer for mobile radio power amplifiers. *IEEE MTT-S International Microwave Symposium Digest*, 831–834. https://doi.org/10.1109/mwsym.1996.511066

Yang, S., & Hanzo, L. (2015). Fifty years of MIMO detection: The road to large-scale MIMOs. *IEEE Communications Surveys and Tutorials*, *17*(4), 1941–1988. https://doi.org/10.1109/COMST.2015.2475242

Yang, W. Y., Cao, W., Kim, J., Park, K. W., Park, H. H., Joung, J., Ro, J. S., Ro, H. L., Hong, C. H., & Hong, C. H. (2020). Applied Numerical Methods Using MATLAB. *Applied Numerical Methods Using MATLAB*, 1–641. https://doi.org/10.1002/9781119626879

Yu, C., Tang, Q., & Liu, Y. (2019). A novel indirect learning digital predistortion architecture only with in-phase component. *Asia-Pacific Microwave Conference Proceedings*, *APMC*, *2018-Novem*, 995–997. https://doi.org/10.23919/APMC.2018.8617557

Zayani, R., Shaiek, H., & Roviras, D. (2019). Ping-Pong Joint Optimization of PAPR Reduction and HPA Linearization in OFDM Systems. *IEEE Transactions on Broadcasting*, *65*(2), 308–315. https://doi.org/10.1109/TBC.2018.2855664

Zhao, Z., Na, W., Gongal-Reddy, V. M. R., & Zhang, Q. (2017). Multi-band behavioral modeling of power amplifier using carrier frequency-dependent time delay neural network model. *2017 IEEE MTT-S International Conference on Numerical Electromagnetic and Multiphysics Modeling and Optimization for RF, Microwave, and Terahertz Applications, NEMO 2017*, 82–84. https://doi.org/10.1109/NEMO.2017.7964194

Zheng, S., & Luong, H. C. (2013). A CMOS WCDMA/WLAN digital polar transmitter with AM replica feedback linearization. *IEEE Journal of Solid-State Circuits*, *48*(7), 1701–1709. https://doi.org/10.1109/JSSC.2013.2253405

Zhou, D., & DeBrunner, V. (2007). A novel adaptive nonlinear predistorter based on the direct learning algorithm. *IEEE Transactions on Signal Processing*, *55*(1), 120–133. https://doi.org/10.1109/icc.2004.1312941

List of Scientific Publications by the Author on the Topic of the Dissertation

Papers in the Reviewed Scientific Journals

Borel, A., Barzdėnas, V., & Vasjanov, A. (2021). Linearization as a Solution for Power Amplifier Imperfections: A Review of Methods. *Electronics*, *10*(9), Article 1073. https://doi.org/10.3390/electronics10091073

Borel, A., Barzdėnas, V., & Vasjanov, A. (2025). Behavioral Modeling of RF Power Amplifiers with Carrier-Frequency Generalization Using Interpolated Memory Polynomials. *Applied Sciences*, *15*(18), Article 9899. https://doi.org/10.3390/app15189899

Papers in Other Editions

Borel, A., & Barzdėnas, V. (2020) A Review of the Basic Power Amplifier Linearization Methods. In *2020 IEEE Open Conference of Electrical, Electronic and Information Sciences (eStream)* (pp. 1–4). IEEE. https://doi.org/10.1109/eStream50540.2020.9108866.

Summary in Lithuanian

Įvadas

Problemos formulavimas

Galios stiprintuvai (GS) yra neatsiejama šiuolaikinių ryšių sistemų dalis, reikalinga signalams patikimai perduoti, tačiau ji sukelia netiesinius iškraipymus, kurie prastina signalo kokybę, ypač prie didžiausio efektyvumo ribos. Šie efektai dažniausiai švelninami taikant tokius linearizavimo metodus kaip skaitmeninis išankstinis iškraipymas (DPD), kuris remiasi elgsenos modeliais, tokiais kaip atminties daugianariai (AD). Tačiau tokie modeliai paprastai taikomi tik jų apskaičiavimo sąlygomis, jų tikslumas prastėja pakeitus stiprintuvo veikimo sąlygas. Tai apriboja šiuolaikinių komunikacinių sistemų, tokių kaip kognytyvinis radijas, taikymą. Šioje disertacijoje sprendžiama ši problema, siūlant elgsenos modeliavimo metodą, kuris parametrizuoja AD modelio koeficientus kaip nešlio dažnio funkcijas – taip leidžiant vienam modeliui veikti ištisiniame nešlio dažnių diapazone. Orientuojantis į vidutinės galios (1–2 W) stiprintuvus 5G FR-1 juostoje (410–7125 MHz) ir naudojant standartinius ryšio signalus, kurių juostos plotis yra nuo 10 kHz iki 2 MHz, šiuo darbu siekiama pagerinti modelio apibendrinamumą, sumažinti pakartotinio charakterizavimo poreikį ir įgalinti efektyvų linearizavimą adaptyviosiose komunikacinėse sistemose.

Darbo aktualumas

Ši disertacija tiria, ar galios stiprintuvo modelis, apskaičiuotas esant vienam nešlio dažniui, gali būti taikomas kitiems nešlio dažniams, sprendžiant esminį iššūkį

šiuolaikinėse plačiajuostėse belaidėse ryšio sistemose, tokiose kaip kognityvinis radijas. Darbe vertinamos modeliavimo paklaidos, atsirandančios keičiantis nešlio dažniui, ir siūlomi metodai joms mažinti, apibūdinant nuo dažnio priklausomą GS elgseną bei įgalinant modelį veikti keliuose darbo taškuose. Šiame darbe pristatomos metrikos skirtos šiems netikslumams kiekybiniškai įvertinti, ir nagrinėjami kompensavimo metodai, gerinantys modelio apibendrinamumą. Parodoma, kad, tinkamai įvertinus dažninius iškraipymus, GS netiesiškumo kompensavimas gali būti efektyvesnis, sumažinant pakartotinio charakterizavimo poreikį ir projektavimo sąnaudas.

Lietuvoje GS buvo anksčiau tyrinėti doc. dr. Aleksandro Vasjanovo ir prof. dr. Vaidoto Barzdėno. Jų indėlis apima įvairios PA architektūros tyrimus (Vasjanov & Barzdėnas, 2016, 2018) ir bendruosius CMOS stiprintuvų lustų projektavimo tyrimus (Barzdėnas & Navickas, 2009; Vasjanov & Barzdėnas, 2020).

Tyrimo objektas

Tyrimo objektas – radijo dažnių galios stiprintuvo elgsenos modelis.

Darbo tikslas

Disertacijos tikslas – sukurti ir patvirtinti dažnio pokyčiams atsparią radijo dažnio galios stiprintuvų elgsenos modeliavimo metodiką, užtikrinančią tikslų veikimo prognozavimą plačiame nešlio dažnių diapazone.

Darbo uždaviniai

Norint pasiekti disertacijos tikslą, reikia atlikti šias užduotis:

1. Suprojektuoti galios stiprintuvo charakterizavimo sistemą, kuri leistų išmatuoti sužadinimo ir atsako signalus bei panaudoti juos galios stiprintuvo elgsenos modeliui sudaryti.
2. Ištirti ir pasiūlyti metrikas, leidžiančias įvertinti nešlio dažnio pokyčio įtaką galios stiprintuvo modelio tikslumui.
3. Eksperimentiškai ištirti sužadinimo signalo charakteristikų įtaką galios stiprintuvų modelio paklaidai, atsirandančiai dėl kintančio nešlio dažnio.
4. Pasiūlyti metodus, skirtus nešlio dažnio pokyčio sukuriamai modeliavimo paklaidai mažinti.

Tyrimų metodika

Šiame darbe taikomi šie metodai:

1. Literatūros apžvalga leido nustatyti pagrindines GS linearizavimo tendencijas ir apibrėžti tyrimo problemą.
2. GS buvo eksperimentiškai charakterizuotas naudojant nuolatinės bangos ir moduliuotus signalus.
3. Išmatuoti duomenys buvo panaudoti elgsenos modeliams apskai taikant polinominę regresiją.

4. MATLAB buvo naudojamas atliekant matavimų valdymą, duomenų apdorojimą, modeliavimą ir vizualizaciją.

Darbo mokslinis naujumas

Rengiant disertaciją gauti šie elektros ir elektronikos inžinerijos mokslo krypčiai nauji rezultatai:

1. Sukurta pusiau automatinė sistema GS charakterizuiti plačiame darbo sąlygų diapazone.
2. Pasiūlytas metodas nuo nešlio dažnio priklausančiai modeliavimo paklaidai kiekybiškai įvertinti ir jos kitimui skirtinguose dažniuose analizuoti.
3. Sukurtas skirtingų dažnių GS įėjimo–išėjimo signalų duomenų rinkinys, skirtas pakartojamai paklaidų analizei užtikrinti.
4. Pasiūlytas parametrizuotas atminties daugianario modelis su nuo dažnio priklausančiais koeficientais, kuris pasiekia esant atskiriems dažniams apskaičiuotų modelių tikslumą ir reikalauja mažiau matavimų ir mažesnių modelio apskaičiavimo sąnaudų.

Darbo rezultatų praktinė reikšmė

Siūloma parametrizuoto atminties daugianario modeliavimo metodika galios stiprintuvams reikalauja mažiau skaičiavimų ir matavimų, palyginti su tradiciniu atminties daugianarių modeliavimo metodu, nes ji leidžia elgsenos modeliui veikti, kai nešlio dažniai skiriasi nuo tų, kuriems esant buvo atliktas modelio apskaičiavimas. Sukurta metodika gali padėti sutrumpinti matavimų ir kalibravimo laiką telekomunikacijų sistemose, veikiančiose kintamais nešlio dažniais, išlaikant deterministinį skaičiavimų sudėtingumą, tinkamą galios stiprintuvui linearizuoti realiu laiku, taikant skaitmeninį išankstinį iškraipymą. Skirtingai nuo metodų, kuriems reikia didelių matavimo duomenų kiekių, siūlomu parametrizavimo metodu pasiekiamas panašus modeliavimo tikslumas, naudojant kur kas mažiau matavimo duomenų rinkinių.

Ginamieji teiginiai

1. Sukurtas galios stiprintuvų elgsenos modelių apibendrinamumo nešlio dažnio atžvilgiu įvertinimo metodas, leidžiantis nustatyti dažninės modelio paklaidos kitimo greitį, analizuoti atminties daugianario modelio paklaidos priklausomybę nuo nešlio dažnio ir įvertinti sužadinimo signalo parametrų – vidutinės galios, moduliacijos juostos pločio ir PAPR – įtaką.
2. Eksperimentiškai nustatyta, kad modeliavimo paklaidos kitimas keičiantis nešlio dažniui yra stipriai koreliuotas su sužadinimo signalo moduliacijos juostos pločiu (koreliacijos koeficientas iki 0,99), o vidutinė signalo galia ir PAPR reikšmingos koreliacijos neturi arba koreliacija pastebima tik esant vienam iš testuotų dažnių, o didėjant dažnio nutolimui nuo modelio išskyrimo taško, paklaida didėja. 3,3–3,8 GHz galios stiprintuvo atveju, padidinus sužadinimo signalo moduliacijos juostos plotį nuo 0,01 MHz iki 2 MHz, modeliavimo paklaidos kitimo greitis dažnio atžvilgiu padidėjo nuo 0,08 dB/MHz iki 0,11 dB/MHz, remiantis normalizuotos vidutinės kvadratinės paklaidos metrika.

3. Pasiūlytas parametrizuotas atminties daugianario modelis su nuo dažnio priklausančiais koeficientais leidžia tiksliai aproksimuoti galios stiprintuvo elgseną 3,3–3,8 GHz ruože, pasiekiant apie −39 dB vidutinę NMSE paklaidą naudojant 10 ir daugiau interpoliacijos taškų, o tai atitinka rezultatą, gautą modeliuojant stiprintuvą 51 skirtingu nešlio dažniu, todėl stipriai sumažinamas matavimų poreikis.

Darbo rezultatų aprobavimas

Disertacijos tema paskelbtos dvi publikacijos, referuojamos *Clarivate Analytics Web of Science* duomenų bazėje (Borel et al., 2021; Borel et al., 2025).

Vienas straipsnis publikuotas konferencijų rinkinyje (Borel & Barzdėnas, 2020).

Tyrimo rezultatai buvo pristatyti keturiose mokslinėse konferencijose:

- Open International Conference of Electrical, Electronic and Information Sciences (eStream), 2020, Vilnius, Lietuva.
- Open International Conference of Electrical, Electronic and Information Sciences (eStream), 2021, Vilnius, Lietuva.
- Workshop on Microwave Theory and Techniques in Wireless Communications (MTTW), 2021, Ryga, Latvija.
- Conference of Doctoral Students and Young Scientists (FizTeCh), 2025, Vilnius, Lietuva.

Disertacijos struktūra

Disertaciją sudaro įvadas, 3 skyriai ir bendrosios išvados. Darbo apimtis – 99 puslapiai, neskaitant santraukos lietuvių kalba; tekste yra 54 numeruotos formulės, 38 paveikslai, 10 lentelių. Rengiant disertaciją naudotasi 100 literatūros šaltinių.

Padėka

Mokslinis darbas niekada nebūna tik autoriaus nuopelnas. Taip ir šis darbas nebūtų įmanomas be kitų pagalbos ir palaikymo.

Norėčiau padėkoti moksliniam vadovui prof. dr. Vaidotui Barzdėnui už nuolatinį ir visapusišką palaikymą ruošiant disertaciją, ilgas valandas, praleistas diskutuojant, ir už tai, kad padėjo nenuleisti rankų kelio viduryje.

Nuoširdžią padėką išreiškiu kolegai doc. dr. Aleksandrui Vasjanovui už kūrybiškumą ir patirtį, kurių įtaką šiam darbui sunku pervertinti.

Dėkoju tėvams Daivai ir Valerijui bei sesutei Jolantai už kantrybę ir palaikymą.

Dėkoju mylimai Rusnei ir jos tėvams Sigitui ir Rasai už palaikymą.

Galiausiai dėkoju Lietuvos visuomenei, kurios darbas sudaro sąlygas mokslo ir studijų plėtrai.

1. Literatūros apie galios stiprintuvų linearizavimo metodus apžvalga

Šiame skyriuje apžvelgiama mokslinė literatūra apie galios stiprintuvų linearizavimo metodus. Apžvalgoje taikytas istorinis dėstymo metodas, t. y. apžvalga pradedama nuo ankščiausių žinomų linearizavimo metodų įgyvendinimo ir pereinama prie šiuolaikinėje pramonėje taikomų metodų.

Išskiriamos trys pagrindinės linearizavimo metodų grupės: tiesioginio koregavimo (angl. *feedforward*), grįžtamojo ryšio, išankstinio signalo iškraipymo (angl. *predistortion*). Apžvelgiama šių metodų istorinė vystymosi raida. Anksčiausiai pritaikytas buvo tiesioginio koregavimo metodas, vėliau jį iš dalies pakeitė grįžtamojo ryšio ir išankstinio iškraipymo metodai. Apžvelgiamos kiekvieno metodo stiprybės ir silpnybės. Tiesioginio koregavimo metodas reikalauja ypač didelio grandinės komponentų verčių tikslumo, bet dėl jo stabilumo nekyla sunkumų, būdingų grįžtamojo ryšio metodui. Grįžtamojo ryšio metodas pasižymį aukštu netiesinių iškraipymų slopinimu, bet taip pat sumažina stiprintuvo stiprinimo koeficientą ir nėra tinkamas aukštų dažnių signalams dėl atsirandančio nestabilumo. Išankstinio iškraipymo metodas skirstomas į dvi dalis: skaitmeninį išankstinis iškraipymą (DPD) ir analoginį išankstinį iškraipymą. Tiek vienu, tiek kitu metodu bandoma sudaryti grandinę, kurios perdavimo charakteristika būtų atvirkštinė linearizuojamo stiprintuvo atžvilgiu. Šiuolaikiniuose galios stiprintuvo linearizavimo metodų tyrimuose dominuoja DPD metodas.

Apžvelgiamas DPD veikimo principas ir problemos, sprendžiamos taikant metodą. DPD linearizacijos metodo problematika suskirstoma į dvi grupes: linearizuojamo galios stiprintuvo grandinės charakterizavimą ir atvirkštinės perdavimo charakteristikos grandinės projektavimą. Išskiriamas vienas pagrindinių stiprintuvo charakterizavimo metodų – elgsenos modeliavimas. Elgsenos modeliavimas – tai modeliavimo būdas, kai stiprintuvo charakteristikos aproksimuojamos matematiniu modeliu, naudojant sužadinimo ir atsako signalų imtis. Išskiriama elgsenos modeliavimo problema – modelis nėra apibendrintas ir paprastai taikomas tik tokiomis sąlygomis, kuriomis jis buvo gautas. Šios sąlygos apima: sužadinimo signalo formą, vidutinį galios lygį, pikinės ir vidutinės galios santykį, moduliacijos plotį, nešlio dažnį ir t. t. Nustatomas disertacijos darbo tikslas – ištirti būdus, leisiančius apibendrinti elgsenos modelio veikimą skirtingais nešlio dažniais, ir pasiūlyti metodus, skirtus mažinti šiai paklaidai.

Atlikus literatūros analizę iškelta ši hipotezė: Nuo nešlio dažnio priklausanti modeliavimo paklaida gali būti nustatyta charakterizuojant galios stiprintuvą tuo pačiu sužadinimo signalu esant įvairiems nešlio dažniams. Gauta paklaida gali būti sumažinta taikant tam tikrą modelio parametrizavimo formą

2. Galios stiprintuvo elgsenos modelio apskaičiavimo metodika

Šiame skyriuje nagrinėjamas elgsenos modelio sudarymo procesas. Projektuojama pusiau automatinė matavimų sistema. Aptariamos matavimų įrangos konfigūravimo ir sinchronizavimo problemos. Analizuojamos galios stiprintuvo elgsenos modelio sudarymo skaičiavimo procedūros.

Norint sudaryti galios stiprintuvo matematinį modelį, reikalingi stiprintuvo sužadinimo signalas ir galimybė išmatuoti stiprintuvo atsaką į šį sužadinimą. Abu šie reikalavimai gali būti įvykdyti naudojant įvairius matavimo prietaisus ir metodus. Tiksli matavimų įrangos konfigūracija priklauso nuo modeliuojamo netiesiškumo rūšies ir laipsnio. Netiesiškumo laipsnis reiškia skaičių k (S2.1) eilutėje:

$$y(t) = \sum_{k=1}^{K} a_k x^k(t), \qquad \text{(S2.1)}$$

čia $y(t)$ yra tiriamos sistemos atsakas, $x^k(t)$ – sužadinimo signalas, a_k – atitinkamo eilutės nario svorio koeficientas. Elgsenos modelio sudarymas yra (S2.1), arba kitos daugianario lygčių sistemos, sprendimas a_k atžvilgiu. a_k vertė yra proporcinga galios stiprintuvo sukuriamų netiesinių iškraipymų stiprumui. Netiesinių iškraipymų stiprumas priklauso nuo galios stiprintuvo veikimo zonos. Veikiant giliai netiesinėje zonoje, netoli soties veikos režimo, netiesiniai iškraipymai yra didesni, todėl a_k yra didesnis. Norint, kad galios stiprintuvas patektų giliau į netiesinio veikimo zoną, žadinimo signalas turi turėti didesnę vidutinę galią. Konkrečios vidutinės galios vertės priklauso nuo modeliuojamų galios stiprintuvo parametrų, tačiau bendra išvada yra tokia: norint modeliuoti aukštesnės eilės netiesinius iškraipymus, sužadinimo signalas turi siekti atitinkamą vidutinės galios lygį, kad galios stiprintuvas būtų pakankamai arti soties veikos režimo. Pavyzdžiui, jei norima apibūdinti penktos eilės galios stiprintuvo netiesinius iškraipymus, reikia užtikrinti pakankamai didelę $x(t)$ vidutinę galią, kad $y^5(t)$ būtų galima atskirti nuo matavimo prietaiso triukšmo lygio.

Be vidutinės galios, galios stiprintuvui charakterizuoti svarbi $x(t)$ forma. Pavyzdžiui, pasirinkus $x(t) = A\cos(\omega t)$ ir apskaičiavus (S2.1) sistemos atsaką, galima pastebėti, kad harmoniniu virpesiu sužadintas stiprintuvas generuoja nuolatinės įtampos poslinkį bei eilę harmonikų, kurių dažniai yra 2ω, 3ω, 4ω ir t. t. Kadangi realiuose komunikacinėse sistemose šie signalo komponentai gali būti lengvai išfiltruoti, jų charakterizavimas nėra labai svarbus. Žymiai svarbesni yra signalo komponentai, atsirandantys šalia praleidžiamų dažnių juostos, kurių išfiltruoti neįmanoma. Pavyzdžiui, pasirinkus $x(t) = A_1\cos(\omega_1 t) + A_2\cos(\omega_2 t)$, ir apskaičiavus (S2.1) sistemos atsaką, galima aptikti papildomus signalo komponentus, kurių dažniai yra $2\omega_1 - \omega_2$ ir $2\omega_2 - \omega_1$. Šie galios stiprintuvo sukurti signalo komponentai vadinami *intermoduliaciniais iškraipymais.* Jų charakterizavimas yra ypač svarbus modeliuojant galios stiprintuvus.

Dar kartą pažvelgus į (S2.1) matyti, kad momentinė atsako vertė priklauso tik nuo dabartinės momentinės žadinimo signalo vertės. Tokia elgsena vadinama statine arba atminties neturinčia elgsena. Be statinės, galios stiprintuvai taip pat pasižymi dinamine elgsena. Dinaminė galios stiprintuvo elgsena nusako jo momentinės atsako vertės priklausomybę ne tik nuo momentinės, bet ir nuo ankstesnių sužadinimo signalo verčių. Tai dar vadinama stiprintuvo atminties efektu. Galios stiprintuvų atminties efektai atsiranda dėl tranzistoriaus sandūros kaitimo ir aušinimo bei elektrinių efektų jo maitinimo

ir suderinimo grandinėse. Norint įtraukti galios stiprintuvo dinaminę elgseną, reikalingi kiti modeliai nei (S2.1).

Sukurti skaitmeniniu būdu moduliuotą signalą, kuris sužadintų tiek statinę, tiek dinaminę galios stiprintuvo elgesenas, galima naudojant vektorinį signalų generatorių (VSG). Be to, šiuo atveju nepakanka elementarios spektrinės analizės, nes ji suteikia informacijos tik apie atsako signalo galios amplitudę. Skaitmeninės moduliacijos schemos, tokios kaip QPSK arba QAM, moduliuoja tiek nešlio amplitudę, tiek ir fazę. Norint sėkmingai demoduliuoti informaciją iš skaitmeniniu būdu moduliuojamo nešlio, patogiausia rinktis vektorinį signalų analizatorių. Atsižvelgiant į tai, S2.1 paveiksle pateikta bandymų stendo struktūra.

Struktūrą sudaro tiesioginis ir tiriamo įrenginio signalų keliai. *SignalHound VSG60A* naudojamas signalui generuoti, o *Tektronix RSA5106A* signalui analizuoti. Ir VSG, ir VSA yra prijungti prie kompiuterio, kuriame veikia MATLAB programinė įranga. Duotam sužadinimo signalui $x(n)$ atliekami keli matavimai, keičiant $x_{\mathrm{RF}}(t)$ nešlio dažnį. Tiesioginis signalo kelias iš VSG į VSA leidžia palyginti $x_{\mathrm{RF}}(t)$ ir $y_{\mathrm{RF}}(t)$, taip palyginant galios stiprintuvo įėjimą su jo išėjimu. Kiekvienam sužadinimo signalui $x(n)$ gaunamas signalų rinkinys:

$$x_{\mathrm{CF}_1}(n), y_{\mathrm{CF}_1}(n), x_{\mathrm{CF}_2}(n), y_{\mathrm{CF}_2}(n), \ldots x_{\mathrm{CF}_l}(n), y_{\mathrm{CF}_l}(n). \qquad \text{(S2.2)}$$

Išmatuoti sužadinimo ir atsako signalai naudojami galios stiprintuvo modeliui apskaičiuoti. Signalo kelyje esantis ateniuatorius užtikrina, kad atliekant matavimus signalų analizatorius nepasiektų soties būsenos ir nebūtų pažeistas.

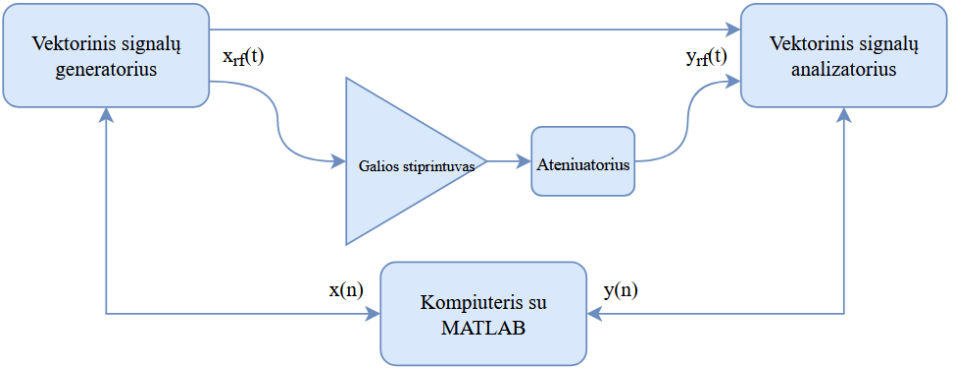

S2.1 pav. Pasiūlyta bandymo stendo struktūra

Kaip jau buvo aptarta anksčiau, (S2.1) lygtyje pateiktas modelis gali apibūdinti tik statinę galios stiprintuvo elgseną, kuri neatspindi galios stiprintuvo atsako į plačiajuosčius moduliuotus signalus, naudojamus šiuolaikiniuose ryšių tinkluose. Norint apibūdinti ir statinę, ir dinaminę galios stiprintuvo elgsenas, reikia naudoti kitus modelius. Vienas iš

labiausiai paplitusių galios stiprintuvo modelių yra atminties daugianaris, kuris yra *Volterra* eilutės supaprastinimas:

$$y(n)=\sum_{k=1}^{K}\sum_{m=0}^{M}a_{km}x(n-m)\left|x(n-m)\right|^{k-1}, \tag{S2.3}$$

čia $y(n)$ yra *n*-oji atsako signalo imtis, *M* − daugianario funkcijos atminties gylis, *K* − daugianario funkcijos laipsnis, $x(n-m)$ – sužadinimo signalo imtis, uždelsta pagal atminties gylį. Palyginus lygtis (S2.1) ir (S2.3), galima įsitikinti, kad pastaroji apima dabartinio atsako signalo imties priklausomybę ne tik nuo dabartinio, bet ir nuo kelių ankstesnių sužadinimo signalo imčių. Tai leidžia į modelį įtraukti ir statinę, ir dinaminę elgsenas.

Žinoma, kad kiekvieno stiprintuvo elgsena priklauso nuo jo konkretaus veikimo dažnio ir kad elgsenos modelis turėtų būti apskaičiuojamas tokiomis sąlygomis, kurios būtų panašios į realaus veikimo sąlygas. Tačiau yra atvejų, kai telekomunikacinė sistema veikia įvairiais nešlio dažniais, pasirinkdama vieną ar kitą priklausomai nuo situacijos tinkle, pavyzdžiui, kognityvinio radijo atveju. Tokiais atvejais elgsenos modeliavimas turėtų apimti kelių nešlio dažnių charakteristikas vienu metu, dėl to modelis turi būti apskaičiuotas didesniam nešlio dažnių skaičiui arba visais atvejais turėtų būti naudojamas modelis, išskirtas esant vienam nešlio dažniui. Pastaruoju atveju, tikėtina, pablogėtų modeliavimo tikslumas. Priklausomai nuo modeliavimo tikslumo sumažėjimo dydžio, reikėtų rinktis iš dviejų blogybių: mažesnio modelio skaičiavimo efektyvumo arba didesnių modeliavimo paklaidų.

Modeliavimo paklaida, susidaranti taikant modelį esant kitiems nešlio dažniams, nei buvo naudoti atliekant jo apskaičiavimą, vadinama dažnine modelio paklaida. Metrika, pagal kurią būtų galima įvertinti šios paklaidos dydį, yra modelio dažninės paklaidos kitimo greitis:

$$FE_{\text{roc}}=\frac{\left|e_{fn}-e_{fk}\right|}{\left|f_n-f_k\right|}, \tag{S2.4}$$

čia e_{fn} ir e_{fk} yra normalizuotos modeliavimo paklaidos decibelais, apskaičiuotos atitinkamai esant dažniams f_n ir f_k, FE_{roc} − dažninės paklaidos kitimo greitis, matuojamas dB/Hz. Šis rodiklis leidžia įvertinti, kaip greitai didėja dažninė modelio paklaida, besikeičiant nešlio dažniui. Pavyzdžiui, NMSE vertės −44 dB ir −33 dB apskaičiuotos atitinkamai esant 3,6 GHz ir 3,7 GHz nešlio dažniams. Taip gautume

$$\text{FE}_{\text{roc}}=\frac{\left|-33\text{ dB}-\left(-44\text{ dB}\right)\right|}{\left|3{,}6\text{ GHz}-3{,}7\text{ GHz}\right|}\cong\frac{0{,}11\text{ dB}}{\text{MHz}}. \tag{S2.5}$$

Matavimai atliekami esant tam tikrai sužadinimo signalo konfigūracijai. Kontroliuojamas sužadinimo signalo charakteristikų keitimas leistų patikrinti minėtų charakteristikų įtaką dažninės paklaidos kitimo greičiui. Tai leistų padaryti bendrą išvadą apie sužadinimo signalo charakteristikų įtaką galios stiprintuvo elgsenos modelio dažninei paklaidai.

Dažninei modelio paklaidai sumažinti siūloma tokia parametrizavimo metodika:

$$y_{\mathrm{PMP}}(n, f_c) = \sum_{k=0}^{K-1} \sum_{m=0}^{M-1} p_{km}(f_c)\, x(n-m) \left| x(n-m) \right|^k , \tag{S2.6}$$

čia įprastiniai atminties daugianario koeficientai a_{km} pakeičiami nuo nešlio dažnio priklausančiomis funkcijomis $p_{km}(f_c)$. Šios parametrinės funkcijos išvedamos panaudojant (S2.2) lygtyje nurodytus sužadinimo ir atsako signalų rinkinius. Kiekvienam surinktam signalų rinkiniui apskaičiuojamas atminties daugianario (S2.3) modelis:

$$\mathrm{A}(f_{c_0}) = \begin{pmatrix} a_{00} \\ a_{01} \\ \vdots \\ a_{km} \end{pmatrix}, \quad \mathrm{A}(f_{c_1}) = \begin{pmatrix} b_{00} \\ b_{01} \\ \vdots \\ b_{km} \end{pmatrix}, \quad \ldots \quad \mathrm{A}(f_{c_N}) = \begin{pmatrix} c_{00} \\ c_{01} \\ \vdots \\ c_{km} \end{pmatrix}. \tag{S2.7}$$

Gauti modelių koeficientai interpoliuojami nešlio dažnių ašyje.

Metodas remiasi prielaidą, kad galios stiprintuvo elgsena modeliuojamame dažnių diapazone yra pakankamai pastovi (t. y. nėra rezonansų ar kitų priežasčių, lemiančių staigius elgsenos pokyčius). Esant šiai sąlygai, parametrinis atminties daugianario modelis gali tiksliai prognozuoti stiprintuvo elgseną bet kuriuose dažniuose tiriamo diapazono ribose, įskaitant ir netirtus dažnius tarp matavimų taškų.

Siūlomo parametrizuoto modelio veikimas vertinamas naudojant pagal nešlio dažnį vidurkinamą normalizuotos vidutinės kvadratinės paklaidos (NMSE) metriką. Jeigu modeliuojama N skirtingų nešlio dažnių,

$$e_{\mathrm{avg}} = 10 \times \log_{10}\left(\frac{1}{N} \sum_{f_c=1}^{N} e(f_c)\right). \tag{S2.8}$$

Kiekvienam nagrinėjamo diapazono nešlio dažniui apskaičiuojama normalizuota vidutinė kvadratinė paklaida, lyginant modelio spėjimą su atitinkamu išmatuotu galios stiprintuvo signalu. Šios nuo nešlio dažnio priklausančios paklaidos reikšmės vėliau vidurkinamos per visą nešlio modeliuojamą dažnių diapazoną, o gauta vidutinė paklaida galiausiai išreiškiama decibelais. Ši procedūra leidžia gauti vieną skaliarinę metriką, apibūdinančią tikėtiną modeliavimo paklaidos dydį modeliuojamame dažnių diapazone.

3. Nešlio dažnio pokyčio poveikio tyrimas galios stiprintuvo modelio tikslumui

Šiame skyriuje daugiausia dėmesio skiriama eksperimento struktūrai, rezultatams ir diskusijoms.

Eksperimentai atlikti naudojant QPA9942 galios stiprintuvą. Tai didelio efektyvumo InGaP/GaAs HBT technologijos tranzistorinis stiprintuvas. Jo darbinis dažnių diapazonas, kaip nurodo gamintojas, yra 3300−3800 MHz. Skelbiama, kad įrenginio PAE yra ~25 %, kai išėjimo galia +28 dBm. Dažnių diapazonas yra 5G FR−1 ribose, stiprintuvas sureguliuotas taip, kad veiktų esant apytiksliai ~1 W išėjimo galios. Taip pat skelbiama,

kad stiprintuvas yra „paruoštas linearizacijai“, t. y. būdamas pradinėse būsenos jis nėra linearizuotas. Platus darbinių dažnių diapazonas taip pat svarbus šio darbo tikslui. Gamintojas nepateikia jokios informacijos apie vidinę įrenginio struktūrą, tik pažymi, kad tai yra 3 pakopų įrenginys. Stiprintuvas išbandytas naudojant gamintojo pateiktą spausdintinę plokštę.

Tikrieji veikimo parametrai gali skirtis nuo gamintojo pateiktų parametrų dėl daugybės priežasčių. Norint suprasti, kaip prietaisas veikia konkrečiomis šiame eksperimente nustatytomis sąlygomis, buvo atlikti kai kurie pagrindiniai matavimai. Pirmiausia buvo išmatuota stiprinimo priklausomybė nuo išėjimo galios verčių ir PAE priklausomybė nuo išėjimo galios verčių. Efektyvumo kreivė, kaip ir tikėtasi, auga kartu su išėjimo galios verte. Esant +28 dBm išėjimo galiai išmatuotas PAE yra apie 27−28 %, t. y. didesnis, nei nurodo gamintojas. Neatitikimą gali lemti PAE sklaida priklausomai nuo stiprintuvo temperatūros. Stiprinimo priklausomybė nuo išėjimo galios lygio rodo netiesinę stiprintuvo elgseną. Stiprinimo koeficiento svyravimas išmatuotos galios diapazone siekia apie 1 dB.

Dažninei modeliavimo paklaidai turi įtakos tiesinio stiprinimo pokytis modeliuojamame dažnių diapazone. Todėl buvo išmatuota tiriamo stiprintuvo dažninė-amplitudinė charakteristika. Matavimas buvo atliekamas per visą galios stiprintuvo darbo dažnių juostos plotį, t. y. 3300−3800 MHz. Matavimo žingsnis buvo 10 MHz. Vidutinė įėjimo signalo galia buvo −15 dBm. Taip užtikrinama, kad rezultatatams didžiausią įtaką turi tiesinė GS stiprinimo dalis, išvengiant netiesinio stiprinimo įtakos. Apskaičiuotos vidutinės kreivės atveju bendras stiprinimo svyravimas yra ~1,54 dB. Išmatuotas skirtumas viršyja matavimo neabirėžtį tarp generatoriaus ir analizatoriaus – jos dydis apytiksliai yra ±0,71 dB. Didžiąją stiprintimo pokyčio dalį lemia jo vertė 3,3−3,5 GHz dažnių diapazone. Šiame diapazone stiprinimas turi apytiksliai tiesinę teigiamą priklausomybę nuo dažnio. Diapazone 3,5−3,8 GHz pasireiškia mažesnė priklausomybė nuo dažnio. Šiame diapazone stiprinimo svyravimas siekia apie 0,3 dB, o tai yra mažiau nei minėtas matavimo neapibrežtumas. Pateiktos charakteristikos įtaka matavimams ir siūlomi būdai jai sumažinti bus parodyti toliau.

Siekiant ištirti galios stiprintuvo elgseną esant skirtingiems sužadinimo signalams, iš viso buvo atlikta dvylika matavimų. Matavimai suskirstyti į tris grupes, kurių kiekvienoje yra keturi matavimų rinkiniai. Grupės sudarytos atsižvelgiant į kiekvieno matavimo metu keičiamą sužadinimo signalo parametrą. Yra trys parametrai, kurių poveikis tiriamas: vidutinė galia, moduliacijos dažnių juostos plotis, aukščiausios ir vidutinės galios santykis (angl. *peak-to-average power ratio,* PAPR). Du iš trijų parametrų kiekvienoje grupėje yra pastovūs, o vienas keičiamas.

Kiekvienas matavimas susideda iš kelių dalinių matavimų, atliekamų esant įvairiems nešlio dažniams. Nešlio dažnių diapazonas pasirinktas taip, kad apimtų visą QPA9942 veikimo dažnių juostos plotį, t. y. 3300−3800 MHz. Matavimų žingsnis pasirinktas toks pat, koks buvo naudojamas apibūdinant stiprintuvo dažninę-amplitudinę charakteristiką, t. y. 10 MHz. Taip gaunamas 51 unikalus sužadinimo ir atsako signalų rinkinys kiekvienam kiekvienos grupės matavimui. Vieno iš šių dalinių matavimų duomenys pasirenkami modeliui apskaičiuoti. Kiti 50 dalinių matavimų duomenys naudojami kaip modelio koeficientų patikros duomenys. Kiekvienam daliniam matavimui apskaičiuojama

normalizuota vidutinė kvadratinė paklaida (NMSE). Gautos paklaidos nubraižomos priklausomai nuo nešlio dažnio, kuriam esant jos buvo nustatytos.

S3.1 paveiksle pateikiami II grupės rezultatai. Modeliams apskaičiuoti buvo naudojami esant 3,55−3,65 GHz dažniams surinkti duomenys. 3,65 GHz atveju NMSE yra mažiausia netoli modelio apskaičiavimo dažnio, t. y. 3,65 GHz. Paklaida didėja didėjant dažnių skirtumui tarp apskaičiavimo dažnio ir dalinio matavimo dažnio. S3.1 lentelėje pateikiami paklaidos vertės svyravimai ir paklaidos kitimo greitis. Modelio veikimas esant 3,8 GHz ir 3,3 GHz dažniams gerokai skiriasi. Viena iš priežasčių gali būti anksčiau aptartas tiesinio stiprinimo skirtumas. Kita priežastis gali būti atstumas tarp 3,65 GHz ir 3,3 GHz taškų, jis yra lygus 350 MHz, o atstumas nuo 3,65 GHz iki 3,8 GHz yra 150 MHz. Modelio paklaidos kitimo greitis nešlio dažnio atžvilgiu rodo stiprią teigiamą koreliaciją, lygią 0,9865 Pearsono koreliacijos koeficiento.

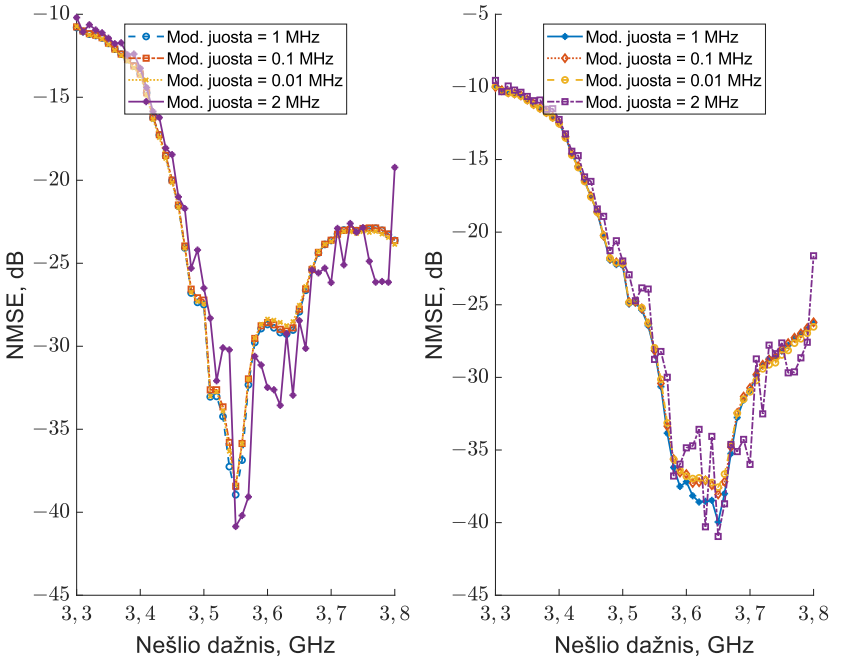

S3.1 pav. II grupės NMSE priklausomybė nuo nešlio dažnio modeliuose, apskaičiuotuose esant 3,55 ir 3,65 GHz dažniui

S3.1 lentelė. II grupės rezultatas, kai modelis apskaičiuojamas esant 3,65 GHz dažniui

Mod. plotis, MHz	NMSE 3,65 GHz, dB	NMSE 3,3 GHz, dB	NMSE 3,8 GHz, dB	NMSE ROC, dB/MHz
2	−40,95	−9,55	−21,63	0,1093

S3.1 lentelės pabaiga

Mod. plotis, MHz	NMSE 3,65 GHz, dB	NMSE 3,3 GHz, dB	NMSE 3,8 GHz, dB	NMSE ROC, dB/MHz
1	−39,96	−10,05	−26,23	0,0885
0,1	−38,06	−10,01	−26,23	0,0796
0,01	−37,56	−9,96	−26,52	0,0762

S3.2 lentelė. II grupės rezultatas, kai modelis apskaičiuojamas esant 3,55 GHz dažniui

Mod. plotis, MHz	NMSE 3,55 GHz, dB	NMSE 3,3 GHz, dB	NMSE 3,8 GHz, dB	NMSE ROC, dB/MHz
2	−40,86	−10,12	−19,23	0,1046
1	−38,94	−10,79	−23,63	0,0869
0,1	−38,43	−10,76	−23,63	0,0849
0,01	−38,38	−10,72	−23,86	0,0843

Rezultatų palyginimas rodo, kad modelio apskaičiavimo taško perkėlimas į 3,55 GHz neturėjo reikšmingos įtakos NMSE 3,3 ir 3,8 GHz taškuose. Tai patvirtina S3.2 lentelėje pateikti duomenys. Iš tiesų, abiem atvejais rezultatai išliko palyginti artimi. Paklaidų kreivių forma S3.1 paveiksle išliko panaši esant abiem dažniams. Abiem atvejais kairioji kreivės dalis pasiekia gerokai didesnes vertes. Tai patvirtina prielaidą, kad tiesinio stiprinimo skirtumai esant skirtingiems nešlio dažniams daro didelę įtaką gautoms modelio paklaidoms. 3,55 GHz modelio atveju taip pat matyti tiesioginė koreliacija tarp klaidos kitimo greičio ir signalo moduliacijos pločio, nors šiuo atveju koreliacija yra silpnesnė − 0,9257 Pearsono koreliacijos koeficiento. I ir III grupių rezultatai nepasižymi minėta koreliacija, o kitos tendencijos sutampa su jau aptartomis, todėl toliau santraukoje tai nagrinėjama nebus.

Vienas iš I grupės duomenų rinkinių buvo panaudotas išbandyti antrame skyriuje pasiūlytai parametrizavimo metodikai. Modelio struktūra parinkta palyginus vidutines NMSE vertes stiprintuvo dažnių juostos intervalo kraštuose: 3,3 GHz ir 3,8 GHz. Analizės rezultatas parodė, kad optimalios modelio struktūros netiesinio laipsnio dydis K = 5, o atminties gylis M = 2.

S3.2 paveiksle pateikiamas standartinio atminties daugianario modelio, apskaičiuoto esant 3,55 GHz dažniui, ir keturių parametrizuotų modelių veikimo palyginimas. Parametrizuoti modeliai buvo sudaryti naudojant 3, 5, 7 ir 11 interpoliacijos taškų, tolygiai paskirstytų 3,3–3,8 GHz dažnių ruože (kiekvieną tašką suapvalinant iki artimiausios išmatuotos dažnio reikšmės). Gauti rezultatai rodo reikšmingą dažninės modelio paklaidos sumažėjimą visame nešlio dažnių diapazone, palyginti su baziniu modeliu. Iš 3 taškų sudarytas parametrizuotas atminties dauginario modelis leidžia pasiekti vidutinį paklaidos sumažėjimą – apie 14 dB. Padidinus interpoliacijos taškų skaičių iki 7 ir 11 taškų, gaunami

dar geresni rezultatai – vidutinė paklaida sumažėja atitinkamai 18 dB ir 20 dB, palyginti su pradiniu atminties daugianariu modeliu.

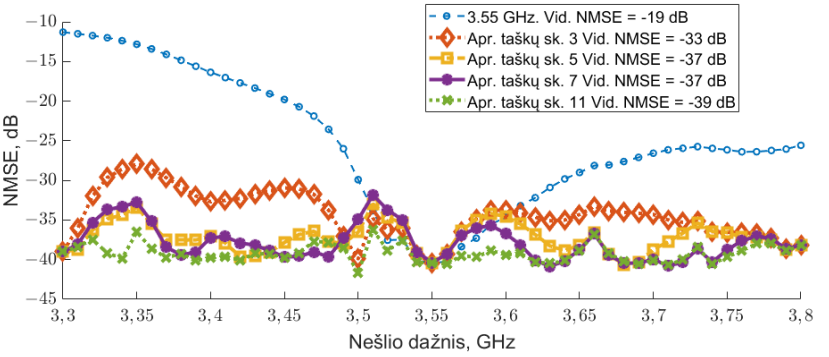

S3.2 pav. Skirtingų eilių parametrinio atminties daugianario modelio paklaida priklausomai nuo nešlio dažnio

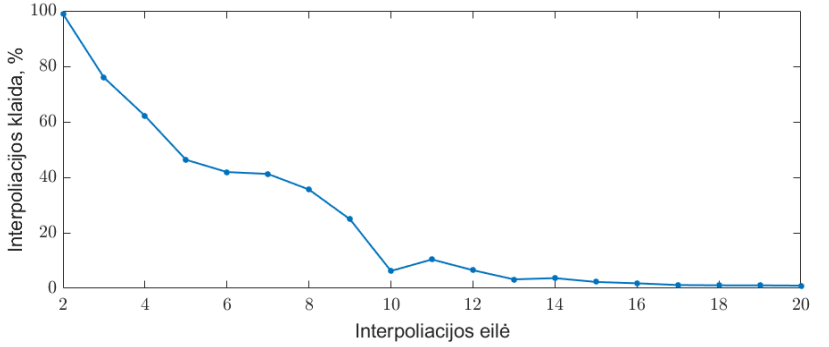

S3.3 pav. Interpoliacijos įnešamos paklaidos įvertinimas

Parametrizuoto modėlio paklaida sudaryta iš dviejų dalių. Pirmoji – tai interpoliacijai naudojamų atminties daugianarių paklaidos esant jų apskaičiavimo dažniams arba, kitaip tariant, jų pradinės paklaidos. Pavyzdžiui, jeigu parametrizuotam modeliui apskaičiuoti naudojami trys taškai, kurių paklaidų vertės yra −40 dB, tai akivaizdu, kad interpoliuoto modelio paklaida šiuose taškuose nesiskirs nuo pradinių modelių paklaidų ir sieks tuos pačius −40 dB. Antroji dalis – tai interpoliavimo paklaida, rodanti, kiek būtent gauta aproksimuojanti funkcija skirsiasi nuo aproksimuojamo originalo. Siekiant įvertinti paminėtos paklaidos dydį, kiekvienam iš tirtų 51 dažnių buvo sudarytas atminties daugianario modelis ir įvertinta to modelio paklaida esant jo apskaičiavimo dažniui. Gauta kreivė buvo palyginta su parametrizuoto modelio rezultatais, kai modeliui apskaičiuti buvo naudojama nuo 2 iki 15 taškų. Rezultatai pateikiami S3.3 paveiksle. Matyti, kad

žemesnėse aproksimacijos eilėse beveik visą modelio paklaidą sudaro būtent interpoliacijos sukuriama paklaida. Didinant interpoliacijos taškų skaičių, mažėja ir interpoliacijos paklaidos santykinis dydis. Nuo 10 aproksimacijos eilės aproksimacijos paklaidos santykinis dydis sumažėja ~90 % ir siekia apie 10 % visos modeliavimo paklaidos.

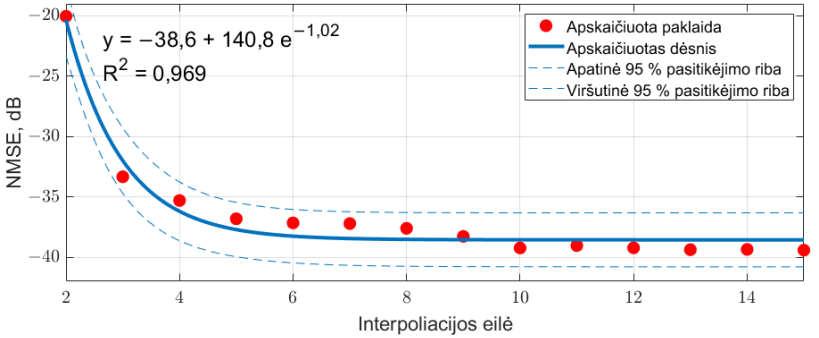

S3.4 pav. Klaidos kitimo dėsnio apskaičiavimas

S3.4 paveiksle pateikiama apskaičiuota sukurto modelio paklaidos priklausomybė nuo interpoliacijos eilės. Priklausomybė atitinka atvirkštinę eksponentinio įsisotinimo funkciją, kurios įsisotimo vertė −38,6 dB artima vidutinei paklaidai, modeliuojant esant visiems 51 dažniams, t. y. − 39,5 dB.

Bendrosios išvados

1. Vienam nešlio dažniui apskaičiuotą elgsenos modelį taikant kitiems nešlių dažniams, padidėja modeliavimo paklaida, kurią vadiname dažnine modelio paklaida. Ši dažninė paklaida gali būti apibūdinama naudojant jos kitimo greičio dažnio atžvilgiu metriką ir vidutinės modeliavimo klaidos tirtame dažnių diapazone metriką. Šios metrikos leidžia palyginti skirtingų elgsenos modelių abibendrinamumą nešlio dažnio atžvilgiu.
2. Sužadinimo signalo moduliacijos plotis tiesiogiai koreliuoja su modeliavimo dažninės paklaidos kitimo greičiu ir 3,55 GHz dažnio modeliui yra būdingas 0,93 koreliacijos koeficientas, o 3,65 GHz modeliui – 0,99 koreliacijos koeficientas. Sužadinimo signalo moduliacijos pločio padidinimas nuo 10 kHz iki 2 MHz pagreitino paklaidos kitimo greitį nuo 0,08 dB/MHz iki 0,11 dB/MHz.
3. Tarp sužadinimo signalo vidutinės galios ir dažninės paklaidos kitimo greičio koreliacijos nebuvo arba ji buvo aptinkama tik viename iš modeliuotų dažnių. Tarp sužadinimo signalo pikinės ir vidutinės galios santykio bei dažninės paklaidos kitimo greičio koreliacijos nebuvo.
4. Siūlomo parametrizuoto atminties daugianario modelio vidutinė paklaida atvirkštinio įsisotinimo eksponentine funkcija priklauso nuo modelio interpoliacijos eilės. Nustatyta, kad parametrizuoto 11 taškų modelio vidutinė

modeliavimo paklaida siekia −39 dB iryra tokia pati, kaip kiekvienam dažniui atskirai apskaičiuotų modelių vidutinė paklaida. Tai rodo, kad pasiūlyto metodo tikslumas plačiame nešlio dažnių diapazone yra artimas individualiai kiekvienam dažniui išskiriamų modelių tikslumui.

5. Dvi pagrindinės parametrizuoto modeliavimo paklaidos dedamosios yra interpoliacijos paklaida ir pradinė modelio apskaičiavimo paklaida. Pirmoji reikšmingai sumažėja didinant interpoliacijos taškų skaičių – padidinus jų skaičių nuo 2 iki 10, interpoliacijos sukuriamos paklaidos santykis su visa modėlio paklaida sumažėja ~90 %. Pradinė modelio pritaikymo paklaida gali būti sumažinta tik mažinant bazinių atminties daugianarių modelių, taikomų interpoliacijai, paklaidas.

Andžej BOREL

INVESTIGATION OF BEHAVIORAL MODELS USED
FOR LINEARIZATION OF RADIO FREQUENCY POWER
AMPLIFIERS OVER A WIDE CARRIER FREQUENCY RANGE

Doctoral Dissertation

Technological Sciences,
Electrical and Electronic Engineering (T 001)

RADIJO DAŽNIŲ GALIOS STIPRINTUVAMS LINEARIZUOTI
TAIKOMŲ ELGSENOS MODELIŲ TYRIMAS
PLAČIAME NEŠLIO DAŽNIŲ DIAPAZONE

Daktaro disertacija

Technologijos mokslai,
Elektros ir elektronikos inžinerija (T 001)

Lietuvių kalbos redaktorė Audronė Jonikienė
Anglų kalbos redaktorė Jūratė Griškėnaitė

2026 05 08. 10,5 sp. l. Tiražas 20 egz.
Leidinio el. versija *https://doi.org/10.20334/2026-026-M*
Vilniaus Gedimino technikos universitetas
Saulėtekio al. 11, 10223 Vilnius
Spausdino UAB „Ciklonas“,
Žirmūnų g. 68, 09124 Vilnius